# THE ROLE OF THE BARENTS SEA IN THE ARCTIC CLIMATE SYSTEM

Lars H. Smedsrud,[1,5] Igor Esau,[2,5] Randi B. Ingvaldsen,[3,5] Tor Eldevik,[4,5] Peter M. Haugan,[4,5] Camille Li,[4,5] Vidar S. Lien,[3,5] Are Olsen,[3,5] Abdirahman M. Omar,[1,5] Odd H. Otterå,[1,5] Bjørg Risebrobakken,[1,5] Anne B. Sandø,[3,5] Vladimir A. Semenov,[6,7] and Svetlana A. Sorokina[2,5]

Received 14 September 2012; revised 3 May 2013; accepted 30 June 2013; published 16 September 2013.

[1] Present global warming is amplified in the Arctic and accompanied by unprecedented sea ice decline. Located along the main pathway of Atlantic Water entering the Arctic, the Barents Sea is the site of coupled feedback processes that are important for creating variability in the entire Arctic air-ice-ocean system. As warm Atlantic Water flows through the Barents Sea, it loses heat to the Arctic atmosphere. Warm periods, like today, are associated with high northward heat transport, reduced Arctic sea ice cover, and high surface air temperatures. The cooling of the Atlantic inflow creates dense water sinking to great depths in the Arctic Basins, and ~60% of the Arctic Ocean carbon uptake is removed from the carbon-saturated surface this way. Recently, anomalously large ocean heat transport has reduced sea ice formation in the Barents Sea during winter. The missing Barents Sea winter ice makes up a large part of observed winter Arctic sea ice loss, and in 2050, the Barents Sea is projected to be largely ice free throughout the year, with 4°C summer warming in the formerly ice-covered areas. The heating of the Barents atmosphere plays an important role both in "Arctic amplification" and the Arctic heat budget. The heating also perturbs the large-scale circulation through expansion of the Siberian High northward, with a possible link to recent continental wintertime cooling. Large air-ice-ocean variability is evident in proxy records of past climate conditions, suggesting that the Barents Sea has had an important role in Northern Hemisphere climate for, at least, the last 2500 years.

**Citation:** Smedsrud, L. H., et al. (2013), The role of the Barents Sea in the Arctic climate system, *Rev. Geophys.*, *51*, 415–449, doi:10.1002/rog.20017.

## 1. INTRODUCTION AND FOCUS

[2] The Barents Sea (BS) is the northernmost Arctic shelf sea with partly ice-free ocean during winter in the present climate. Because of this, the BS exhibits a number of special properties that make it an interesting region for studying interactions between the atmosphere, sea ice, and ocean.

[3] First, the relatively easy access due to open waters has allowed for good, year-round observations. The first explorers visited the region more than 500 years ago [*van Linschoten*, 1601]. They discovered abundant wildlife and rich fishing on the many shallow banks of the BS. These bounties have drawn a steady stream of visitors over time, providing us with a good historical record of conditions in the BS. For instance, old sailing logs [*Vinje*, 2001] reveal that the winter of 1866 was particularly severe, with the April sea ice edge reaching its southernmost recorded position. In comparison, recent years have seen the smallest ice extents with less than 30% of the BS ice covered annually [*Årthun et al*., 2012b]. Second, the limited depth (< 300 m for the most part) and surrounding islands create a confined oceanic basin that is reasonably simple to monitor. Despite limited observations in the northern straits (Figure 1), the net heat transport (volume and temperature) over the last decade is well known [*Smedsrud et al*., 2010]. This information has been used to evaluate regional and global models and to constrain the previously wide ranges [*Simonsen and Haugan*, 1996] in heat budgets.

[4] The northward flowing Atlantic Water (AW) that keeps the BS partly ice free also keeps the Greenland Sea ice free during winter. These regions provided the first observations of decadal-scale oscillations in the air-ice-ocean system [*Ikeda*, 1990]. Around 1970, there was a long cold period with lower temperatures than average over the Arctic (Figure 2). We term this period "Cool 70s" here, although it also incorporates some years at the end of the 1960s. The

[1]Uni Climate, Uni Research, Bergen, Norway.
[2]Nansen Environmental and Remote Sensing Centre, Bergen, Norway.
[3]Institute of Marine Research, Bergen, Norway.
[4]Geophysical Institute, University of Bergen, Bergen, Norway.
[5]Also at Bjerknes Centre for Climate Research, Bergen, Norway.
[6]Helmholtz Centre for Ocean Research Kiel, GEOMAR, Kiel, Germany.
[7]Also at A. M. Obukhov Institute of Atmospheric Physics, Russian Academy of Sciences, Moscow, Russia.

Corresponding author: L. H. Smedsrud, Uni Climate, Uni Research, Allegaten 55, Bergen 5007, Norway. (larsh@gfi.uib.no)





8755-1209/13/10.1002/rog.20017
Paper number 2012RG000418

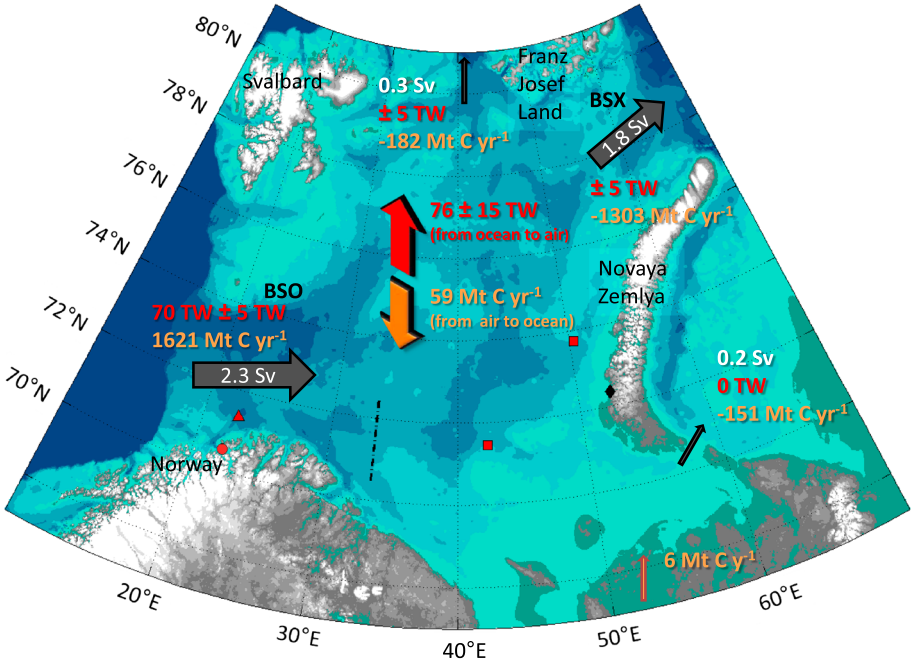


**Figure 1.** The mean oceans transports to the Barents Sea and present-day mean value of surface flux of heat (TW $=10^{12}$ W) and carbon (Mtyr$^{-1}$ $=10^{12}$ gyr$^{-1}$). Locations of station data used are shown as diamond, triangle, square, and circle; and the Kola section is shown as the dashed black line. Locations of the Barents Sea Opening (BSO) and the Barents Sea Exit (BSX) are also included.

cooling was particularly pronounced in the Barents and Greenland Seas, which were about 2°C colder than average [*Ikeda*, 1990]. In the recorded air temperature from Novaya Zemlya (Figure 2b), the cold anomaly is ~2°C, while the cold anomaly in ocean temperature in the Kola section is ~0.5°C (Figure 2a). The Cool 70s was also characterized by greater-than-average Arctic sea ice extent, primarily caused by anomalies in the Barents and Greenland Seas [*Ikeda*, 1990]. In the same records, there is a warm period termed the "Early Warming," between the mid-1920s and the 1940s (Figure 2). At its peak in the 1930s, the anomaly in Northern Hemisphere (> 60°N) surface air temperature (SAT) was of the same magnitude as that during the Cool 70s. Increased ocean heat transport into the BS, driven by local wind forcing, with an associated sea ice retreat, has been suggested as the main drivers of the Early Warming [*Bengtsson et al*., 2004].

[5] How much influence can the small, shallow BS have on an Arctic scale? The BS area is about 10% of the Arctic Ocean, or about 1.4 million km$^2$, and the mean depth is only 230 m. Despite this limited volume, the BS occupies a key position on the eastern side of the main gateway between the Arctic and the other world oceans, and here, much of the heat transport occurs, both in the air and ocean. The BS is thus favorably located to couple the oceanic heat brought northward by the AW to the atmosphere. Being small and shallow may be an advantage in some respects: The AW transported to the BS by the Norwegian Atlantic Current is well exposed to the air above and is therefore vertically mixed and cooled very efficiently. For the ocean, the heat loss creates dense water that sinks below the upper mixed layer of the Arctic Ocean, bringing along $CO_2$ sequestered from the atmosphere. For the atmosphere, the resulting decline of winter sea ice cover [*Screen and Simmonds*, 2010] has been suggested to increase the probability of cold winters in Europe by triggering circulation changes over a much larger region [*Yang and Christensen*, 2012], though the mechanisms behind such a link are debated [*Honda et al*., 2009; *Overland and Wang*, 2010; *Inoue et al*., 2012]. In these ways, the BS may influence larger regions, both the Arctic to the north and Europe to the south, via atmospheric and oceanic pathways.

[6] A series of cause and effects in the coupled Barents air-ice-ocean climate appears well established from the published literature. Taken in sequence, these links suggest the possibility of positive feedback loops operating in the Barents system. Consider an anomalously high transport of Atlantic heat in the BS Opening (BSO) (Figure 1). This may occur because of increased volume transport and/or temperature of the water being transported (Figure 3a). This leads to a warmer BS, which requires more cooling before it reaches the freezing point, such that less winter sea ice is formed, and there is a larger temperature contrast between the cold air and the warm ocean (Figure 3b). As a consequence, there is increased net surface heat loss from the ocean to the atmosphere (Figure 3c). This three-step series of events was introduced more than 20 years ago by *Ikeda* [1990] and *Ådlandsvik and Loeng* [1991] and forms the common axis of the two positive feedback loops that will be our focus here.

[7] Atmospheric circulation responses to the large surface heat loss in the BS have been proposed as one way to facilitate a positive feedback loop and thus maintain decadal oscillations in the Arctic air-ice-ocean system [*Ikeda* 1990; *Mysak and Venegas*, 1998; *Ikeda et al*., 2001; *Bengtsson et al*., 2004]. We call this loop the "wind feedback." In this feedback loop,

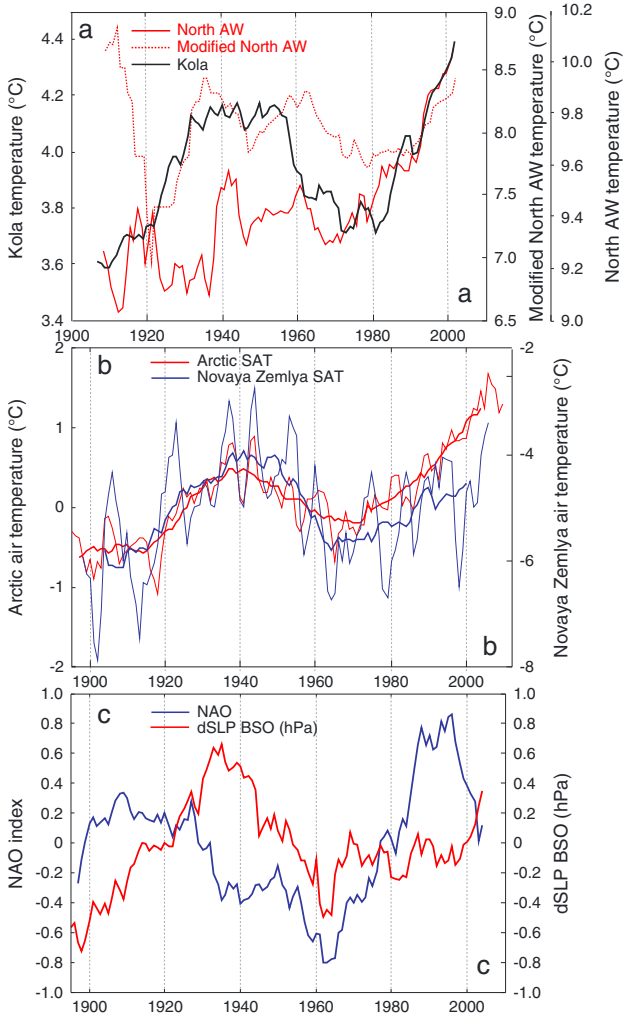


**Figure 2.** Long-term observations of key parameters for the Barents Sea climate. Locations are shown in Figure 1, and a 15 year moving average filter was used for all plots. (a) Black line shows annual mean ocean temperature between 0 and 200 m depth in the Kola section (data from the Polar Research Institute of Marine Fisheries and Oceanography, Russia). Red lines show two different types of upstream Atlantic Water temperature in the Faroe-Shetland Channel (data from *Yndestad et al.* [2008]). (b) Surface air temperature for the Arctic (mean 60°N–90°N, CRUTEM3 [*Brohan et al.* 2006]) and observed temperature at Mayle Karmakuly, Novaya Zemlya. Thin lines show annual values. (c) NAO winter (DJFM) index [*Hurrell*, 1995] and pressure SLP difference between Norway and Svalbard (HadSLP2 data [*Allan and Ansell*, 2006]).

the increased surface heat loss warms the lower atmosphere and leads to a local reduction in surface pressure (Figure 3d). The resulting cyclonic circulation anomaly produces strong westerly winds over the BSO (Figure 3e). Local wind forcing, in part, drives the inflow of AW to the BS, so the stronger westerlies reinforce the initial perturbation of increased Atlantic heat transport through the BSO to close the wind feedback loop and produce a new warmer mean climate. The feedback loop is considered to be nonaccelerating, stable, and self-maintaining, but the initial anomalous perturbation is likely to be forced externally by variations in the large-scale oceanic or atmospheric circulation [*Ådlandsvik and Loeng*, 1991].

[8] Complementary to the wind feedback, we hypothesize the existence of a new positive "ocean feedback" (Figure 3). The existing, relevant ocean observations are reviewed in section 2.2, and climate model simulations are presented in section 3.4.2 to support this new idea. A large portion (>60%) of the BSO inflow is transformed into Cold Deep Water (CDW) with temperature <0°C [*Midttun*, 1985; *Schauer et al.*, 2002], dense enough to sink below the Atlantic layer in the Arctic Ocean. Most of the CDW flows northeastward and leaves the BS in the Barents Sea Exit (BSX) between Franz Josef Land and Novaya Zemlya (Figure 1). Because the downslope speed and transport on the shelf slope increases with increasing density gradients [*Shapiro et al.*, 2003b], denser water on the BS shelf is associated with increased BSX outflow. This is consistent with a lower sea surface height at the BSX with respect to the BSO and favors larger throughflow and larger inflow of AW at the BSO through barotropic forcing. Increased inflow is part of the "common axis" of the feedback loops referred above, with less sea ice and more heat loss to the atmosphere as the result (Figures 3–3c). The hypothesized loop is closed when the increased heat loss feeds back to increase the density of BSX outflow.

[9] In terms of the two feedback loops (Figure 3), warm periods like the Early Warming should be associated with increased AW inflow and reduced winter sea ice cover. During such periods, we hypothesize that the BS loses most of the extra ocean heat it receives to the atmosphere. Cold periods (around 1905 and the Cool 70s) (Figure 2) should experience decreased AW inflow and expanded winter sea ice cover, less surface heat loss to the air, and less dense water outflow through the BSX. Overall, the feedback loops may also operate differently depending on the mean state of the BS ice cover, a topic we will get back to in section 3.6.

[10] Different processes affect BSO inflow in the wind and ocean feedback loops. To set the stage, we first survey the available literature on the Barents air-ice-ocean system and review earlier relevant results (section 2). In particular, we will provide a detailed and up-to-date review on available observations of key parameters in the BS region. After the review, we present new results addressing the operation of these processes and existence of the feedback loops (section 3). We finish by summarizing the most important processes occurring in the Barents Sea and their relevance to the Arctic climate (section 4). Terms and abbreviations used are listed in a separate section at the end.

## 2. REVIEW

[11] The BS is one of two major pathways for AW entering the Arctic Ocean. It is a transition zone for warm and saline water from the Atlantic on its way to the Arctic and for cold and less saline water returning south from the Arctic. The first in-depth analysis of the BS was made by *Helland-Hansen and Nansen* [1909], suggesting that variations in the marine climate of the BS are primarily dependent on ocean transport. Cooling of the AW passing through the BS contributes to the ventilation of the Arctic Ocean [*Aagaard and Woodgate*, 2001; *Schauer et al.*, 2002], and the heat transferred annually to and from the atmosphere is large [*Simonsen and Haugan*, 1996].

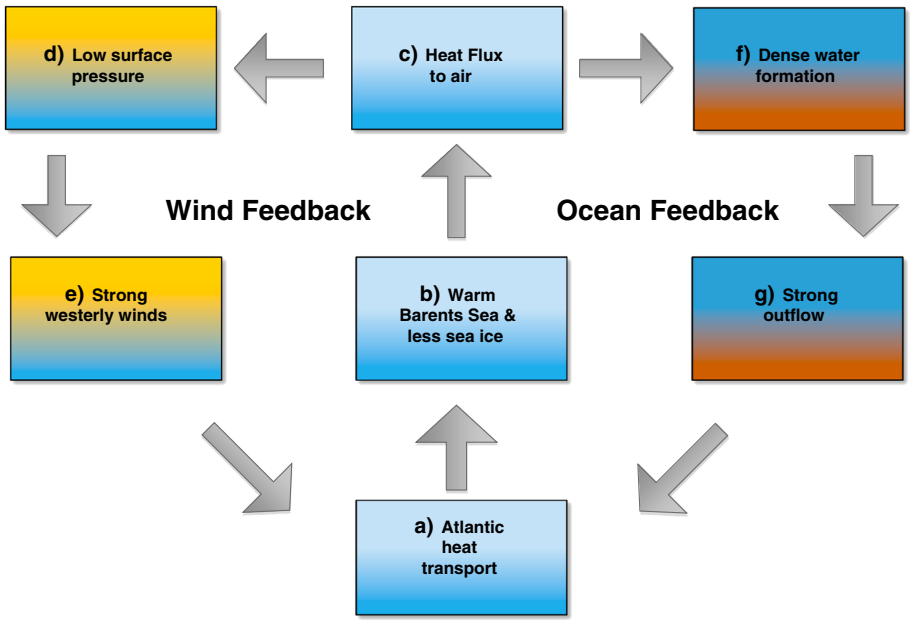


**Figure 3.** The two hypothesized positive feedback loops for the Barents Sea. The feedback loops are not considered to be accelerating but stable, self-maintaining cycles. Figures 3a–3c show that the loops share the main axis. Both loops could be started anywhere within the loop, and negative perturbations will also occur.

In this way, the BS ventilates the Arctic Ocean below the halocline [*Rudels et al*., 1994; *Schauer et al*., 1997].

[12] The fact that the BS dominates the seasonal Arctic heat budget and has the most vigorous ocean-air exchange in the Arctic makes it a "hot spot" of influence on the high-latitude climate system [*Serreze et al*., 2007]. This influence may be direct, through the ocean-atmosphere heat fluxes themselves, or indirect, through the forcing of atmospheric circulation anomalies. The atmosphere above the BS gains heat when the ocean cools to the freezing point and sea ice forms (section 2.3). Once established, the sea ice cover effectively limits the air-sea heat exchange and controls the surface heat budget climatology (section 2.4). The advance and retreat of the sea ice cover itself are, however, also tied to variations in atmosphere and ocean heat transport [*Bjerknes*, 1964; *Polyakov et al*., 2003; *Klimenko*, 2008], which model studies suggest may be anticorrelated (−0.7 to −0.8) [*van der Swaluw et al*., 2007; *Jungclaus and Koenigk*, 2010]. The rest of this section reviews current understanding about these interactions in the context of the BS.

### 2.1. Atmosphere

[13] The tropics are net absorbers of solar heating. This heat is redistributed by the atmosphere and ocean toward the poles. Although atmospheric transport dominates the 1000–1700 TW (1 TW = $10^{12}$ W) of global heat transported across 70°N [*Trenberth and Stepaniak*, 2004], the contribution in the BS region is estimated to be ~5% of this total, or around 60–80 TW [*Sorokina and Esau*, 2011]. The ocean heat transport through the BSO is better constrained and estimated to be ~70 TW [*Smedsrud et al*., 2010]. Thus, there is a critical balance between atmospheric and ocean heat transport in the heat budget of the BS.

[14] The prevailing notion that the marine climate of the BS region is primarily controlled by the ocean [*Helland-Hansen and Nansen*, 1909] has been challenged in recent years. Studies arguing for the importance of the atmosphere for driving climate variability in the Barents region have highlighted the role of anomalies in large-scale atmospheric circulation and cyclone activity [*Deser and Teng*, 2008; *Zhang et al*., 2008; *Sorteberg and Kvingedal*, 2006], in northerly winds driving ice import from the Arctic Ocean [*Koenigk et al*., 2009; *Kwok*, 2009], and in surface heat fluxes generated locally [*Schlichtholz*, 2011] or in the Norwegian Sea [*Vinje*, 2001; *Francis and Hunter*, 2007].

[15] The flow of AW into the BS is undoubtedly linked to atmospheric conditions (see wind feedback, section 1), but the exact nature of the relationship is not clear from observations. For example, the North Atlantic Oscillation (NAO) is the leading pattern of extratropical atmospheric variability in the Atlantic sector (Figure 4) [*Walker*, 1925; *van Loon and Rogers*, 1978]. The NAO index is defined as the pressure difference between the Azores high and the Icelandic low. In addition to exhibiting variability on daily to interannual time scales, the NAO index underwent a shift from persistent negative values in the 1960s to persistent positive values in the 1990s (Figure 2). This shift is closely related to Arctic warming trends over the last three decades of the twentieth century [*Moritz et al*., 2002] and was accompanied by pan-Arctic climate responses, including an intensification of the storm track and increased winter precipitation in the Nordic Seas. *Dickson et al*. [2000] suggested a related increase in AW inflow to the Arctic Ocean. Of particular relevance for this review, ocean volume transport into the BSO and sea ice cover over the BS were correlated with the NAO up until the 1990s [*Loeng et al*., 1997; *Dickson et al*., 2000]. The AW inflow in the BSO has likely increased steadily since the Cool

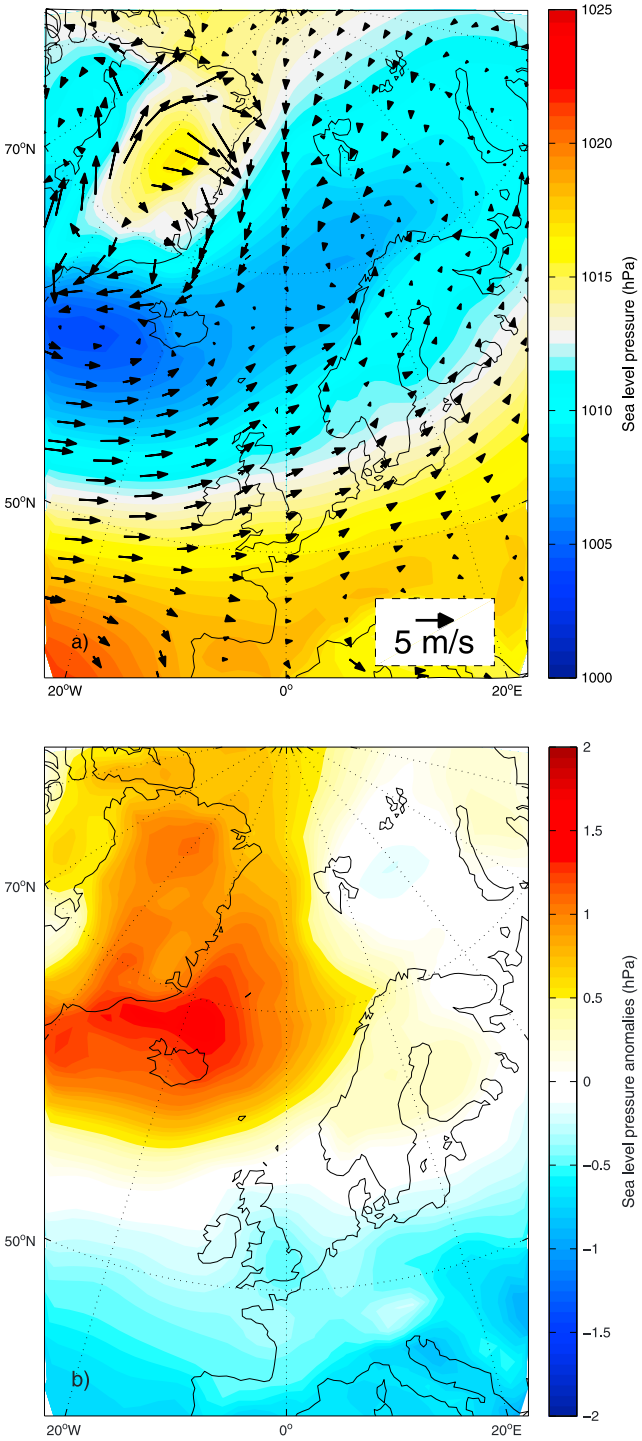


**Figure 4.** Sea level pressure (SLP) of the Barents Sea and the North Atlantic region from the ERA-Interim reanalysis project. (a) Mean over all months between 1979 through 2010. Black arrows indicate near-surface wind speed. (b) Anomalies for 2000–2010 showing change from the 1979–1999 period.

70s and has remained high in recent years [*Årthun et al.* 2012b], despite the return to lower values of the NAO index (Figure 2c). The correlation broke down sometime around year 2000, but the high heat transport since then has been consistent with the sea level pressure (SLP) gradient across the BSO (Figure 2c).

[16] It is possible that the NAO does not capture the atmospheric circulation anomalies most important for the BS. *Skeie* [2000] introduced the Barents Oscillation as the second empirical orthogonal function (EOF) of Northern Hemisphere winter sea level pressure variability (1958–1999) north of 30°N (the first EOF is the Arctic Oscillation pattern). Though its temporal robustness is debated [*Tremblay*, 2001], the Barents Oscillation pattern has a center of action over the BS and is correlated with sensible heat loss over the Nordic Seas and SAT variability over Eurasia after the Arctic Oscillation related signal has been removed [*Skeie*, 2000]. This is in line with findings by *Rogers and Mosley-Thompson* [1995], which show that Siberian winter temperature anomalies are linked to the northeast extension of the Icelandic low toward the BS more so than to the NAO index or to the strength of the Siberian High. Similarly, the North Atlantic winter storm track was found to be more closely related to sea level pressure anomalies in the far northeastern Atlantic than to the NAO index itself [*Rogers*, 1997].

[17] A typical response of atmospheric models to prescribed sea ice anomalies is to set up a cyclonic near-surface circulation anomaly over the regions experiencing a reduction in sea ice cover [*Bengtsson et al.*, 2004; *Alexander et al.*, 2004; *Deser et al.*, 2004]. Likewise, an expansion of sea ice cover sets up an anticyclonic circulation. For the BS region, recent studies have suggested a nonlinear atmospheric circulation response to gradually declining sea ice cover, such that anticyclonic circulation anomalies develop for only a certain range of sea ice concentrations [*Petoukhov and Semenov*, 2010]. This anticyclonic anomaly is accompanied by weakened midlatitude westerlies over Eurasia with cooling over the continent and increased probabilities of anomalously cold spells [*Yang and Christensen*, 2012]. The low sea ice concentrations currently observed in the Barents and Kara Seas may fall within this range, possibly explaining the increased probability of anomalously cold winters in Europe and northern Asia during the first decade of the 21st century. *Hopsch et al.* [2012] examined atmospheric circulation and temperature signals associated with negative sea ice anomalies in the Arctic and found similarly suggestive, but not definitive, relationships.

[18] In summary, an increasing number of studies suggest that the BS influences atmospheric circulation over a much larger geographic area. Although the fraction of the atmospheric changes that is response versus forcing is not settled, the existence of a link between the BS ice cover and the atmosphere is unmistakable, and the associated climate impacts for Europe and Siberia are large.

## 2.2. Ocean

[19] The oceanographic conditions of the BS are mainly determined by two factors: ocean transport and heat exchange with the atmosphere. This was noted by *Helland-Hansen and Nansen* [1909], and during the following century, the mean state and variability have been described with improved detail [*Mosby*, 1962; *Häkkinen and Cavalieri*, 1989; *Simonsen and Haugan*, 1996; *Smedsrud et al.*, 2010; *Sandø et al.*, 2010; *Årthun and Schrum*, 2010; *Ozhigin et al.*, 2011]. The main

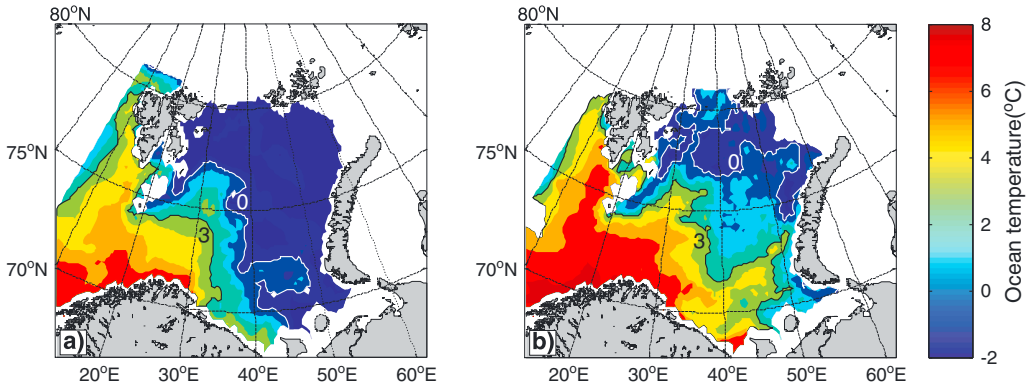


**Figure 5.** Mean temperature between 50 and 200 m depth in late summer (August–September) in (a) 1979 and (b) 2006. Isotherms are included, the 0°C as a gray line and the 3°C as black. Temperature data are from the Institute of Marine Research (Norway) and the Polar Research Institute of Marine Fisheries and Oceanography (Russia).

oceanic exchanges occur through the BSO and the BSX. The exchanges in these major openings are an order of magnitude larger than the exchange through the northern opening and the Kara Gate [*Loeng et al*., 1997; *Maslowski et al*., 2004; *Aksenov et al*., 2010; *Årthun et al*., 2012b].

[20] In the BSO, relatively warm AW and coastal waters enter. Although the importance of this heat transport for general ocean conditions was realized early on, it has only been properly quantified over the last decade [*Ingvaldsen et al*., 2004; *Smedsrud et al*., 2010; *Ozhigin et al*., 2011; *Skagseth et al*., 2011]. The absorbed solar radiation during summer is also important [*Sandø et al*., 2010], but less so than the ocean transport [*Ozhigin et al*., 2011]. Smaller amounts of (modified) AW also enter the BS as submerged flows through the northern opening [*Mosby*, 1938; *Pfirman et al*., 1994; *Lind and Ingvaldsen*, 2012] and in the BSX [*Hanzlick and Aagard*, 1980; *Schauer et al*., 2002]. Although these transports may have substantial impact on the local scale, their contribution to the total BS heat budget is low.

[21] The mean ocean heat transport to the BS over the last decade has been ~70 TW (Figure 1, heat referenced to 0°C), with ~30% carried by the Norwegian Coastal Current [*Skagseth et al*., 2011], and ~70% by the AW [*Smedsrud et al*., 2010]. The net volume transport of 2.3 Sv ($1\ \mathrm{Sv} = 10^6\ \mathrm{m^3\ s^{-1}}$) in the BSO consists of an inflow of ~2 Sv AW and ~1.2 Sv in the Norwegian Coastal Current. An outflow south of Bear Island balances roughly the ~1.2 Sv of the coastal current. The transport is stronger during winter than summer [*Ingvaldsen et al*., 2004]. Regional models suggest a positive trend in heat transport since the Cool 70s [*Årthun and Schrum*, 2010], causing the large observed changes in mean ocean temperature from the Cool 70s. Figure 5 illustrates the regional pattern of cold temperature of 1979 compared to 2006, and Figure 2a illustrates the gradual increase in time.

[22] Spatially, the BS oceanographic variability varies in phase, but there are differences in the amplitude of the long-term fluctuations [*Lind and Ingvaldsen*, 2012]. The warming since the Cool 70s has been stronger in the north and northeast than in the south and has been more pronounced since 2000. The cause of the northern amplification is related to the local atmospheric forcing [*Lind and Ingvaldsen*, 2012], which, in turn, is likely to be related to observed changes in the larger-scale circulation patterns [*Zhang et al*., 2008].

[23] The dense CDW exiting in the BSX may contribute with the densest fraction of the North Atlantic Deep Water [*Mauritzen*, 1996]. It flows north in the St. Anna Trough, recirculates along the slope of the Arctic Ocean, returns south through the Fram Strait, passes the Greenland Sea, and, finally, becomes a source of upper Norwegian Sea Deep Water, supplying the Greenland-Scotland ridge overflow feeding the deep water of the North Atlantic. This formation process is supported by observations from the Greenland Sea [*Mauritzen*, 1996]. The fate, if not the rate, of the water exiting the BS is set by the density [*Jones et al*., 1995] and determines the contribution to deep water in the Norwegian Sea and the Atlantic Ocean.

[24] Water mass transformation occurs in the BS due to cooling of AW and subsequent brine release from sea ice growth. In this way, the BS ventilates the Arctic Ocean more effectively than the other Arctic shelf seas. This is because the other shelf seas are even more shallow and have a larger river input, making the flow in the BSX high in salinity and relatively constant over time [*Rudels et al*., 1994; *Schauer et al*., 2002]. Again, processes within the BS have a documented influence on the Arctic and contributes to the overall overturning in the Atlantic Ocean.

### 2.3. Sea Ice

[25] The surface heat loss produces sea ice in the BS. The solar heating during summer melts most of the BS ice and produces a high seasonal variability of sea ice [*Vinje*, 2001; *Sorteberg and Kvingedal*, 2006]. The minimum occurs in late summer (August–September) while the maximum occurs in late winter (March–April).

[26] Both the interannual and the long-term BS ice variability are large. In cold periods, the eastern and southeastern parts of the BS have been ice covered during winter. Figure 6a shows the winter ice cover for 1979 showing maximum ice cover for the last decades. In warm periods, most of

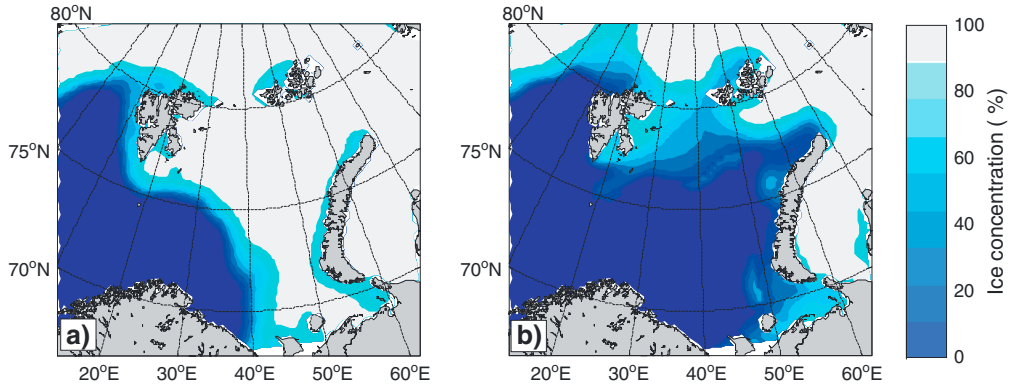


**Figure 6.** Barents Sea ice concentration in late winter (March–April). (a) 1979 illustrates maximum ice cover during the recent decades, while (b) 2006 shows minimum cover during recent years. Sea ice concentration is from the National Snow and Ice Data Center, USA [*Cavalieri et al*., 1996; *Meier et al*., 2006].

the BS is ice free even during winter, illustrated by 2006, which shows a small winter ice cover typical for the years 2005–2007 (Figure 6b). The winter ice cover has retreated northward since the 1850s [*Shapiro et al*., 2003a], but with large year-to-year variations [*Vinje*, 2001]. The ice-covered area has decreased over the last decades [*Årthun et al*., 2012b] and more so in the northern BS than in other regions in the Arctic [*Screen and Simmonds*, 2010; *Serreze and Barry*, 2011]. Longer time series of observed sea ice thickness are rare in the BS as elsewhere in the Arctic. One series of fast ice thickness exists from Hopen Island [*Gerland et al*., 2008] and has shown a thickness decrease of 0.1 m/decade since the 1960s, with variability in the 2 to 4 year window.

[27] Winter sea ice loss in the BS is fundamentally different than sea ice loss occurring in other parts of the Arctic Ocean. The greatest losses of Arctic sea ice are mostly in the Siberian sector and during summer [*Comiso*, 2012]. This summer ice loss is caused by more efficient melting inside the basin [*Kwok and Cunningham*, 2010] and a larger export of ice southward in the Fram Strait [*Smedsrud et al*., 2011]. Most of the ice in the BS is formed locally, but the wintertime import from the Arctic Ocean can explain much of the year-to-year variability [*Kwok*, 2009; *Ellingsen et al*., 2009]. On average, 40 $km^3$ of Arctic sea ice is imported to the BS each winter, but net import may reach 340 $km^3$ and net export 280 $km^3$ out of the sea [*Kwok et al*., 2005]. Some years, there is also a high ice transport north of Novaya Zemlya into the northeastern BS [*Ellingsen et al*., 2009; *Ozhigin et al*., 2011].

[28] Most of the BS ice cover used to form during winter when surface heat loss cooled the ocean to the freezing point, but in recent years, large areas of the BS have not formed ice. This is largely due to the recent high AW heat transport [*Årthun et al*., 2012b]. The link between AW transport and winter ice variability is well known [*Loeng et al*., 1997; *Dickson et al*., 2000], although the winter ice variability has also been linked to northerly winds and the number and intensity of cyclones [*Sorteberg and Kvingedal*, 2006]. Stronger northerly winds give lower AW transport, and this is, thus, consistent with *Årthun et al*. [2012b]. Time series of annual mean ice cover correlates significantly with ocean temperature from the Kola section [*Schlichtholz*, 2011] and air temperature at Bear Island and Franz Josef Land (1951–2000) [*Ozhigin et al*., 2003]. Most of the loss of BS ice in the winter has thus not been ice that melted but rather ice that never froze.

[29] In the 1950s and 1970s, the BS annual mean ice cover was around 30% of the BS area. In the 1960s, the ice cover was somewhat larger, but recently, it has dropped to only 200,000 $km^2$, or 14% of the area [*Årthun et al*., 2012b]. Sea ice cover (Figure 6) and ocean temperature (Figure 5) are closely linked. A loss of sea ice corresponds to increased heat fluxes and thus higher surface temperatures [*Screen and Simmonds*, 2010; *Årthun et al*., 2012b]. Based on model simulations, *Semenov and Latif* [2012] suggested considerable negative sea ice anomalies during Early Warming using this link between surface air temperature and sea ice cover. Although an indirect method, the estimates are based on the more reliable temperature data, and particularly, winter sea ice observations are lacking for the Early Warming years and those before.

[30] The BS is thus a location where long time series of sea ice cover are available and document that decadal-scale oscillations have occurred. In addition, the BS ice loss is dominating Arctic ice loss during winter and contribute to "polar amplification" by present and warmer open waters in the formerly ice-covered areas.

### 2.4. Air-Ice-Ocean Heat Exchange

[31] The Barents air-ice-ocean heat exchange is characterized by large differences in the surface heat fluxes under the influence of warm ocean-air transport from the south and cold ocean-air transport from the north. Changes in the high-latitude Arctic climate have been linked to a number of local feedback mechanisms where modifications of the surface features and the vertical surface fluxes of heat, moisture, and momentum play an important role. Two primary feedbacks are the ice-albedo and long-wave radiation feedbacks connected to the extent of the sea ice cover [*Serreze and Barry*, 2011; *Winton*, 2006]. Considering annual averages in the BS, the atmosphere cools the ocean, i.e., positive

**TABLE 1. List of Data Sets Utilized in the Analysis**

| Data Set | Parameters Used | Period, Area, Resolution | Comments | Reference |
|---|---|---|---|---|
| OAFLUX (Objectively Analyzed air-sea Fluxes) | LHF, SHF, LW, SW, SST, SAT | 1958–2007 Global fields 1°×1° deg | Woods Hole Oceanographic Institution http://oaflux.whoi.edu/dataproducts.html Algorithm: COARE bulk flux algorithm 3.0 [*Fairall et al*., 2003] | *Yu and Weller* [2007] |
| ISCCP (International Satellite Cloud Climatology Project) | LHF, SHF, LW, SW, SST, SAT | 1984–2007 Global fields 1° × 1° | Subset of AOFLUX with radiative fluxes http://www.isccp.giss.nasa.gov | *Rossow and Dueñas* [2004] |
| HOAPS3 (Hamburg Ocean Atmosphere Parameters and fluxes from Satellite data) | LHF, SHF, LW, SW, SST, | 1987–2005 | http://www.hoaps.zmaw.de/ Algorithm: COARE bulk flux algorithm 1.0 [*Fairall et al*., 2003] | *Andersson et al*. [2010] |
| ERAI (European Centre for Medium range Weather Forecast Interim reanalysis) | LHF, SHF, LW, SW, SLP | 1979–2010 Global fields 1.5° × 1.5° | http://www.ecmwf.int/research/era | *Dee et al*. [2011] |
| NOAA20C V2 (National Oceanographic and Atmospheric Administration, twentieth century reanalysis, version 2) | LHF, SHF, LW, SW | 1871–2010 Global fields 2° × 2° | http://www.esrl.noaa.gov/psd/data/gridded/data.20thCent Reanalysis.html | *Compo et al*. [2006] |
| NCEP | SLP, SAT | 1948–2012 | http://www.esrl.noaa.gov/psd/data/gridded/data.ncep.reanalysis.html | *Kalnay et al*. [1996] |
| BCM<br><br>Bergen Climate Model | LHF, SHF, LW, SW, | 600 years Global fields 2° × 2° (sea ice) 2.8° × 2.8° (atmosphere) | - | *Otterå et al*. [2009] |

heat flux dominates. Different estimates of the BS vertical fluxes are available from independent data sets based on remote sensing and model retrospective analyses (Table 1). Climatological values of the different heat flux components are given in Table 2. Although each data set has its limitations, we use the International Satellite Cloud Climatology Project (ISCCP) (Table 1, 1984–2007) as a standard for comparison based on the analyses presented here (Table 2 and Figures 7, 12, and 13). The mean total BS surface heat flux based on the ISCCP data is 56 W $m^{-2}$ and corresponds to an annual surface heat loss of 76 TW, with large seasonal variability (Figure 7b).

[32] In wintertime, when incoming solar radiation is negligible, the heat loss increases. In particular, the relatively warm open water surface creates favorable conditions for convective instability and therefore strong turbulent heat flux in the planetary boundary layer. Turbulent sensible and latent heat fluxes depend largely on air properties. The large turbulent fluxes during winter (Figure 7a) can only be explained through persistent advection of cold air masses from surrounding continents and regions covered by sea ice. Such advection events are known as cold air outbreaks. Figure 8 shows the typical spatial pattern of the atmospheric convection during a cold air outbreak over the eastern part of the BS on 24 April 2002. During such events, heat fluxes as large as 500 $Wm^{-2}$ can be found over the southern BS, even on monthly time scales [*Ivanov et al*., 2003]. These very large heat fluxes not only couple the atmosphere and the ocean and induce strong turbulence self-organization but also feed intense meteorological mesoscale cyclones known as polar lows. The large wintertime heat fluxes above 150 W $m^{-2}$ (Figure 7) is associated with a planetary boundary layer ~ 1000 m thick (not shown).

[33] Paradoxically, stronger convective motions reduce the total cloudiness and increase the long-wave heat flux due to clustering of upward and downward motions, as seen in the cloud patterns in Figure 8. Turbulent air-ocean interactions in the region were studied by *Brümmer* [1999] using field observations and *Brümmer and Pohlmann* [2000] using satellite images for the years 1985–1995. The occurrence of organized convective patterns (cloud streets, rolls, and cells) over open water varied in this period from ~50% in the southern BS to ~10% in the northern part of the area. The organized convection enhanced surface turbulent fluxes by 15%–30%. In the north, convection was organized in rolls and linked to cold air outbreaks in 47%–100% of the cases. In the south, convection was observed in 50%–80% of the cases, indicating a deep and well-developed planetary boundary layer. The characteristic distance between the cloud streets in the rolls was ~14 km, while the diameter of the convective cell was 20–30 km . The majority of the cold air outbreaks lasted about 1 day. The cell convection was more persistent events lasting 3–5 days, while the longest continued period with convection was 20 days. The offshore and off-ice winds drive strong air-ocean interactions, while on-ice flow decouples the atmosphere and the planetary boundary layer above the ice [*Vihma et al*., 2003; *Tjernström et al*., 2005].

[34] On average, 12 polar lows per year are found in the BS and Nordic Seas using satellite data covering the last decade, with the maximum number observed in January [*Noer et al*., 2011]. Using reanalysis and climate models, the identification of polar lows is based on indirect indicators and thus carries substantial uncertainties. *Zahn and von Storch* [2008] found 4.3 polar lows per year in the BS for the reanalysis period 1948–2006 and, more importantly, no significant trend. Modeling studies suggest that polar lows will follow the retreating ice edge northward such that more polar lows may appear in the northern BS in the future [*Kolstad and Bracegirdle*, 2008]. On the other hand,

**TABLE 2. Climatological Values of Barents Sea Heat Budget Components Obtained From Different Data Sets[a]**

| Data Set (Period) | Total heat flux [TW] | Turbulent heat flux [TW] | Radiative heat flux [TW] | Comments |
|---|---|---|---|---|
| ISCCP (1984 – 2007) | +76 | +111 | −35 | |
| HOAPS−3 (1987 – 2005) | +99 | +92 | +7 | SW radiation is taken from ISCCP data |
| ERAI (1979 – 2010) | +67 | +88 | −21 | |
| NOAA20C (1871 – 2010) | +62 | +98 | −35 | Since 1979 |
| **Models** | | | | |
| BCM (600 years) | +69 | +99 | −30 | |
| ERA−40 (1990−1999) | +73 | | | *Segtnan et al*. [2011] |
| NCEP−2 (1990−1999) | +63 | | | |
| COADS and ECMWF (1985 – 1990) and Coastal stations (1950 – 1990) | +42 to +162 | +118 to +183 | −30 to −68 | *Simonsen and Haugan* [1996] |
| Regional model (1958 –1997) | +40 | +58 | −18 | *Årthun and Schrum* [2010] |
| Ocean CTD data northern part of BS (1979 – 2011) | +240 | +320 | | *Ivanov et al*. [2012] |
| Column model and climatology | +88 | +95 | −8 | *Smedsrud et al*. [2010] |
| **Overall average estimates** | +76 ±15 | +97 ±10 | −20 ± 17 | Using ISCCP, HOAPS−3, ERAI and NOAA20C |

[a]Values given are rounded off to the nearest integer because uncertainties are generally above ±10 TW. The new estimates (ISCCP, HOAPS−3, ERAI and NOAA20C) are calculated as an area averaged mean flux for grid cells with available data, and multiplied with the same Barents Sea area of $1.36 \times 10^{12}$ m².

atmospheric warming may lead to fewer polar lows developing in areas where they appear today as the necessary temperature difference between the relatively warm ocean and the air above weakens.

[35] Between May and August, the incoming solar radiation compensates the surface heat loss and warms the ocean (Figure 7a). The sea surface temperature rise significantly only in the southern BS. Here the upper few tens of meters warm, stratifying the ocean and preventing downward mixing of heat. The surrounding continents and the air above them warm faster than the ocean due to the lower heat capacity of the air. This creates a stably stratified layer of relatively cold marine air over the BS, with a thickness of a few hundred meters. This layer prevents turbulent heat exchange with the higher atmospheric layers, as was clearly shown during the Arctic Ocean Experiment by *Tjernström et al*. [2005]. During summertime, both the deeper ocean and the free troposphere are thus insulated from near-surface processes. The mean planetary boundary layer thickness reduces to less than 300 m over open water in summer in the NOAA20C data set. Despite higher surface temperatures in summer than in winter, the long-wave radiation loss is smaller due to increase in summertime cloudiness (Figure 7a) [*Chernokulsky and Mokhov*, 2012]. For the March–September period, when solar radiation is strong, the sea ice also insulates the ocean below due to the high albedo of the ice. This leads to smaller summer warming of the ice-covered areas and larger warming of the open ocean areas (Figure 7b).

[36] The sea ice cover is an especially good insulator for the latent heat flux. However, Barents ice cover can be significantly fractured (Figure 8), and this reduces the insulation. The ISCCP data suggest that the total heat flux in the mostly ice-covered areas is 30%–50% of the open ocean values during winter (Figure 7b). On average, ~62 TW of the heat is lost in the open water parts, or 82% of the total heat loss. The main difference in the winter heat budget between sea ice–covered and open ocean is caused by the turbulent heat loss, because long-wave radiative flux is nearly the same. Over sea ice–covered areas, the turbulent fluxes are large (~ 80 W $m^{-2}$) over the small fractions of open water, and are reduced to modest values over the ice surface. The difference in these turbulent heat fluxes over areas with open water and ice is quite sensitive to the number of fractures in the sea ice. In reanalysis data, where sea ice cover fractures are not resolved, e.g., in the NOAA20C data set, the wintertime turbulent heat flux over sea ice is a factor of 6 smaller than the corresponding flux over open water. This indicates that sea ice fractures are a critical parameter for estimating BS heat loss.

[37] Generally, more clouds are expected over open ocean than over sea ice–covered ocean. Using active remote sensing, *Palm et al*. [2010] found the largest and thickest cloud cover over Arctic areas with little sea ice based on observations since 2003 and increased cloudiness in October (7%) and March (10%) associated with recent sea ice loss. Disagreement between limited surface observations and passive satellite cloud detection has until recently hampered observations of changes in cloudiness, especially during winter, in both the BS and the Arctic in general. More Arctic clouds will likely affect the surface heat loss in the future, with an expected decrease in short-wave radiation reaching the surface and an increase in net long-wave radiation [*Sorteberg et al*., 2007].

[38] The BS heat loss is composed of turbulent and radiative components of comparable magnitude and vary with sea ice cover. The differences in BS heat loss estimates from the products analyzed here are considerable (Table 2), but all results point to the fact that this heat loss is large by Arctic standards.

## 2.5. Air-Ice-Ocean Variability

[39] The BS climate shows substantial variations on different time scales, ranging from seasonal to multidecadal [*Loeng et al*., 1997; *Ingvaldsen et al*., 2003; *Bengtsson et al*., 2004; *Skagseth et al*., 2008; *Levitus et al*., 2009]. High ocean temperature tends to occur during the same periods as high air temperature [*Ozhigin et al*., 2011; *Boitsov et al*., 2012] (Figure 2). Fluctuations in Barents air and ocean temperature also tend to vary in phase with the sea ice

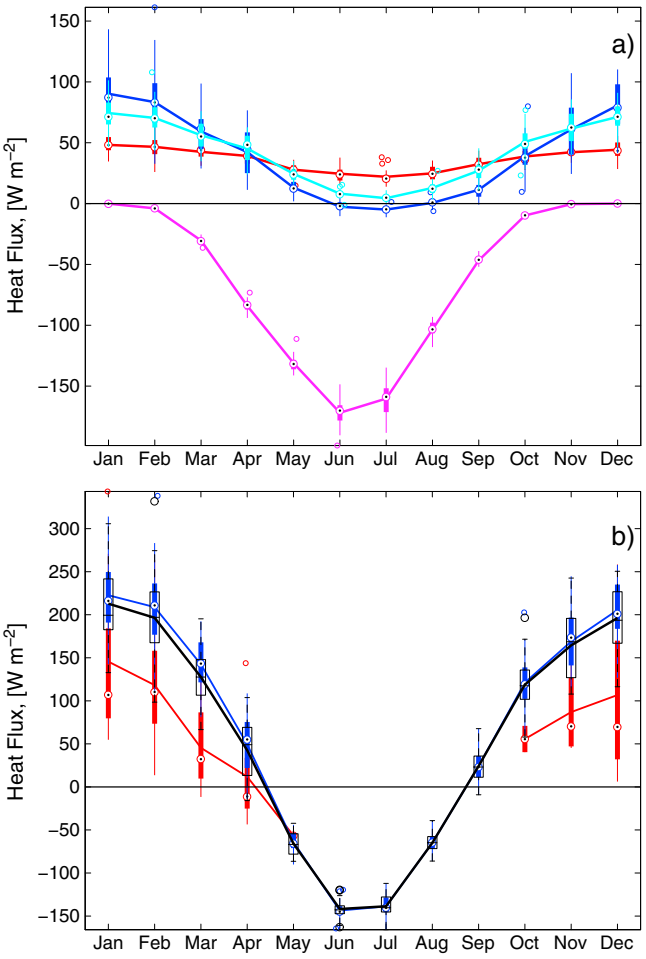


**Figure 7.** Surface heat flux climatology averaged over the Barents Sea from the ISCCP data set (Table 1). Positive values are upward heat flux and heat gain to the air, and a Barents Sea area of 1.36 $10^{12}$ m$^2$ can be used to convert from W m$^{-2}$ to TW. The monthly climatology is plotted using solid lines for the mean values. Box plots surrounding the mean indicate (thin vertical lines) the smallest and largest monthly values, (thicker vertical lines) the lower and the upper quartile, and (open circle with black dot) the median value. Outliers are included using open circles and are identified as outside 1.5 times the interquartile range. (a) The different components of the total surface heat flux. Turbulent sensible flux is shown in blue (mean: 39 W m$^{-2}$, or 54 TW), turbulent latent flux in cyan (mean: 42 W m$^{-2}$, or 57 TW), the total long-wave radiation in red (mean: 36 W m$^{-2}$, or 49 TW), and the short-wave radiation as magenta (mean: −62 W m$^{-2}$, or −85 TW). (b) The total heat flux and dependence on sea ice cover. Total heat flux is shown in black (mean: 56 W m$^{-2}$, or 76 TW; open box plots and black horizontal line for the median). Open water area (no sea ice) is included as blue (mean of 61 W m$^{-2}$) and areas with sea ice cover >80% in red (mean heat flux over the open water fraction is 83 W m$^{-2}$).

cover[*Ozhigin et al.*, 2011]. The short-term climate variability (3–10 years ) is strongly correlated with changes in AW volume and temperature [*Loeng*, 1991; *Ingvaldsen et al.*, 2004; *Sandø et al.*, 2010], as well as with regional heat flux [*Häkkinen and Cavalieri*, 1989; *Ådlandsvik and Loeng*, 1991; *Simonsen and Haugan*, 1996; *Årthun and Schrum*, 2010]. *Ikeda* [1990] and *Ådlandsvik and Loeng* [1991] suggested that warm periods of 5 to 10 year duration are related to a stable low-pressure situation over the area with cyclonic circulation, while cold periods tend to occur in high-pressure situations with anticyclonic wind circulation.

[40] During the last 100 years, the multidecadal variability in the BS has changed from cold at the beginning of the twentieth century, the Early Warming period in the 1930–1950s, followed by the Cool 70s, and, finally, further warming in recent years [*Bengtsson et al.*, 2004; *Levitus et al.*, 2009; *Boitsov et al.*, 2012] (Figure 2). Associated with the positive temperature trend in the BS over the last 3 decades, the extent of the warm Atlantic region has increased, the cold Arctic region has declined [*Johannesen et al.*, 2012], and the ice cover has decreased [*Årthun et al.*, 2012b]. However, comparing the two warm periods, a shift between the air temperatures in the eastern BS and ocean temperatures is clear. While the ocean temperature (Figure 2a) is now higher than any time during the last century, the air temperature on Novaya Zemlya (Figure 2b) is still below that of the Early Warming.

[41] The cause of the recent warming in the BS is likely to be a combination of oceanic and atmospheric changes. The ocean influence is evident as there is a strong relation

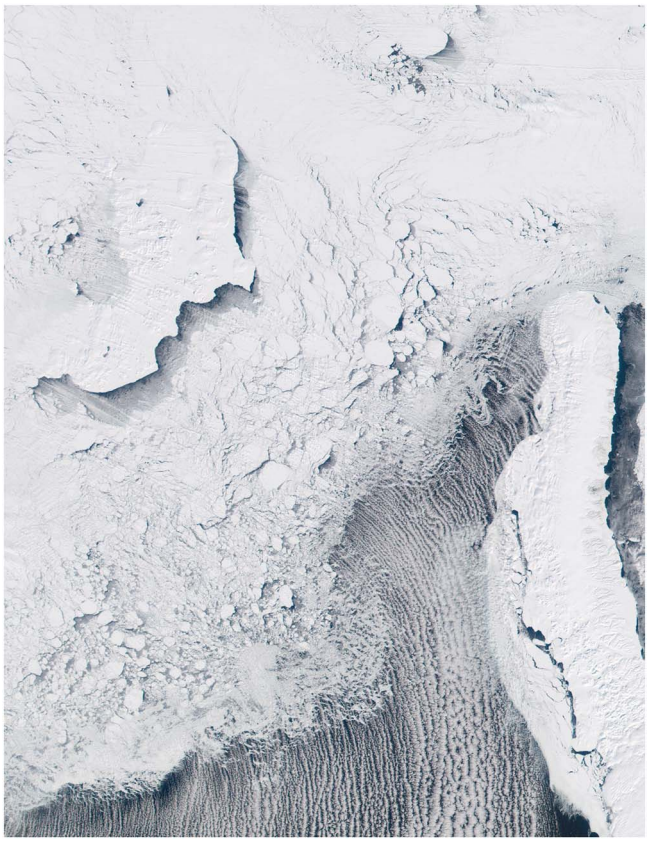

**Figure 8.** A typical spatial organization of cloud patterns over the Barents Sea during a cold air outbreak. Parallel rolls of the clouds (cloud streets) show strong clustering of clouds with significant area of clear sky in between. MODIS (Moderate Resolution Imaging Spectroradiometer) image was acquired 24 April 2002. Credit is given to Jacques Descloitres, MODIS Land Rapid Response Team, NASA/GSFC.

between upstream and BS ocean temperatures (Figure 2). *Skagseth et al*. [2008] and *Yndestad et al*. [2008] found the multidecadal climatic variation observed in the southern BS to be a local manifestation of a larger-scale climate fluctuation covering at least the North Atlantic Ocean, and model simulations by *Årthun and Schrum* [2010] showed a substantial increase in the oceanic heat transport over the last decades.

[42] Others have argued that the recent warming is caused by an increase in the atmospheric heat transport [*Overland et al*., 2008; *Overland and Wang*, 2005b]. Similar long-term fluctuations as in the ocean are found in air temperature in several areas throughout the North Atlantic and North European Seas [*Boitsov*, 2006] (Figure 2). The importance of the ocean-air interaction in the BS is highlighted by analyses of the recent accelerated sea ice loss since 2000 and temperature increase that have proceeded despite negative NAO tendency [*Overland and Wang*, 2005a] (Figure 2c). It has been suggested that the recent warming and the fast summer sea ice decrease are linked to the dramatic shift of the atmospheric circulation, resulting in the emergence of the meridional variability pattern that has been described in particular as the third Arctic pattern, the dipole anomaly pattern or the Arctic Dipole [*Overland and Wang*, 2005b; *Zhang et al*., 2008; *Overland et al*., 2008; *Overland and Wang*, 2010]. The Arctic Dipole pattern has the opposite sign centers of action in the BS region and in the central western Arctic that resembles the Barents Oscillation [*Overland and Wang*, 2010].

[43] Interdecadal variations in Arctic winter temperature have distinct patterns with maxima in the BS and Baffin Bay [*Semenov and Bengtsson*, 2003]. While NAO has contributed considerably to the Arctic mean warming between the 1970s and 1990s, this other pattern explains the major temperature change during the Early Warming and the recent warming in the Arctic [*Semenov and Bengtsson*, 2003]. This pattern (termed the multidecadal pattern) is closely linked to the pressure gradient between northern Norway and Svalbard in Figure 2c [*Bengtsson et al*., 2004]. This SLP difference represents an index of the atmospherically driven inflow in the wind feedback (Figure 3). This positive feedback may amplify the regional climate variability and lead to rapid climate changes [*Ådlandsvik and Loeng*, 1991; *Goosse et al*., 2003; *Bengtsson et al*., 2004; *Arzel et al*., 2008; *Semenov et al*., 2009]. High negative correlations between observed winter horizontally averaged Arctic SAT and spatially varying SLP are located in the BS region (Figure 9a). The pattern is similar to the results of *Bengtsson et al*. [2004] and, thus, confirms their findings using more recent data for the 1920–1970 annual variability. Using other periods modifies the pattern, but the region with strongest correlations remains in the eastern Arctic. The increased inflow could be triggered by a powerful internal atmospheric circulation as suggested by *Bengtsson et al*. [2004]. It could also be the low-frequency variability of the inflow related to the Atlantic multidecadal variability that brings the local atmospheric response [*Semenov*, 2008; *Semenov et al*., 2010].

[44] The positive wind feedback (Figure 3) in the BS requires that the sea ice retreat is associated with negative SLP anomaly in the region of enhanced surface heat flux to the atmosphere [*Bengtsson et al*., 2004]. Such a link is suggested by the observational data showing the strongest correlation between low-frequency variations of Arctic SAT and the December–January–February SLP field located in the BS region (Figure 9a). Many modeling studies have reported on significant impact of altered Arctic sea ice conditions on atmospheric circulation. In general, the local circulation response of atmospheric general circulation models is baroclinic, resulting in rather shallow near-surface warming and SLP decrease. The associated large-scale circulation response in the free troposphere projects onto a negative phase of the Arctic Oscillation in the Atlantic sector [*Alexander et al*., 2004; *Magnusdottir et al*., 2004; *Deser et al*., 2004; *Seierstad and Bader*, 2009]. Declining sea ice cover also impacts cyclogenesis in the BS region with possible consequences for weather regimes in Siberia and East Asia as reported by *Inoue et al*. [2012].

[45] The atmospheric circulation response, however, can be essentially nonlinear and depend on the magnitude of sea ice anomalies in the BS, as recently demonstrated by *Petoukhov and Semenov* [2010]. Sea ice reduction in the BS in a certain range that is close to the current state may result in a strong anticyclonic circulation anomaly contrasting to cyclonic-type response for lower and higher sea ice concentrations. The anticyclonic response pattern projects on negative NAO (shifted eastward), leads to anomalous large scale easterly flow over Eurasia accompanied by cooling and increased probabilities in strong negative temperature anomalies, and may reduce atmosphere and ocean heat transport to the Arctic.

[46] Arctic wintertime circulation may have been impacted not only by sea ice anomalies in the eastern Arctic directly but also by summer and autumn sea ice changes through oceanic heat storage and planetary wave excitation mechanisms [e.g., *Overland and Wang*, 2010; *Honda et al*., 2009; *Liu et al*., 2012].

[47] In summary, there is evidence for air, ice, and ocean decadal oscillations centered on the BS region. These oscillations are coupled, and while the mechanisms and causes are not entirely clear, changes in the BS and the Arctic appear to be synchronized.

### 2.6. Carbon Transport and Fluxes

[48] When considering inorganic carbon in the BS and its relationship to climate, it is worthwhile to separate the fluxes, transports, and concentrations into their anthropogenic and natural components. The fluxes of natural carbon represent the exchange of carbon between the air and the ocean resulting from heating, cooling, and biological activity, in combination with ocean circulation. These fluxes are neutral on a global scale and include contributions from rivers, sedimentation, and weathering of mountains [*Gloor et al*., 2003]. They have been in near–steady state since the termination of the last ice age and have served to maintain the atmospheric $CO_2$ stable at approximately 280 ppm until the industrial revolution. With the industrial revolution came emissions of $CO_2$ from combustion of fossil fuel, changes in land use, and other sources like, for example, emission

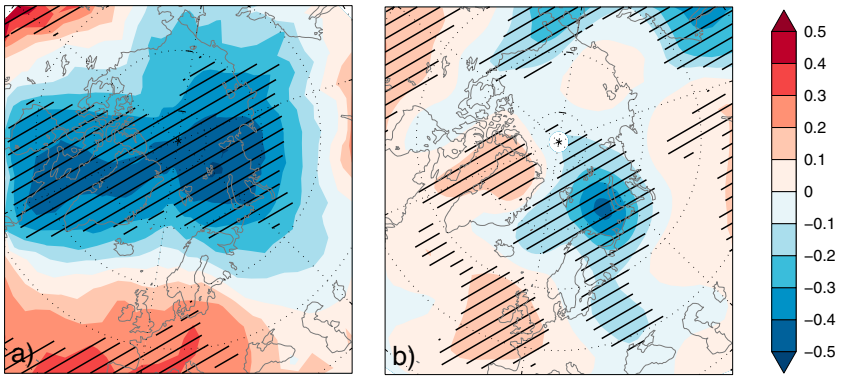


**Figure 9.** Correlation maps of winter (December through February) SLP anomalies and time series of winter Arctic SAT (area-weighted average over 60°N–90°N). (a) Observed SAT values from 1920–1970 (CRUTEM3) [*Brohan et al*., 2006] and SLP data (HadSLP2) [*Allan and Ansell*, 2006]. (b) Simulated SAT and SLP in a 600 year control run with the BCM [*Otterå et al*., 2009]. Hatched areas indicate statistically significant correlations at the 95% confidence level. The observed correlations were calculated using annual data, whereas the simulations have been filtered using a 15 year Butterworth low-pass filter prior to the correlation analysis.

from cement production. This is anthropogenic $CO_2$, and global emissions are now ~9000 megatonne (Mt) C $yr^{-1}$ (1 Mt = $10^{12}$ g) and rising [*Peters et al*., 2012], and ~25% is currently absorbed by the world oceans [*Gruber et al*., 2009]. The uptake of anthropogenic $CO_2$ occurs, in principle, everywhere at the ocean surface, but is strongest in divergence zones [*Tjiputra et al*., 2010].

[49] Anthropogenic carbon is sequestered, or shielded from the atmosphere and ocean surface layer, in a few special places. Estimates of the inventory of anthropogenic $CO_2$ in the ocean converge on very high values in the North Atlantic [*Khatiwala et al*., 2009], the Nordic Seas [*Olsen et al*., 2010], and the Arctic Ocean [*Tanhua et al*., 2009]. This is due to efficient deepwater ventilation, bringing water recently exposed to the atmosphere, with high concentrations of anthropogenic $CO_2$, downward. This process is critical for maintaining the ocean sink for anthropogenic $CO_2$ [*Broecker and Peng*, 1974].

[50] The BS may be regarded as a strong sink of $CO_2$ because the ocean cooling increases the solubility of $CO_2$. There is also extensive primary production, reducing the ocean summer $pCO_2$. Reported flux densities range between 29 and 51 g C $m^{-2}$ $yr^{-1}$ [*Fransson et al*., 2001; *Kaltin et al*., 2002; *Nakaoka et al*., 2006; *Omar et al*., 2007; *Årthun et al*., 2012a]. The spread reflects to some extent not only regional variations in the BS but also uncertainty in methods. These estimates give a total uptake of $CO_2$ from the atmosphere between 44 and 77 Mt C $yr^{-1}$, a modest contribution to the global ocean uptake of 2200 Mt C $yr^{-1}$. However, the flux density is much greater than the global annual average of 4 g C/$m^2$ [*Takahashi et al*., 2009]. The BS contributes significantly to the total uptake of $CO_2$ in the combined Nordic Seas and Arctic Ocean, which is estimated at 110 Mt C $yr^{-1}$ [*Lundberg and Haugan*, 1996].

[51] These reported estimates of carbon uptake from the Barents atmosphere are for the total present uptake, the sum of natural and anthropogenic components. Published estimates of each of these components are lacking, but the BS surface $pCO_2$ increases at a rate which is indistinguishable from the global atmospheric $pCO_2$. This implies that the uptake of anthropogenic $CO_2$ from the air is probably small within the BS and that horizontal transport into the area is a more important source [*Omar et al*., 2003]. *Jeansson et al*. [2011] estimated a net anthropogenic transport across the BSO of 41 Mt C $yr^{-1}$ as part of their Nordic Seas carbon budget. If we assume that all of this remains within the BS and given a BS volume of 227,000 $km^3$ [*Jakobsson*, 2002], this would translate to an annual concentration increase of 15 µmol/kg in the entire BS. This exceeds by far the growth rate estimate of *Omar et al*. [2003], illustrating that there must also be considerable drainage of anthropogenic carbon from the BS.

[52] Transports and fluxes of dissolved inorganic carbon (DIC) into and out of the BS were presented by *Kivimäe et al*. [2010]. Their estimate of net BSO transport into the BS was 2700 ± 700 Mt C $yr^{-1}$ of DIC, much larger than the 1800 Mt C $yr^{-1}$ estimate by *Jeansson et al*. [2011]. The difference is due to *Kivimäe et al*. [2010] using a net volume flux of 3.3 Sv from *Maslowski et al*. [2004], while the best estimate in the period 1998–2008 is close to 2.0 Sv [*Smedsrud et al*., 2011; *Jeansson et al*., 2011]. We have therefore adjusted the *Kivimäe et al*. [2010] transports associated with ocean currents, accordingly, to 60% of their original value (Figures 1 and 10). This adjustment also brings the DIC transport estimate for the BSX closer to the 1260 Mt C $yr^{-1}$ value derived by *Anderson et al*. [1998a] as part of their Arctic Ocean carbon budget. The advective transport of DIC dwarfs the uptake of $CO_2$ from the atmosphere (Figure 10), which is 59 Mt C $yr^{-1}$. For comparison, the BSO inflow transports 27 times more DIC, 1621 Mt C $yr^{-1}$. The mean annual export can be separated into 605 Mt C $yr^{-1}$ leaving with the surface water and 1031 Mt C $yr^{-1}$ leaving with the CDW in the BSX (Figure 10). Of the DIC entering in the BSO, 63% is thus, on average, sequestered into the deep Arctic Ocean. The surface export has smaller contributions from the Kara Gate (151 Mt C $yr^{-1}$) and the northern opening between Svalbard and Franz Josef Land (182 Mt C $yr^{-1}$) (Figure 1) [*Kivimäe et al*., 2010].

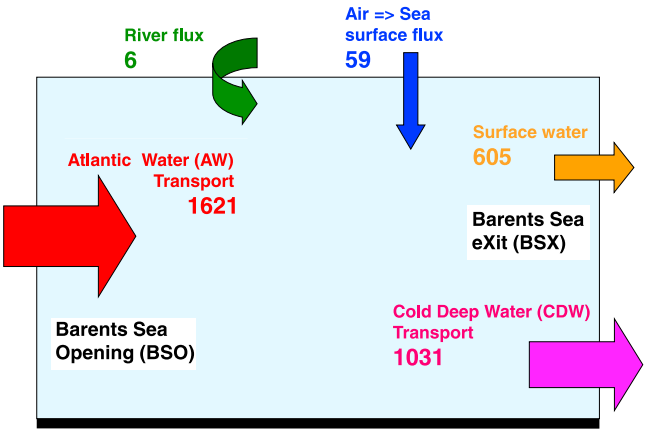


**Figure 10.** Barents Sea climatic mean fluxes of dissolved inorganic carbon (DIC). The values are revised from *Kivimäe et al.* [2010] as described in the text. Values are rounded off to the closest 1 Mt $Cyr^{-1}$ but uncertainties are generally larger. The major carbon export occurs in the BSX between Franz Josef Land and Novaya Zemlya, and smaller contributions occur in the other gates as shown in Figure 1. The total budget here and in Figure 1 is not balanced because organic components, sedimentation, and inventory increase are not included.

[53] The above transport estimates are for the present or last decade and are sums of the natural and anthropogenic components. Based on estimates of the two transport types in the BSX [*Anderson et al.*, 1998a] and the BSO [*Jeansson et al.*, 2011], these can be split into ~97% natural and ~3% anthropogenic. Apart from the trend estimate presented by *Omar et al.*, [2003], knowledge about time changes of the BS carbon budget and its sensitivity to climate change is lacking. Based on empirical relationships between $pCO_2$, temperature, salinity, and phosphate, *Omar et al.* [2007] estimated a year-to-year variability of the BSO ocean-air carbon flux density. Assuming that the data are representative for the full year, the average for the 1990s was 51 g $C/m^2$, and the interannual standard deviation was 3 g $C/m^2$ [*Omar et al.*, 2007]. However, the quality of these empirical relationships remains unknown due to the scarcity of observations.

[54] In summary, we have found that the BS takes up DIC very effectively. The net uptake of atmospheric $CO_2$ of ~60 Mt C $yr^{-1}$ is about 50% of the earlier estimated combined carbon uptake of the Nordic Seas and the Arctic Ocean. A much larger mass of DIC is transported into the BS with the AW, and the major part (>60%) is transformed to dense water in the BS that sequesters the carbon from the ocean surface layer and stores it effectively in the deep Arctic Ocean.

### 2.7. Long-Term Changes of Barents Climate

[55] At time scales from centuries to millennia, the Barents climate has experienced a range of changes beyond those observed in instrumental records. At several occasions, during history, a grounded ice sheet has covered the shallow BS. The latest Barents ice sheet occurred ~20,000 years ago during the last glacial maximum [*Vorren et al.*, 2011]. As this ice sheet disintegrated and interglacial conditions were established, major environmental and climatic changes took place. Through the deglaciation, the southwestern BS switched between severe polar conditions with extensive sea ice cover, periods with open cold surface water, winter sea ice cover, and weak subsurface inflow of AW [*Aagaard-Sørensen et al.*, 2010; *Chistyakova et al.*, 2010].

[56] During the early phase of the present interglacial, 11,000–7500 years ago, warm bottom water occurred in the southwestern BS [*Risebrobakken et al.*, 2010]. During this time, a warm summer mixed layer occurred at the surface, sea ice formed in the winter, and the position of the winter sea ice edge (Polar Front) changed as a circulation pattern like today established [*Risebrobakken et al.*, 2010]. The northern BS deglaciated at about the same time as the southern parts [*Junttila et al.*, 2010], possibly as a response to influence of AW entering through the northern troughs [*Polyak and Solheim*, 1994]. Cold conditions, occasionally interrupted by intrusions of AW, prevailed in the north until 8000–7000 years ago, when marked subsurface warming of about 2°C occurred [*Lubinski et al.*, 2001]. Reduced AW presence and cold rather stable conditions occurred subsurface both in the northeast and southwestern BS from approximately 7000 years ago, while more variable conditions were seen throughout the last millennia [*Duplessy et al.*, 2005; *Risebrobakken et al.*, 2010; *Voronina et al.*, 2001]. Sea ice growth and brine release took place throughout the last 10,000 years in the eastern BS [*Duplessy et al.*, 2005].

[57] In the southwestern BS, the last 2500 years were characterized by episodes with reduced surface and subsurface salinity, warm water at the bottom, and a strongly stratified water column. This corresponds with expansion of the area influenced by coastal water and more sea ice growth [*Risebrobakken et al.*, 2010]. These episodes are interpreted as cold due to weaker southwesterlies, consistent with the effect of a weak NAO [*Blindheim et al.*, 2000] (section 2.5). The amplitude of natural changes at centennial scale is larger than the scale of variability observed through the last decades [*Risebrobakken et al.*, 2010].

[58] Sea ice extent reconstructed for the last ~300 years show ice-free conditions in the southwestern BS, at least during spring [*Vare et al.*, 2010]. They also show consistent sea ice occurrence in the northern region, with a reduced occurrence in the recent decades, and fluctuating sea ice variability. Episodic expansions of the sea ice cover, corresponding to colder periods, are also seen in the eastern BS [*Voronina et al.*, 2001]. In the northern part of the BSO, close to Bear Island, gradual warming of the bottom water characterized the last 1400 years, interrupted by slight cooling during the Little Ice Age [*Wilson et al.*, 2011].

[59] Reconstructed temperatures from the southwestern BS correspond well with pollen-based temperatures from northern Norway [*Chistyakova et al.*, 2010]. Similarly, temperature variability in the eastern BS compares with reconstructed temperatures from Russia [*Voronina et al.*, 2001]. *Sjögren* [2009b] found significant changes in the strength of southwesterlies through the past 3000 years, based on accumulation of aeolien sediment in the BSO. A common cause, or a causal link, between the wind pattern and oceanographic changes

was suggested by *Sjögren* [2009b]. Reconstructed temperatures based on historical observations from terrestrial sites surrounding the BS show increasing temperatures from 1450 to 2000 A.D., with substantial decadal scale variability superimposed on the increasing long-term trend [*Klimenko*, 2008].

[60] BS ocean temperature, sea ice conditions, and influence on atmospheric circulation have occurred beyond the BS and, in particular, for the Arctic Ocean, in the instrumental record (sections 2.1–2.5). This influence would also have occurred over longer time scales, but the responses have likely differed depending on the time scale. During times when the BS was covered by a grounded ice sheet, no AW could enter in the BSO, and the air-ice-ocean coupling must have been fundamentally different. In these glacial times, all the northward flowing AW would have entered the Arctic Ocean through the Fram Strait.

### 2.8. Modeling of the Barents Sea

[61] Simulating circulation and air-ice-ocean processes in the BS region is a challenging problem. The challenges are, in part, related to the dynamic behavior of the sea ice margin, a feature that is sensitive to small long-term residuals of large short-term fluctuations in horizontal heat transport. Phenomena that are important for the sea ice margin—ocean mesoscale eddies, coastal currents, polar lows, and self-organized convection—have small horizontal scales that are unresolved in state-of-the-art global climate models. Studies comparing model simulations [*Chapman and Walsh*, 2007] and observational (including reanalysis) data sets [*Alexeev et al*., 2012] clearly indicate enhanced scatter in the Arctic region. More than half the global models overestimated the sea ice in the southern BS, and models that performed well for present-day sea ice did not necessarily simulate a realistic poleward heat transport [*Arzel et al*., 2006]. We shortly summarize recent model studies which have produced results of direct relevance to the BS circulation and AW transport. Global simulations of the Nordic Seas and the Arctic Ocean are not included.

[62] *Hibler and Bryan* [1987] were among the first to couple a 3-D ocean model to a dynamic-thermodynamic ice model for the Arctic Ocean. They showed that the ocean model was essential for providing the heat required to prevent unrealistically large ice cover in the western BS. Using a wind-driven barotropic model, *Ådlandsvik and Loeng* [1991] found very low mean BS throughflow (0.06 Sv), indicating that the local wind forcing may influence variability on daily to interannual time scales, but is not a significant driver of mean throughflow on decadal or centennial time scales. *Harms* [1992] reached similar conclusions.

[63] *Gerdes and Schauer* [1997] used a numerical model covering the Atlantic from 20°S and the entire Arctic Ocean, focusing on transport of AW across the BS and its influence on Arctic conditions. The net heat transport into the BS was 74 TW in the standard case associated with a 3.2 Sv throughflow and varied between 66 and 79 TW in different case experiments. The simulated flow through the BS captured such properties as sinking out of the St. Anna Trough, displacement of the Fram Strait branch from the shelf slope there, and affecting the intermediate water of the Eurasian Basin in agreement with observations. The model had high vertical resolution (60 levels), and a version with 19 levels generated a weaker throughflow (1.4 Sv) and less heat divergence (38 TW). In later years, a wide range of model studies have been performed with focus on the BS, and new advances in supercomputer modeling have made it possible to move toward an eddy-resolving regime even for regional applications.

[64] Several models suggest strong year-to-year variability [*Zhang and Zhang*, 2001; *Harms et al*., 2005; *Budgell*, 2005; *Maslowski et al*., 2004]. *Harms et al*. [2005] found this variability to be highly dependent on the BSO inflow, which had the strongest effect. The ocean-atmosphere heat flux proved to be the most sensitive parameter for ocean and air anomalies, while the ice extent and the corresponding salt input were more invariant to different boundary conditions. Year-to-year variability in hydrographic sections and sea ice cover has been successfully reproduced [*Budgell*, 2005], but the high-resolution regional models are still dependent on correct boundary conditions. Too much AW transport leads to less sea ice and overly warm temperatures in the central BS [*Budgell*, 2005]. *Årthun and Schrum* [2010] suggested a long-term increase in the AW transport since 1950, and *Sandø et al*. [2010] studied shorter-term lead and lag correlations and found that heat transport leads the heat content, which, in turn, leads the heat fluxes to the atmosphere. A further step was taken in *Årthun et al*. [2011], who combined observations and model results to study locations of dense water formation in the BS and how these formation locations relate to the BSO inflow variability.

[65] The spatial scales of dynamical processes in the atmosphere are usually much larger than those in the ocean. However, the BS region is rather unique in this sense. Vigorous air-ice-ocean interactions create large fluxes of heat and moisture driving not only convective turbulence but also mesoscale cyclones known as polar lows, whose development is critically controlled by latent heat release [*Bracegirdle and Gray*, 2008]. Mesoscale dynamics are not parameterized in global models but are very important in the BS region, meaning that proper simulations of its climate require regional meteorological model resolutions of 20 km or less [*Grønås and Kvamstø*, 1995; *Brümmer and Pohlmann*, 2000; *Skeie and Grønås*, 2000; *Sandvik and Furevik*, 2002].

[66] *Keup-Thiel et al*. [2006] simulated the Barents region from 1961 to 2100 with a regional atmospheric model with a horizontal resolution of 55 km. Inconsistency of the gridded observations in the region [*Alexeev et al*., 2012] resulted in ambiguous evaluation of the simulated climatology with large differences between simulations and observations. As expected, the strongest warming for 2100 was found along the sea ice edge, but surprisingly, this warming did not lead to a considerable sea ice retreat. The simulated long-term variability and trends were not consistent with the observations. A detailed study of the influence of fractured sea ice cover on the atmosphere found that the Barents atmosphere has almost no sensitivity

to variations in summer sea ice concentration (May through October), but the wintertime sensitivity is large [*Rinke et al*., 2006].

[67] *Koenigk et al*. [2011] conducted future Arctic scenario experiments with a coupled regional climate model. A remarkable feature of the simulation was the large variability of sea ice extent and sea ice trends. They found several periods with sea ice loss and partial recovery in the following years, but this was sensitive to the details of the model forcing and parameterization. A specific model setup can strongly modulate the BS ice variability as it seems dependent on the configuration of the narrow passages in relation to climatological wind directions [*Dethloff et al*., 2001; *Kwok et al*., 2005]. Regional air-ice-ocean models are important tools for studying the Barents climate as they attempt to resolve the important mesoscale dynamics in the region. To date, the present-day standard resolution (~50 km) and the methodologies used to force the simulations are probably not adequate for representing the physical processes in the region. Many models simulate too little sea ice and therefore greatly reduced climate variability.

## 3. SYNTHESIS OF NEW RESULTS

[68] Some of the key observational records reviewed in section 2 are too short to consider variability on decadal time scales [*Skagseth et al*., 2008]. We also found that most model studies focusing on the BS used regional models and, thus, cannot properly address the fully coupled air-ice-ocean system. The longer time series that do exist are based on reanalysis, and we found significant differences between these products as described below. In order to advance, we use a 600 year simulation of the Bergen Climate Model (BCM) [*Otterå et al*., 2009] and a number of reanalysis and satellite-based data sets (Table 1). The BCM is a global, fully coupled air-ice-ocean model that simulates variability on interannual and decadal time scales in the Atlantic and Arctic Oceans quite realistically compared to observations and reanalysis [*Otterå et al*., 2009; *Medhaug et al*., 2011; *Langehaug et al*., 2012]. A coarse scale global model is unable to resolve processes that shape specific features of the regional climate, but does resolve decadal time scale variability and teleconnections that are more important for the regional climate at these larger time scales. Consistently, we use the BCM to study regional-scale dependencies on longer time scales. The ocean component of the BCM uses density as the vertical coordinate and has a grid size of ~90 km in the Barents area. The atmosphere component is a low-top spectral atmospheric model with a spatial resolution of ~300 km (2.8°). The results presented are mostly based on a preindustrial control run, where the external forcing from, e.g., solar insolation and greenhouse gases, is set at constant preindustrial values [*Otterå et al*., 2009]. The only variability is, thus, the model's internal climate variability.

[69] Our aim is to understand what drives the warm and cold periods in the BS and if feedback loops are important in maintaining such periods. The atmosphere has large natural variability, so heat flux anomalies of ±20 TW and the resulting effects on atmospheric circulation could be difficult to discern. Similarly, ±20 TW heat transport anomalies carried by the inflowing AW could be smaller than other perturbations. We thus need a large number of occurrences to draw any conclusions on the importance of the feedbacks. There may also be some kind of an upper limit for how much extra heat the BS atmosphere can handle, possibly influencing the feedbacks. If such a limit exists, what is the threshold? Has it been reached in the past? Is this threshold the brake for the positive feedback loops, bringing an end to events such as the Early Warming?

[70] The inflow of AW to the BS accounts for about half of the northward heat transport to the Arctic Ocean and the BS combined. The other main share is through the Fram Strait, contributing about 30% [*Tsubouchi et al*., 2012]. However, the fate of the ocean heat carried by the two branches is substantially different. The Fram Strait branch meets the Arctic sea ice north of Svalbard. The upper AW layer melts some ice in this localized region [*Rudels et al*., 1996], but the deeper AW layer continues around the Arctic Ocean and releases heat gradually over a much larger region. The BS branch releases ~70 TW of heat to the atmosphere in the BS [*Smedsrud et al*., 2010], resulting in a decrease in water temperature from ~6°C in the BSO [*Årthun and Schrum*, 2010] to ~0°C in the BSX [*Gammelsrød et al*., 2009].

[71] Given that the ocean and air are necessarily coupled at the surface, our new results start at this interface with the sea ice cover (section 3.1) and ocean-air heat fluxes (section 3.2), variables that are closely related. These sections compare satellite-based products, reanalyses, and BCM simulations; evaluate the uncertainties; and present the climatology, variability, and trends in ice cover and heat fluxes. Next, we return to the ocean-air heat exchange relationships (section 3.3). Earlier studies have shown that these relationships are of great importance in the BS, and we also evaluate the importance on the Arctic climate system. The hypothesized feedback loops presented in Figure 3 are evaluated in section 3.4 before we look at recent changes in atmospheric circulation and heat transport (section 3.5) and present new results on the relative roles of the ocean and the atmosphere as drivers of the sea ice variability (section 3.6). The heat loss from the ocean to the atmosphere leads to dense water production and export of carbon to the Arctic Ocean, and these processes are presented in section 3.7. The relatively recent air-ice-ocean variability is contrasted with variability over the last 2500 years in section 3.8. We finish by presenting a possible future BS scenario from dedicated dynamical downscaling of 21st century climate model projections (section 3.9).

### 3.1. Sea Ice Cover

[72] The BS may be classified in two regions: a permanently open water area in the southwest and a region with a gradually increasing sea ice cover moving toward the BSX (Figure 11). Important features of the BS ice are large portions of open water within the ice pack and a generally thin cover because it is mostly seasonal ice. The thin, patchy ice cover results in uncertainties and cross–data set differences in the sea ice

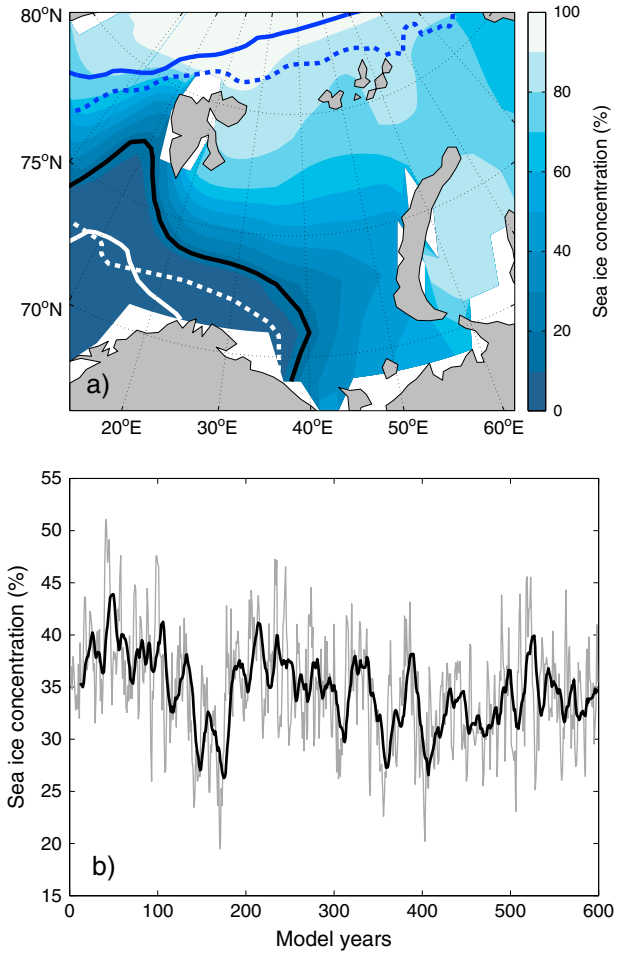


**Figure 11.** Barents Sea ice concentration in the Bergen Climate Model control simulation. (a) Annual average over 600 years and the climatic mean sea ice extent taken as the 15% (black solid line) sea ice concentration line. White solid line is the maximum monthly extent (April, year 41), and the blue solid line is the minimum monthly extent (October, year 168). Historical winter maximum ice extent from April 1866 is shown as the white dashed line [*Vinje*, 2001; *Macias Fauria et al.*, 2010] and the summer minimum for September 2007 as the blue dashed line (NSIDC data). (b) Spatial average over 67°N–81°N, 21°–55°E, black line is 11 year running mean.

determination, which, in turn, lead to related uncertainties in the surface heat budgets (Table 2). The uncertainties among the reanalysis and satellite data products are clearly evident in the time series of the annual mean sea ice cover anomalies for 1960–2010 (Figure 12a). While all series agree on the decline in the BS ice cover, they all differ in both trends and annual averages. The annual satellite-based trend is −3.7%/decade, while the reanalysis data sets show smaller trends (maximum loss of −2.5%/decade and minimum loss of −0.89%/decade) (Figure 12a). Focusing on the long-time variability of the BCM (Figure 11), the annual mean ice extent (here taken as the15% sea ice concentration) resembles the observations from the 1980s. Also, the mean seasonal variation (not shown) is close to the observed. Since the 1980s, the satellite observations have shown an ice cover mostly smaller than the simulations (Figures 13a and 13b). This is expected because the BCM simulations use preindustrial values of natural (solar and volcanic) and anthropogenic (tropospheric aerosols, greenhouse gases) forcing.

[73] Despite the generally larger BCM-simulated ice cover, the maximum and the minimum span both the 1866 maximum and the recent minimum in the observations (Figure 11). This indicates that even though the recent decades have seen little ice cover, we are still above the minimum levels of the long-term variability. The decadal-scale fluctuations (Figure 11b) indicate multiannual excursions of order 10% lower or higher than the mean BS ice concentration of 35%. However, the recent ice retreat seems now to have lasted longer than earlier events, and the present-day ice cover is at consistently lower concentrations than the range spanned by the BCM simulation (Figures 13a and 13b).

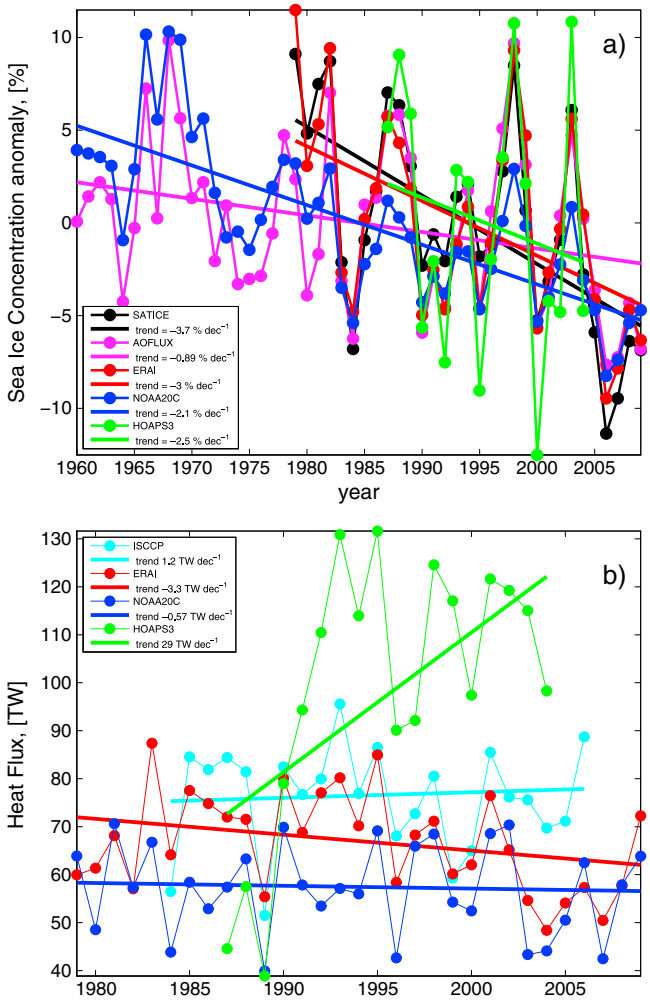


**Figure 12.** Annual sea ice cover anomalies and heat loss from the reanalysis and satellite data products (Tables 1 and 2). Winter-centered values are used. (a) The sea ice-covered area is the sum of areas with >80% sea ice concentration. (b) The heat loss, or total upward heat flux, is the turbulent and radiative fluxes combined for areas of the Barents Sea were data is available. The area averaged values are then multiplied with the same Barents Sea area of 1.36 $10^{12}$ $m^2$.

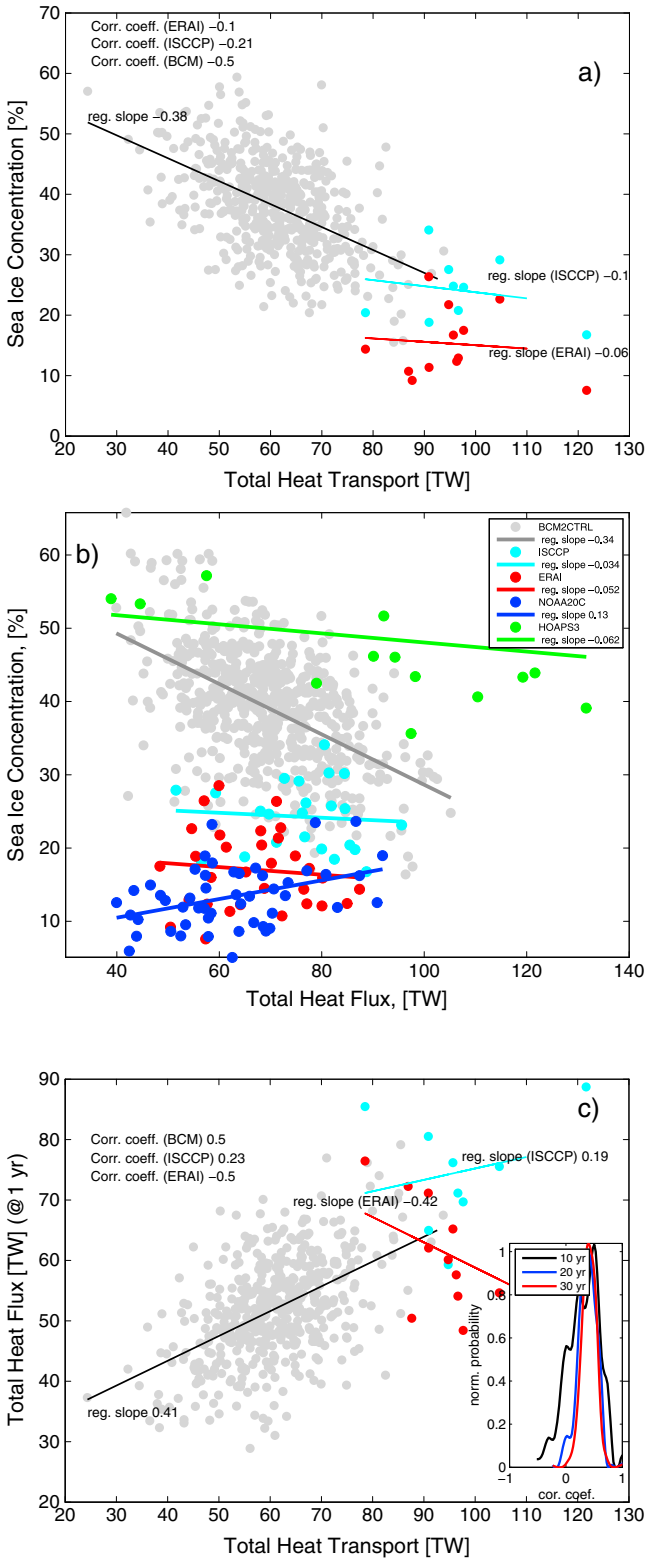


**Figure 13.**

### 3.2. Surface Heat Fluxes

[74] The data scatter among the different reanalysis and satellite data products (Table 1) is large. Uncertainties in the sea ice cover alone, as discussed above, result in estimated errors comparable to the interannual variability [*Bourassa et al.*, 2013]. Also, during the last decades of instrumental observations, estimates of surface fluxes show large scatter. This is related to differences in estimated basic meteorological parameters (temperature, wind speed, and cloudiness), as well as to differences in the algorithms used to calculate fluxes from those parameters. Moreover, the algorithmic difficulties are of two types: (1) It is difficult to estimate the role of cloudiness and the ubiquitous temperature inversions on the long-wave radiation balance. Those quantities are poorly known from observations and poorly reproduced in reanalysis products. (2) It is equally difficult to account for the near-surface static stability in the atmosphere and therefore to obtain a correct turbulent exchange coefficient. The applied bulk turbulent exchange algorithms [*Fairall et al.*, 2003] were fitted to the Pacific tropical areas where the stability is nearly neutral. With reservations for those problems, we mostly use the ISCCP data, a part of the Objectively Analyzed air-sea Fluxes (OAFLUX) data, (Table 1) as reference to discuss the BS surface heat budget climatology (Table 2).

[75] Summarized over the BS area, the climatological mean heat loss from all available data sets becomes 76 ± 15 TW (Figure 1) or a heat flux of 56 ± 11 W $m^{-2}$. The uncertainty is based on the different values from Table 2. The yearly cycle is pronounced with a net heat gain during summer of ~150 W $m^{-2}$ and a loss of ~200 W $m^{-2}$ during winter (Figure 7). During winter, the upward heat flux is reduced in partially ice covered areas but remains ~100 W $m^{-2}$ for horizontally averaged values, presumably due to the presence of open water within the fractured sea ice cover (Figure 7b).

[76] The wintertime fluxes in the BS are higher than those found elsewhere in the Arctic, consistent with more thin and fractured sea ice in the BS. The dominant and most variable component of the budget in wintertime is the sensible heat flux (Figure 7a). It is followed by the turbulent latent heat flux and the surface long-wave radiation balance. This ranking is preserved in all the data products. As the open water temperature of the BS changes just by a few degrees and

**Figure 13.** Winter-centered annual averages of key variables for the Barents Sea area. Gray dots are simulations from the Bergen Climate Model, the other data sets are described in Table 1 (red—ERAI reanalysis; cyan—ISCCP satellite data product; blue—NOAA20C; green—HOAPS3). The lines show the best fit linear regressions to the different data sets. (a) Barents Sea ice cover as a function of ocean heat transport. Observations of temperature and currents in the Barents Sea Opening are used here and in (c) for ISCCP and ERAI to achieve values for total heat transport. (b) Barents Sea ice cover as a function of total surface heat loss. The surface heat flux is the sum of the radiative and turbulent fluxes, and positive values mean ocean heat loss. (c) Total surface heat loss as a function of ocean heat transport. The surface heat loss is lagged by 1 year (suggested by lag-correlation analysis). The inserted plot shows the probability (normalized by its maximum value) to find a given correlation coefficient between the ocean transport and the surface flux in the BCM data broken into 10, 20, and 30 year intervals. The probability to find small and negative correlations increases significantly for shorter intervals.

**TABLE 3. Cross–Data Set Correlations for the Barents Total, Radiative and Turbulent Heat Fluxes[a]**

| | Total Heat Flux | | | Turbulent Heat Flux | | | Radiation Heat Flux | | |
|---|---|---|---|---|---|---|---|---|---|
| | HOAPS3 | ERAI | NOAA20C | HOAPS3 | ERAI | NOAA20C | HOAPS3 | ERAI | NOAA20C |
| ISCCP | 0.53 | 0.7 | 0.62 | 0.67 | 0.8 | 0.64 | 0.2 | 0.1 | 0.1 |
| HOAPS3 | | 0.37 | 0.39 | | 0.47 | 0.49 | | 0.1 | 0.2 |
| ERAI | | | 0.63 | | | 0.54 | | | 0.9 |

[a]Values are calculated using annual averages.

cloudiness variations are poorly resolved in the data sets, the long-wave radiation budget remains an almost constant 40 W m$^{-2}$ across the year (Figure 7a). As the air temperature rises, the lower atmosphere becomes statically stable with the sea surface temperature lower than the air temperature near the surface. This inhibits the turbulence exchange from May through September. The result is that the BS has uniform upward surface heat fluxes independent of the surface type during summer, while the fluxes show strong dependence on the ice fraction during winter (Figure 7b). At present, it is difficult to evaluate the reliability of the components for the available data sets as observations are very limited, especially in wintertime [*Bourassa et al*., 2013].

[77] The BS thus has a climatological heat gain through the radiation balance (26 W m$^{-2}$), and the bulk share of this gain is in the southern part of the sea (Table 2). The strong loss of heat is achieved through turbulent vertical mixing due to development of intense convection above open water in cold air outbreaks. The turbulent heat loss of 81 W m$^{-2}$ is almost entirely achieved in the winter months of September through May.

[78] The interannual variations of the surface heat flux may reach about 30 TW, or ~50% of the mean (Figure 12b). This is true for all the considered data sets in Table 1, but the differences between data sets are even larger. The smallest heat loss occurs in the ISCCP data, and the largest occurs in ERAI data (Figure 12b and Table 2). The data sets share largely the same sea ice, temperature, and wind observations, but the correlations among many of them are surprisingly low (0.2–0.6) (Table 3).

[79] The trends in the heat loss since 1979 are also different (Figure 12b). The ISCCP and NOAA20C data sets demonstrate clear positive trends in the heat loss that could be explained by the observed BS ice reduction (Figure 12a). They show that the sea ice retreat is faster than the heating of the atmosphere. ERAI, on the other hand, shows a significant negative trend. HOAPS data generally show too high ice concentrations (Figure 13b), and the large increase in heat loss over time (Figure 12b) does therefore seem to be less consistent than the other data sets. All data sets show positive heat loss trends if only the open water area is considered (not shown), indicating that they agree in the warming of the southern ice-free region of the BS and a larger heat loss from this area.

### 3.3. Air-Ice-Ocean Heat Exchange

[80] A series of cause and effects in the coupled Barents air-ice-ocean heat exchange is evaluated using the data sets presented in sections 3.1 and 3.2. These also form the common axis of the proposed feedback loops. In addition, the relationships between the BS heat exchange and the large-scale Arctic climate are evaluated.

[81] Starting with the link between ocean and ice (Figures 3a and 3b), the BCM simulations reveal a stable relationship throughout most of the 600 years between AW inflow and BS ice variability. The relationship is shown in Figure 13a, partly supported by the reanalysis data, and as a running correlation from the BCM simulation in Figure 14a. Because a stronger inflow leads to less ice, the correlation is negative. Sea ice cover limits the heat loss to the BS atmosphere as discussed above, so years with a larger sea ice cover have lower annual heat loss, as shown in Figure 13b. The BCM and ISCCP data agree on this negative relationship. Similar dependence (with a logarithmic correlation coefficient of 0.7) was obtained by *Ivanov et al*. [2003] from direct field measurements in the central BS marginal ice zone. These negative correlation relationships suggest that oceanic variability is an important driver of sea ice variability, with high ocean heat transport leading to smaller sea ice cover and large total heat fluxes from the ocean to the atmosphere. While these relationships and, hence, the common axis of the two feedback loops (Figure 3) are supported by the ISCCP data and BCM simulation, the ERAI and NOAA20C data sets show unclear opposite relationships (weakly negative or neutral to positive slopes). These differences based on the total heat flux remain the same when only turbulent heat loss is used (not shown). A positive correlation between sea ice and surface heat fluxes would suggest that the atmosphere drives sea ice changes. The fundamentally different behavior between the data sets may be linked to the different treatments of heat fluxes over sea ice. The NOAA20C data show, for example, lower fluxes over open water than the other data sets (not shown).

[82] The lead-lag coupling between heat transport and surface heat fluxes (Figure 13c) shows consistently increased heat fluxes the year after a heat transport increase ($r \sim 0.5$). Thus, a higher heat transport prevents formation of sea ice and thereby increases the open water area (Figures 3a and 13a). Cooling of the ocean therefore occurs over an increased area, and the overall heat loss increases (Figures 3b and 3c and 13b and 13c). Further details of Figure 13c, including a possible threshold for the surface fluxes that might limit the cooling of the BS, are explored in section 3.6.

[83] To further evaluate the importance of the atmospheric forcing and the ocean forcing in the Barents air-ice-ocean system, we have calculated the lead-lag relationships between the surface heat flux (atmospheric forcing) and the ocean heat transport (ocean forcing) from the BCM

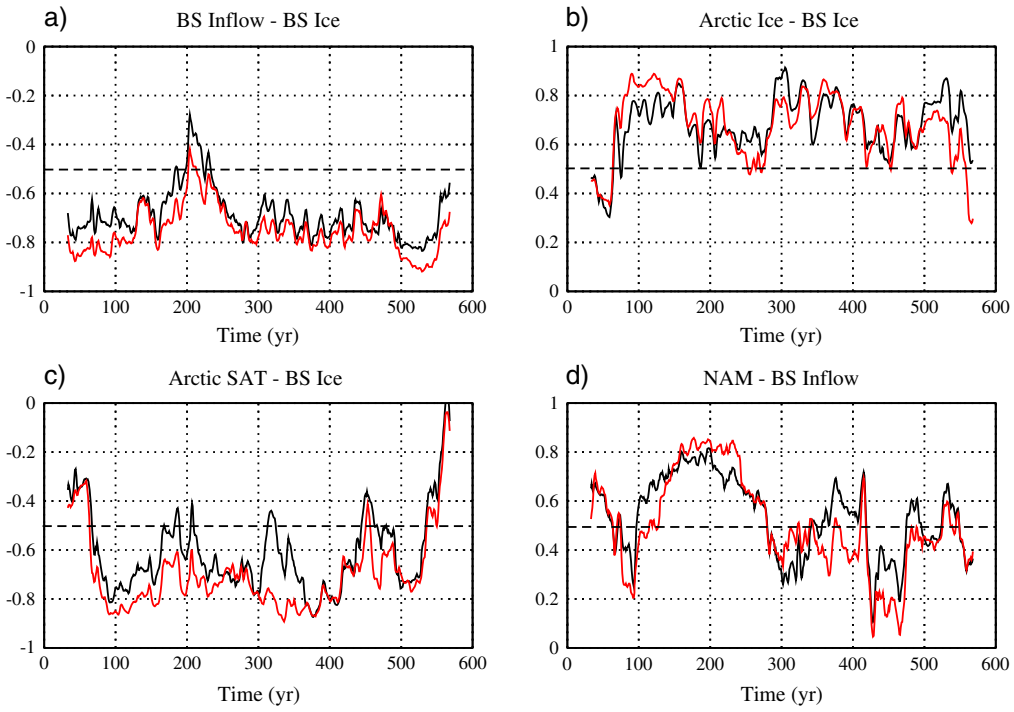


**Figure 14.** Correlation time series from the Bergen Climate Model 600 year control run. Annual averages are red and winter (December – February) averages are black. (a) Barents Sea inflow and Barents Sea ice. (b) Arctic sea ice and Barents Sea ice. (c) Arctic surface air temperature (mean for 60°N–90°N) and Barents Sea ice. (d) Northern Annular Mode index and Barents Sea inflow. Data have been smoothed using a 5 year low-pass filter, and correlations were calculated using a 60 year window. Dashed lines show the 95% confidence levels calculated using a double-sided *t* test. The first and last 30 years are missing due to the 60 year window.

simulations on different time scales. Although the ocean heat transport leads the heat fluxes by 1 year for the annual means, the results are opposite for the monthly data; the ocean lags the atmosphere by about 2–3 months (not shown). This is consistent with the short-term lead and lag analysis in *Fang and Wallace* [1994], who found that the atmosphere leads by about 2 weeks. The short-term variability within one winter is thus governed by the atmosphere. There are indications that the heat flux is also variable on multidecadal scales [*Bjerknes*, 1964; *Polyakov et al*., 2003; *van der Swaluw et al*., 2007; *Jungclaus and Koenigk*, 2010]. Some model simulations show anticorrelation between the meridional atmospheric heat transport and the corresponding horizontal heat transport in the ocean.

### 3.3.1. Heat Exchange and the Arctic Climate

[84] In the analysis presented here, we used detrended winter-centered yearly averages from the BCM control simulation. Time series of various key parameters are then smoothed using a 5 year low-pass filter and correlated using a 60 year moving window. The 5 year smoothing is done to focus on decadal to multidecadal scale variability, while the choice of a 60 year window is motivated by the length of observational records and commonly used reanalysis data (Table 1). Because relationships obtained from analysis of observations may change over time, climate simulations give a possibility to evaluate to what extent these relationships vary over longer time periods. Analyzing correlations in a moving window with a length approximately corresponding to available data coverage is therefore useful.

[85] To evaluate the effects of the BS air-ice-ocean heat exchange variability on the Arctic as a whole, we first note that the BS ice variability correlates well with the sea ice variability over the entire Arctic in the BCM (Figure 14b). This indicates common driving processes for the simulated Arctic and BS ice covers. Also evident in the BCM simulations is a robust connection between the Arctic SAT and Arctic sea ice variations, particularly on a decadal time scale ($r = -0.86$, not shown). This is perhaps self-evident, but that these two vary together does not indicate whether the sea ice controls the SAT or vice versa. Not surprisingly, the BS ice and the Arctic SAT are also correlated at almost as high a value ($r = -0.65$) (Figure 14c). This is explained by the similar high correlation between sea ice in the BS and the Arctic Ocean (Figure 14b). The results thus suggest a link between the BS ice and the Arctic SAT (Figure 14c) and that the simulated BS ice variability is responsible for a large part of the Arctic sea ice variations (Figure 14b).

[86] We know already that the AW inflow drives variations in the BS ice cover (Figure 14a), and correlations between the BS inflow and the Arctic SAT vary between 0.6 and 0 over the BCM simulation (not shown). Given the above correlations, there is a plausible link between the BS inflow and the Arctic SAT as well, although the relationship is not stable over time. This means that

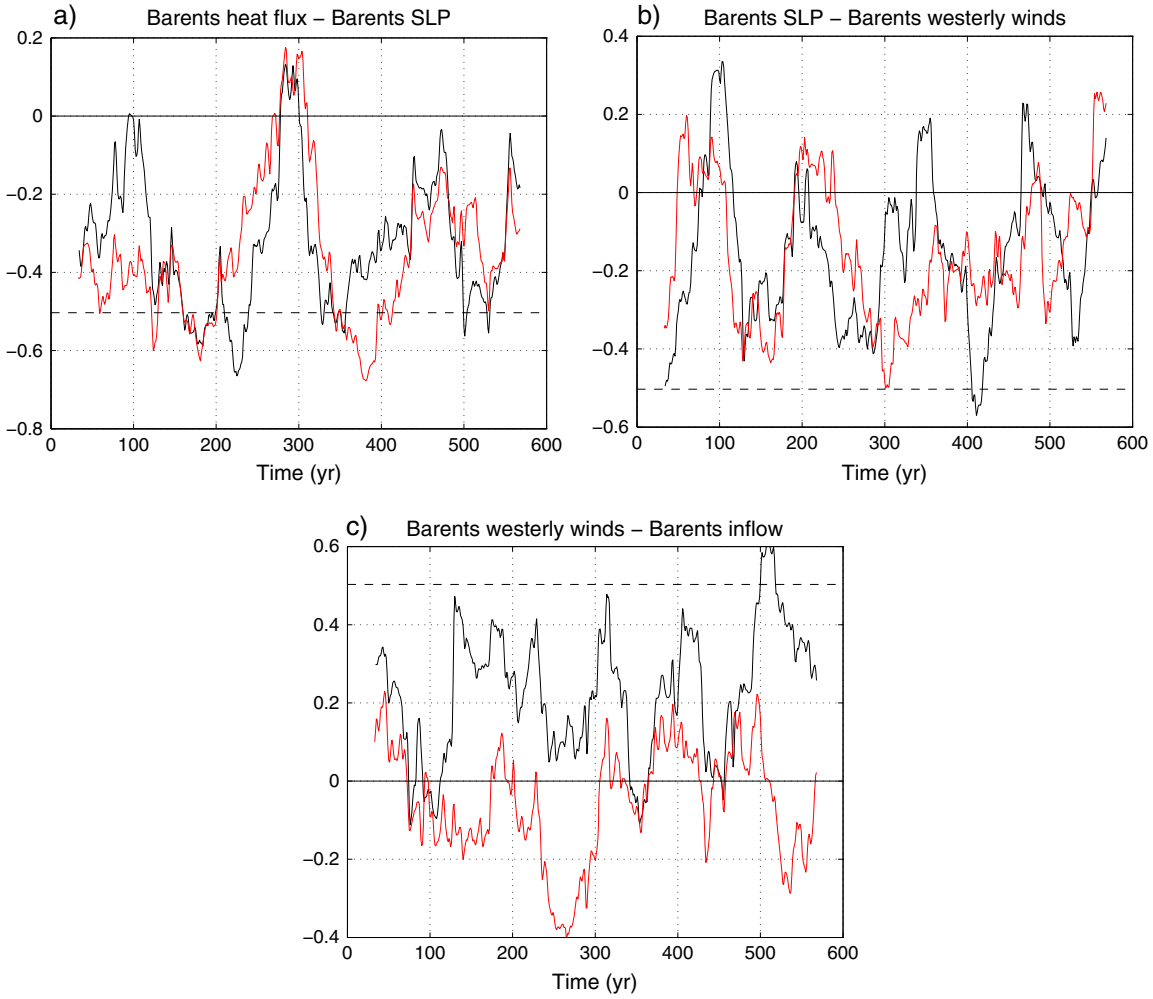


**Figure 15.** Correlation time series from the Bergen Climate Model 600 year control run. Annual averages are red and winter (December – February) averages are black. (a) Total Barents heat flux correlated with sea level pressure over the Barents Sea. (b) Sea level pressure correlated with westerly winds in the Barents Opening. (c) Westerly winds correlated with Atlantic Water inflow in the Barents Opening. Data have been smoothed using a 5 year low-pass filter, and correlations were calculated using a 60 year window. Dashed lines show the 95% confidence levels calculated using a double-sided *t* test. The first and last 30 years are missing due to the 60 year window.

processes other than those driving the BS inflow also contribute to the Arctic SAT as expected.

[87] The results of this section reveal a series of cause and effects in the BS air-ice-ocean system. This series of events is evident in the global-coupled BCM, earlier regional modeling studies as well as in observations, and forms strong support for the existence of the common axis of the two feedback loops. In the next section, the rest of the two feedback loops in Figure 3 are evaluated.

## 3.4. The Feedback Loops

[88] As in the former section, the analysis presented here is performed on detrended yearly averages from the BCM control simulation. Time series of various key parameters are smoothed using a 5 year low-pass filter and correlated using a 60 year moving window. The analyses for the BCM are presented in Figure 15 for links on the air side of Figure 3 and in Figure 16 for links on the ocean side.

### 3.4.1. The Wind Feedback

[89] The wind feedback loop requires changes in atmospheric circulation over the BS. The atmospheric circulation may not only respond to surface temperature and sea ice variability (Figures 3c–3e) but can also cause the ocean and sea ice cover to change (Figures 3e, 3a, and 3b). Observed decadal variations in regional climate and oceanic inflow into the BS have been suggested as evidence for the operation of the wind feedback in the real world [*Ådlandsvik and Loeng*, 1991]. However, the observational record is too short to assess the stationarity of the hypothesized relationships, particularly on multidecadal time scales [*Bengtsson et al.*, 2004], and different processes within the coupled air-ice-ocean system may dominate during different periods.

[90] Strong internal atmospheric variability further complicates the picture, making it difficult to unambiguously identify the wind feedback in available observational data. For example, internal variability patterns such as the Northern Annular Mode (NAM) or the North Atlantic oscillation (NAO) may

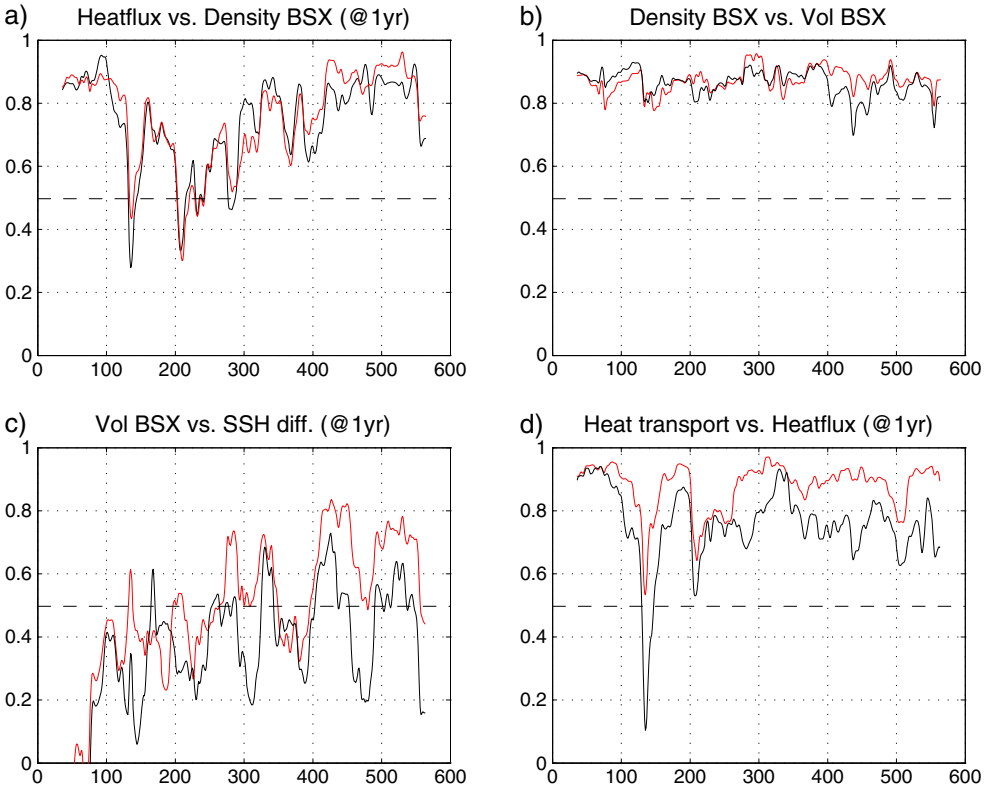


**Figure 16.** Correlation time series from the Bergen Climate Model 600 year control run. Annual averages are red and winter (December – February) averages are black. (a) Total ocean-air heat flux from the BS and average density in the BSX at 1 year time-lag. (b) Average BSX density and net volume BSX transport. (c) Net BSX volume transport and the difference in sea surface height between the BSX and the BSO at 1 year time lag. (d) Net heat transport into the Barents Sea (through all openings) and total ocean-air heat flux at a 1 year time lag. Data have been smoothed using a 5 year low-pass filter, and correlations were calculated using a 60 year window. Dashed lines show the 95% confidence levels calculated using a double-sided *t* test. BSO area used is 71°N–75°N, 19°E–23°E and, for the BSX, 77°N–79°N, 49°E–59°E. Thirty years are missing at the end and beginning due to the 60 year window.

influence AW heat transport through wind changes (Figure 3a) or atmospheric heat fluxes through anomalous warm/cold advection over the BS (Figure 3c). The relationship between internal variability patterns and the Barents climate is complicated though, as evidenced by the highly variable running correlations between the NAM and the BS inflow (Figure 14d) or the BS ice cover (not shown) throughout the simulation. This result is consistent with other coupled models that exhibit similar nonstationarity [*Goosse and Holland*, 2005; *Semenov*, 2008] and further suggests that empirical links between atmospheric variability patterns and Arctic climate established for the recent period should be treated with caution when considering past and future climate changes.

[91] A link between the observed long-term Arctic SAT and SLP variations for the winter period highlights the BS region as a hot spot (Figure 9a). The strongest negative correlations are found in the BS when using the period 1920–1970, following *Bengtsson et al*. [2004], and remain in the eastern Arctic for other periods (not shown). A similar link was also found in the control simulation of the BCM (Figure 9b). The significant negative correlations centered over the BS indicate a relationship between the Arctic SAT warming and the BS ice retreat, most likely through atmospheric circulation changes, although, again, the relationship appears to be highly variable through time (Figure 14c). In the BCM, the reduced BS ice is primarily driven by an increased inflow of AW as discussed earlier (Figure 14a), resulting in larger total heat fluxes from the ocean to the atmosphere.

[92] According to the hypothesized wind feedback, larger surface heat fluxes should lead to a local reduction in surface pressure (Figure 3d) and stronger westerly winds in the BSO (Figure 3e). These relationships are not particularly strong in the BCM. Heat flux and SLP are generally negatively correlated (Figure 15a), while the SLP and westerly winds show mostly insignificant correlations of both positive and negative signs (Figure 15b). This suggests that local circulation changes in the BS are related to large-scale atmospheric circulation variability more so than to the local perturbations in heat flux. Interestingly, stronger westerlies in the BSO are somewhat coincident with stronger BS inflow during winter (Figure 15c), providing some support for the last step of the wind feedback (Figures 3e and 3a), though the annual relationship fluctuates around zero. The wind-inflow correlation in winter is also consistent with recent observations [*Ingvaldsen et al*., 2004] and results from earlier coupled and regional modeling studies [*Bengtsson et al*., 2004; *Loeng et al*., 1997].

[93] In summary, our analyses reveal weak but significant correlations between heat flux and SLP on shorter (e.g. 10 to 50 year) time scales, as well as consistently positive correlations between westerly winds and Barents inflow during winter (Figure 15c). Although the strength of these relationships varies through the simulation period, they suggest that the wind feedback (Figures 3e and 3a) might be in operation at times, though not likely dominant. Whether the wind anomalies are linked to the BS ice loss is more of an open question. An additional consideration for future work is that relationships between SLP, heat flux, and westerly winds in the BS region are likely sensitive to the averaging area and externally (to the BS) forced variations in sea ice extent and atmospheric circulation (section 3.6).

#### 3.4.2. The Ocean Feedback

[94] The possible existence of an ocean feedback loop, as briefly described in section 1, is evaluated here. The main idea is that dense water formation and overflow into the Arctic Ocean will cause AW to enter in the BSO (Figures 3f, 3g, and 3a). Such a relationship was first proposed by *Midttun* [1985], but a feedback loop based on this process has neither been hypothesized nor tested before. Although predominantly oceanic, the loop also interacts with the atmosphere through the ocean heat loss that is an essential element of dense water formation in the BS. The simulated BCM heat transport into the BS is lower than that observed in the recent decade (Figures 13a and 13c), but the annual variability covers a reasonable range. The model thus appears adequate for the BS ocean climate in particular, and the coupled air-ice-ocean climate model enables investigation of cause and effects in the climate system that concerns the flow of AW through the BS (Figure 3).

[95] A feedback loop can be entered at any stage of the loop, and we start the analysis with investigating the relation between the dense water formation and the ocean-air heat flux. Comparing the total BS heat loss to the atmosphere and the average ocean column density in the BSX area, we find that a denser water column is generally preceded by greater heat loss. The two correlate closely throughout the simulation ($r = 0.3$–$0.8$) (Figure 16a).

[96] The denser water forms a horizontal density gradient between the BS and the Arctic Ocean. Because the downslope speed and transport increases with increasing density gradients [*Shapiro et al*., 2003b], denser water on the shelf is associated with increased BSX outflow, and this is specifically the case in the BCM. Enhanced BSX density is associated with increased volume transport ($r \sim 0.8$) (Figure 16b). Increased heat loss is thus associated with enhanced dense water formation both in the sense of denser and more BSX outflow.

[97] A denser water column is associated with a reduction in sea surface height in the BSX, even when the contraction caused by the density increase is accounted for. Furthermore, an increased eastward flow through the BSX is positively correlated with a reduced sea surface height in the BSX relative to the BSO (SSH difference) 1 year later ($0.2 < r < 0.8$) (Figure 16c). The correlation remains positive but is insignificant for much of the period, especially for the winter values. However, the correlations largely remain significant using the annual nonfiltered values because the 95% confidence level then drops to $r = 0.25$ (not shown). The increase in density and subsequent acceleration of the outflow in the BSX thus causes the sea surface height in the BSX to drop relative to the sea surface height in the BSO. The relative reduction in the BSX sea level affects the AW inflow by changing the barotropic forcing in favor of increased throughflow.

[98] Advection through BSO accounts for the major part of the net ocean heat transport into the BS (not shown), and this heat—less changing storage—is given up to the atmosphere. The anomalous heat balance is quantified to $r = 0.4$–$0.8$, with the ocean heat transport leading the flux to the atmosphere (Figure 16d). The possible positive feedback loop is thus closed. The closure is corroborated by the fact that regional ocean models forced with reanalysis data [e.g., *Sandø et al*., 2010; *Årthun et al*., 2012b] respond to changes in ocean heat transport in a similar way. However, a possible threshold for the surface fluxes that might limit the cooling of the BS is explored in section 3.6.

[99] Our finding that relative warm years with less sea ice and consequently more heat loss (Figures 3a–3c) support more dense water formation would appear at odds with the original inference of *Midttun* [1985]. In his case, very dense bottom water was formed by cooling and ice formation during cold years. This is, however, not inconsistent with our finding that concerns the average BSX water column. Years with less sea ice cover have a stronger Atlantic influence and higher salinity. Nevertheless, the water is cold upon reaching the BSX and, thus, more homogeneously composed of Cold Deep Water (CDW).

[100] Earlier sections established that the BS is central in the SAT variability of the Arctic and the Northern Hemisphere and that these variations are related to the AW inflow and the response in the BS ice and heat fluxes. However, in this section, we could not find much support in our BCM simulations for the wind feedback that seemed fairly well established from the review. Our results suggest that the BS hot spot is externally driven by large-scale atmospheric circulation, but much of the AW inflow variability is indeed wind driven. We found on the other side of the surface a quite promising support for our new hypothesis of the existence of an ocean feedback. This suggests that an externally forced change in AW inflow will tend to be self-amplified through creation of dense water, stronger outflow, and lowering of the sea surface height in the BSX.

### 3.5. Recent Changes in the Barents Sea Climate

#### 3.5.1. Atmospheric Circulation

[101] The analysis of recent atmospheric circulation changes in the Arctic suggests a transition to a more meridional flow structure (section 2.5) that may lead to more stationary weather patterns (blocking events) accompanied by extreme weather events [*Francis and Vavrus*, 2012]. How such atmospheric changes may be connected to a warmer Arctic and a reduced BS ice cover is suggested by an empirical orthogonal function (EOF) analysis of the 500 hPa geopotential height field north of 40°N in the BCM control simulation. Among the four leading variability patterns (or

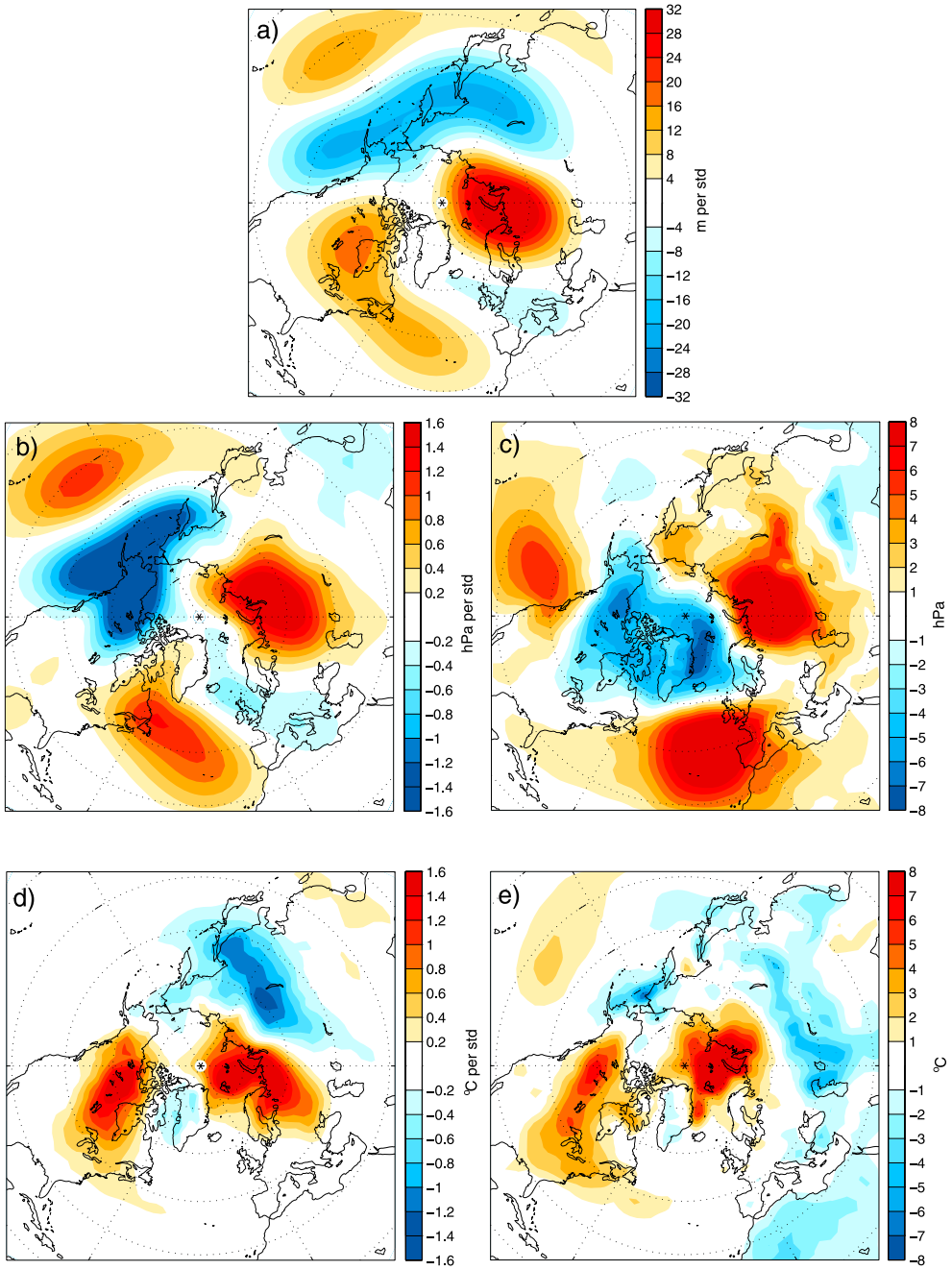


**Figure 17.** Northern Hemisphere winter anomalies of sea level pressure (SLP), surface air temperature (SAT), and geopotential height. The months of December through February are used. (a) The second EOF of the simulated geopotential height at 500 hPa north of 40°N in the 600 year long preindustrial control run for the BCM. (b) Regression of SLP onto the principal component of EOF2. (c) SLP anomalies for the winter of 2011/2012 calculated from the NCEP reanalysis. Reference period used is 1948–2012. (d) Regression of SAT onto the principal component of EOF2. (e) SAT anomalies for NCEP 1948–2012 similar to Figure 17c.

EOFs), the principal component times series associated with the second (EOF2) exhibits the highest correlations with the Arctic SAT ($r = 0.43$) and the BS ice ($r = -0.41$). A regression of the 500 hPa geopotential height field onto this principal component shows a wave number 3 pattern in the northern midlatitudes with a positive center of action south of the BS and a weaker negative center to the west over the Nordic Seas (Figure 17a). This pattern indicates more meridional flow over Scandinavia, reminiscent of a Scandinavian blocking pattern identified by cluster analysis [*Cassou et al.*, 2004]. A similar pattern is found by regressing this principal component onto the simulated SLP field (Figure 17b).

[102] The SLP anomalies associated with EOF2 bear some resemblance to observed SLP anomalies for the 2011/2012 winter (Figures 17b and 17c), especially in the Kara and Barents Seas. More striking is the similarity between SAT

anomalies associated with EOF2 and observed SAT anomalies for this winter (Figures 17d and 17e), with a strong warming signal over the BS, Northern Russia, and Canada and cooling over Siberia, central Russia, and, to a lesser extent, over Greenland. One realization in 2011/2012 is clearly not enough to speculate about a link between the BS surface climate and a particular pattern of internal atmospheric variability. However, the BCM results may provide a clue about the observed trend toward circulations with more meridional flow over the BS region (such as that observed during the recent winter) in the current period of very low BS ice cover and high Arctic SATs. The model reveals a positive correlation of the second principal component with Arctic SAT and negative sea ice anomalies in the BS. This highlights a potentially important role for internal atmospheric variability, such as the more meridional flow associated with EOF2 in Figure 17, for modifying the regional Northern Hemisphere winter climate.

#### 3.5.2. Ocean Heat Transport

[103] In the recent decade, the AW heat transport into the BS has been high [*Årthun and Schrum*, 2010]. This is visualized here by the observations of AW heat transport from the BSO onward from 1998 [*Årthun et al*., 2012b] included in Figures 13a and 13c (ERAI and ISCCP data) compared to the BCM simulations. The BCM thus suggest a lower AW heat transport for the long-term climatic mean, which is reasonable given the 600 year control run, the high recent transports, and the overall warming trend in the last 100 years (Figure 2).

[104] Another interesting aspect arises when comparing the magnitudes of the heat fluxes and the heat transports from the BCM simulations (Figure 13c). It shows that at low heat transports, ~40 TW, the magnitudes of the heat flux and the heat transport in the BS are comparable. Thus, at low heat transports, all the heat added by the ocean is removed by the atmosphere within the following year. At higher heat transports, on the other hand, the heat transported in 1 year is not removed entirely within the next year, and some of the heat is stored. A regression coefficient of ~ 0.5 implies that a heat transport anomaly of 10 TW in the mean results in a compensating heat flux anomaly of 5 TW the following year (Figure 13c). Because the heat is conserved (in the BCM and nature), the remaining 5 TW is not lost but warms up the BS or goes to melting imported sea ice. This, in turn, indicates two things: (1) that there might be a possible threshold for the surface fluxes that might limit the cooling of the BS and (2) that the recent warming (Figure 2) of the BS is strongly linked to the ocean forcing, i.e., more heat has been transported in with the ocean than has been removed by the atmosphere. The latter is also consistent with the two reanalysis estimates and the BSO heat transports; although the relationships between heat transport and heat flux are not as clear as in the BCM simulations, they do show a substantial stronger heat transport than heat flux during the last decade (Figure 13c).

[105] The results of this section reveal that the recent warming of the BS is driven by increased ocean heat transport in combination with possible large-scale changes in the atmospheric circulation. What would happen if the BS became ice free year round? This question and other possible thresholds for the BS surface fluxes will be explored in the next section.

### 3.6. Thresholds in the Air-Ice-Ocean System

[106] We will use here a simple conceptual model to frame our understanding of the relationships between the Barents air-ice-ocean components. Assuming that the strong surface cooling mixes the 265 m mean BS water column each winter [*Smedsrud et al*., 2010], the sea surface temperature and the sea ice cover are determined by two competing factors, namely, the total surface heat loss $F$ and the net ocean heat transport $H$. From the BCM simulations, the ranges in $F$ and $H$ are both between 40 and 70 TW (Figure 13c). Heat loss from open water is generally larger per unit area than for areas covered by sea ice. Figure 7b confirmed that this is true also for the BS, and for the areas with above 80% ice cover, much of the heat loss probably occurs in the small portions of open water or leads. This means that the total surface heat loss $F$ depends on the fraction of the sea ice cover ($f_{\mathrm{SIC}}$).

[107] Open water in the BS is mostly restricted to areas where the AW temperature remains above the freezing point [*Årthun et al*., 2012b]. A flushing time scale can be defined based on the BS volume and the mean volume transport [*Smedsrud et al*., 2010], and this implies that—on average—water in the BS is exchanged every 2 years. For time scales longer than 2 years, changing heat storage may thus be ignored and

$$H - F = 0. \tag{1}$$

[108] This simple equation can be used to determine the sensitivity of the average BS ice cover to the variability of $H$ and $F$. $H$ is largely determined by the AW inflow. To proceed further with our conceptual model, we assume that the heat loss through the ice is small enough to be ignored, and $F$ thus depends solely on the open water surface heat flux per unit area $q$ ($\mathrm{Wm}^{-2}$). $q$ is governed by the atmosphere through the surface air temperature, because the sea surface temperature variability is relatively small. Processes such as the number of cold-air outbreaks occurring each year contribute to the atmospheric variability. The total BS surface heat loss then becomes

$$F = (1 - f_{\mathrm{SIC}}) A_{\mathrm{BS}} q, \tag{2}$$

where $A_{\mathrm{BS}} = 1.36\ 10^{12}\,\mathrm{m}^2$ is the BS area. The scaling here accounts for the total surface heat flux, including short- and long-wave radiation, although for the ice-free area $(1 - f_{\mathrm{SIC}})$ only. The year-to-year variability in long- and short-wave radiation is also relatively small (Figure 7a). Substituting (2) into (1), we find the following expression for the sea ice fraction:

$$f_{\mathrm{SIC}} = 1 - \frac{H}{A_{\mathrm{BS}} q}. \tag{3}$$

[109] The BS ice fraction ($f_{\mathrm{SIC}}$) thus depends on both $q$ and $H$; it is directly proportional to $H$ but reciprocally proportional to $q$. This dependence is nontrivial with respect to $q$.

Indeed, the specific sea ice concentration sensitivities to $H$ and $q$ are

$$\frac{\partial f_{\mathrm{SIC}}}{\partial H} = -\frac{1}{A_{\mathrm{BS}}\, q} \quad \text{and} \tag{4}$$

$$\frac{\partial f_{\mathrm{SIC}}}{\partial q} = \frac{H}{A_{\mathrm{BS}}\, q^2}. \tag{5}$$

[110] The absolute ratio of sensitivities is

$$\frac{1}{A_{\mathrm{BS}}} \frac{\left|\frac{\partial f_{\mathrm{SIC}}}{\partial q}\right|}{\left|\frac{\partial f_{\mathrm{SIC}}}{\partial H}\right|} = \left|\frac{\frac{H}{A_{\mathrm{BS}}{}^2 q^2}}{-\frac{1}{A_{\mathrm{BS}} q}}\right| = \left|\frac{H}{A_{\mathrm{BS}} q}\right| = 1 - f_{\mathrm{SIC}} \leq 1. \tag{6}$$

[111] Thus, the sensitivity of the sea ice concentration to the ocean heat transport is always larger than the sensitivity to the atmospheric variability, scaled to the upper limit of an ice-free BS ($A_{\mathrm{BS}}\, q$). The importance of the atmospheric conditions increases with sea ice retreat. This supports the present understanding of a Barents region dominated by AW inflow and is in agreement with much of the reviewed literature onward from *Helland-Hansen and Nansen* [1909] to *Ikeda* [1990] and *Årthun et al*. [2012b]. Other model studies, however, suggested the opposite. For instance, *Ivanova et al*. [2012] concluded, on the basis of a high-resolution model study for 1979–2002, that wintertime sensitivity to the surface heat loss is about 4 times larger than the sensitivity to the ocean heat transport.

[112] The dependence on heat transport can be approximated directly from the BCM simulations. Figure 13a gives that $\Delta f_{\mathrm{SIC}}/\Delta H = -0.38$, and there is, thus, a loss of 3.8% ice cover with an added 10 TW of ocean heat transport. This is close to the 5% loss of sea ice cover for an additional 10 TW found by *Årthun et al*. [2012b].

[113] The general linear response of the BS ice variability to the ocean heat transport is seen in Figure 13a, and the conceptual model [equations (2)–(5)], in addition, illustrates how the sea ice cover moderates the air-ice-ocean coupling. In this way, surface heat fluxes respond to the ocean and sea ice cover (Figures 13b and 13c). When $f_{\mathrm{SIC}} \sim 1$, large changes in open water surface heat flux (per area) $q$ are required to counterweight small changes in ocean heat transport $H$. The role of the atmosphere increases for years with less ice cover and, more generally, in warm periods with southerly winds and smaller air-sea temperature difference (smaller $q$). This scaling is independent of the cause of such conditions, whether it is natural variability, regional sea ice advection, or impact of long-term climate change.

[114] This analysis reveals that the sea ice sensitivity to oceanic versus atmospheric forcing is conditioned by the sea ice cover itself. Although the instrumental observations are too short and the climate simulations do not have the desired spatial resolution to settle the question, one may speculate that the realization of the two feedback loops (Figure 3) could depend on the sea ice condition at the given time. In the BCM control run between years 150 and 200, such an event is possibly occurring. This period has first two events with quite low sea ice concentration (Figure 11), and then, the correlation between the BS inflow and the BS sea ice breaks down at year 200 (Figure 14a). With the diminishing sea ice cover in the future (section 3.9), it is then also likely that the air-ice-ocean coupling will change. The new state of the BS may then have sea ice variability more sensitive to variations in heat flux $q$. The atmospheric circulation is more variable than the ocean inflow, and because cold winds not only increase the heat loss but also advect more ice into the BS, the BS natural variability could be amplified in a future warmer climate.

[115] The ocean heat transport is strongly localized to the BS, but the atmospheric heat transport is distributed over the whole Arctic. Locally, over the BS, the impact of the ocean heat transport should therefore prevail during the positive phase of the Bjerknes oscillation mentioned earlier (section 3.3). The positive phase has positive sea surface temperature anomalies in the Atlantic sector [*Bjerknes*, 1964], and it seems like such a phase has been observed during the last few decades [*Polyakov and Johnson*, 2000]. Due to the lack of historical observations, it remains unclear whether the meteorological variability takes over during the negative Bjerknes oscillation phase.

[116] This section found that the sensitivity of the BS ice cover to ocean transport and heat fluxes changes with the ice cover itself. The ocean heat transport is a necessary condition for low ice cover, while the atmospheric heat loss is a necessary condition for ice cover in general. When the ice cover is large, the sea ice variability is dominated by the ocean transport, but when the ice cover decreases, variations in heat flux become more important.

### 3.7. Sinking of Carbon-Rich Water

[117] Large heat loss and formation of cold dense water take place in the Barents Sea [*Midttun et al*., 1985; *Årthun et al*., 2011]. This sets the stage for efficient transport of $CO_2$ to the deep Arctic Ocean. This transport of inorganic carbon from the ocean surface to the deep ocean where it will be shielded from the atmosphere, through the BS ( section 2.6), may be significant on a large scale. The carbon budget is dominated by the advective transport of dissolved inorganic carbon (DIC), supplied by AW inflow in the BSO and leaving in the BSX [*Kivimäe et al*., 2010] (Figures 1 and 10). Little is known about the variability in the BSX outflow, but given that the ocean feedback (Figure 3) is present, it would have a direct influence on the carbon transport. Here we will assess the BSX contribution to the global surface-to-deep sea carbon transport and its potential variability.

[118] We base our new analysis on published hydrography and carbon data from the BS combined with BCM simulations. We differ between total (DIC, natural and anthropogenic combined) and anthropogenic ($\mathrm{DIC_{ant}}$) carbon transport. We calculate $\mathrm{DIC_{ant}}$ for a specific year by using the difference between DIC concentration in that year and

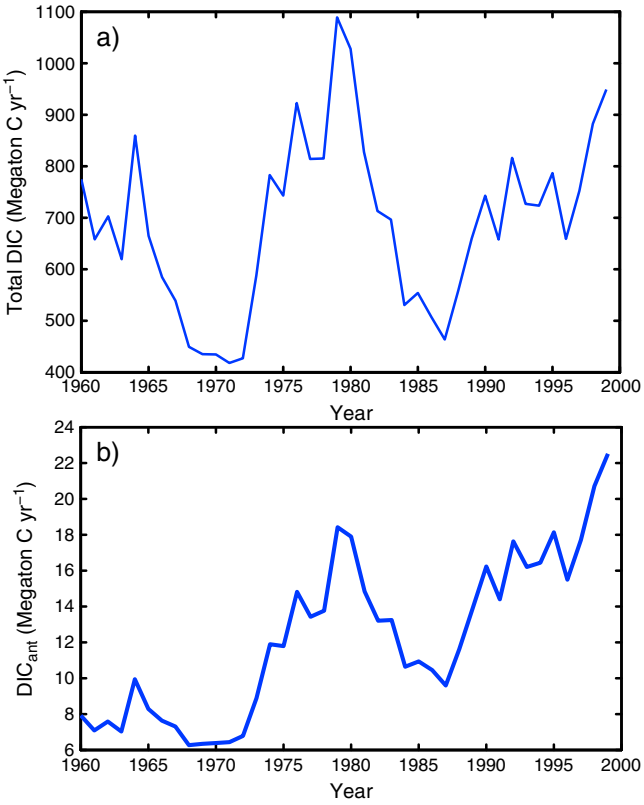


**Figure 18.** Calculated transports of dissolved inorganic carbon (DIC) by outflowing Cold Deep Water from the Barents Sea. The export mostly occurs between Franz Josef Land and Novaya Zemlya in the Barents Sea Exit, and values (Mt C yr$^{-1}$, =10$^{12}$ g C yr$^{-1}$) are based on simulations with the Bergen Climate Model and observations. (a) Total DIC (natural + antropogenic) and (b) the anthropogenic component.

that of the preindustrial era. This can be determined following *Gruber et al.* [1996]:

$$DIC_{\text{ant}} = DIC\left(S,T,Alk,fCO_{2\ \text{year}} - fCO_{2\ \text{diseq}}\right) - DIC\left(S,T,Alk,fCO_{2\ \text{PI}} - fCO_{2\ \text{diseq}}\right). \quad (7)$$

[119] Here $fCO_{2\ \text{year}}$ is the atmospheric $CO_2$ concentration for the year in question, and we use an $fCO_2$ of 280 µatm for preindustrial (PI) times. Alkalinity (Alk) was estimated from the simulated salinity ($S$) using the relationship identified by *Omar et al.* [2005]. To account for the fact that surface ocean $fCO_2$ in the BS is not in equilibrium with the atmospheric $CO_2$ concentration, we use $fCO_{2\ \text{diseq}}$, and the difference $fCO_{2\ \text{year}} - fCO_{2\ \text{diseq}}$ is the sea surface $fCO_2$. We assume that the disequilibrium term has been constant since preindustrial times. This assumption is supported by *Omar et al.* [2003], who found that summertime disequilibrium in the BS was the same in 1967 as in 2001. The $fCO_{2\ \text{diseq}}$ value of 70 µatm was calculated by setting the first term on the right-hand side of (7) equal to 2160 µmol kg$^{-1}$ for the year 1996. This value was chosen because it is the mean DIC value for the BSX in 1996 which was estimated using the results of *Kivimäe et al.* [2010]. Carbon transport is then computed according to

$$TR = DIC \times V \times \rho \times molar\ mass. \quad (8)$$

[120] The volume transport ($V$) used is the average of five ensemble BCM simulations forced with historical volcanoes, aerosols, solar activity, and increasing concentrations of greenhouse gases [*Otterå et al.*, 2010]. For DIC and density, mean values were based on estimates from *Kivimäe et al.* [2010] for AW and Barents Sea bottom water, 2160 µmol kg$^{-1}$ and 1028 kg m$^{-3}$, respectively. Variations in these two variables, typically a few percent, are neglected since the variability in the volume dominates the variability of the transport [*Jeansson et al.*, 2011].

[121] Our results are shown in Figure 18a, and the mean DIC transport (natural + anthropogenic) is 690 Mt C yr$^{-1}$. The variability is large, about ~25% (±1 standard deviation = ±170 Mt C yr$^{-1}$), and caused by volume transport variability. It is interesting to compare the DIC export at the BSX with that supplied through the BSO. Using a similar procedure as described above, we estimate a net BSO DIC transport of 1060 ± 190 Mt C yr$^{-1}$, implying that 65% ± 10% is exported into the deep waters of the Arctic Ocean. These long-term values from both the BSX and the BSO are smaller than the reviewed values found in section 2.6 (Figure 10). The main cause of this difference is the overall high recent volume transport, giving rise to larger carbon flux values in the 1990s and a rising trend (Figure 18a). The long-term averages calculated here are, thus, lower than these. The range in annual DIC$_{ant}$ transport through the BSX is 7–25 Mt C yr$^{-1}$ with a large year-to-year variability (±6 Mt C yr$^{-1}$) (Figure 18b). This is also related to changes in volume transport.

[122] Present emissions of fossil carbon are ~9000 Mt C yr$^{-1}$ globally [*Peters et al.*, 2012] and drives a net ocean uptake of about 2200 Mt C yr$^{-1}$ [*Gruber et al.*, 2009], representing uptake of anthropogenic carbon. The total DIC transport through the BSO (1620 Mt C yr$^{-1}$) (Figure 1) compares in magnitude to ~70% of this, and changes in the transport and deepwater formation in the BS may therefore have consequences for the net ocean carbon uptake at regional and global scales. The BS covers about 10% of the Arctic Ocean area, but in terms of DIC$_{ant}$ sequestration, it has a much larger impact than the small area suggest. An annual DIC$_{ant}$ inventory increase of 26 Mt C yr$^{-1}$ for the Arctic Ocean was determined by *Anderson et al.* [1998b]. Our estimates indicate that roughly 50% of this (Figure 18b) flows into the Arctic through the BSX.

### 3.8. The Last 2500 Years

[123] Processes in the BS operate on a range of time scales, and relationships that appear stable for over hundred years do change over longer time (Figure 14). The proposed feedbacks were suggested from instrumental knowledge the last 100 years and evaluated here using the BCM simulations. Can the same relationships provide useful concepts for interpretations of past climate changes at longer time scales?

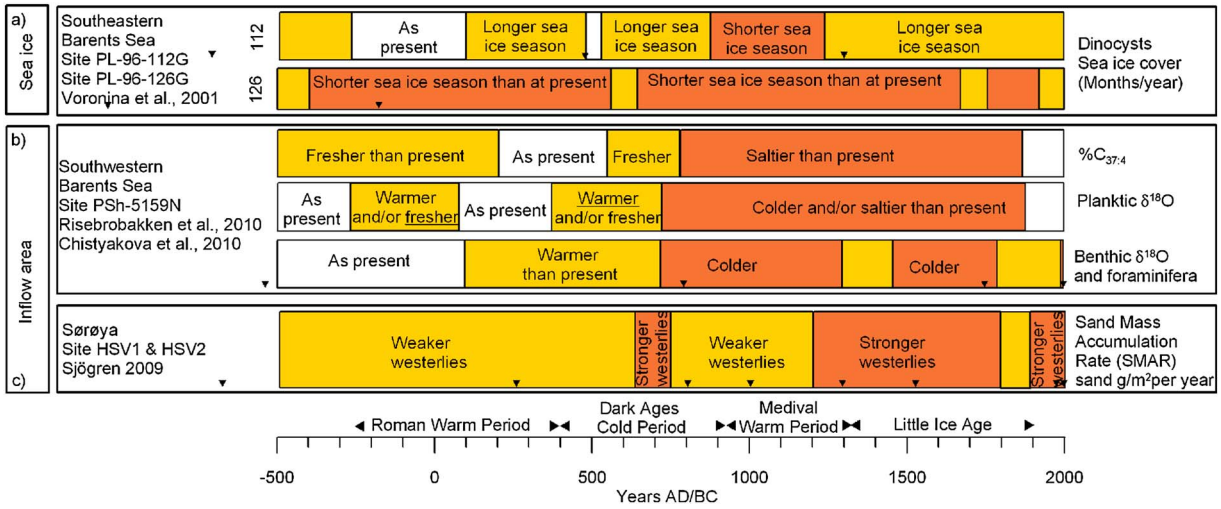


**Figure 19.** Climate characteristics of the Barents Sea air-ice-ocean variability during the last 2500 years. (a) Length of the sea ice season in the southeastern Barents Sea [*Voronina et al*., 2001]. (b) Temperature and salinity of the inflow through the BSO [*Chistyakova et al*., 2010; *Risebrobakken et al*., 2010]. The different proxies represent different depths of the water column (0–20 m; planktic δ18O: thermocline and below; benthic $\delta^{18}O$: 422 m). (c) Strength of the westerlies [*Sjögren*, 2009a]. The two records from HSV1 and HSV2 are resampled at 25 year steps, and the mean of the two records is used to provide a reference record for the strength of the westerlies. The black triangles represent age control points for each site as given by the original publications. White boxes represent conditions comparable to today. Yellow (brown) boxes reflect conditions interpreted to be a response to weaker (stronger) southwesterly wind forcing. Locations are shown in Figure 1 as red squares for (a), a red triangle for (b) and a red circle for (c).

Reconstructions are utilized to investigate air-ice-ocean coupling and the proposed feedbacks (Figure 3) at centennial time scales. A few records are available that provide information related to parts of the wind-feedback mechanism, but the full two feedback loops cannot be traced based on available reconstructions covering the last 2500 years.

[124] We have compared three BS records: (1) the length of the sea ice season in the southeastern BS given by a dinocyst-based transfer function [*Voronina et al*., 2001] (Figure 19a), (2) ocean variability given by a multiproxy study from Ingøydjupet in the southwestern BS [*Chistyakova et al*., 2010; *Risebrobakken et al*., 2010] (Figure 19b), and (3) an aeolien sediment record from two near-shore peat profiles from Sørøya giving relative strength of the westerlies in the BSO area [*Sjögren*, 2009a] (Figure 19c). The extracted information reflects the original interpretations of the proxies but is presented as relative anomalies of the core top values. Given ages follow the published age models, and the records have resolutions of 170 years/sample or better [*Risebrobakken et al*., 2011; *Sjögren*, 2009b; *Voronina et al*., 2001].

[125] A correspondence between weaker southwesterly wind forcing and freshening of the surface water is visible (Figure 19). The surface freshening is in line with present-day observations showing a northward expansion of coastal water as a response to weaker wind forcing. Higher salinity can reflect a warmer and wider inflow of AW related to stronger wind forcing [*Ingvaldsen*, 2005]. Fresher surface water in the BSO, interpreted to represent a northward expansion of the coastal water zone due to a weaker wind forcing, does also, at times, correspond with a longer sea ice season at the southeastern BS site located closest to the coast. The ocean and sea ice response is, however, not consistent with the wind forcing through time.

[126] In the AW domain of the southwestern BS, the suggested wind-feedback mechanism (Figure 3) will produce AW cooling for weaker wind and heat transport. Likewise should warming of the AW correspond to stronger winds and higher BSO heat transport. The reconstructions of southwestern BS AW conditions do not indicate a response that consistently can be put into such a framework. Occasional warming of deeper water masses occurs at times with weaker wind, and fresher surface water is suggested to represent reduced heat exchange with the atmosphere related to a shielding winter sea ice cover and summer freshwater lid [*Risebrobakken et al*., 2010].

[127] Based on the available reconstructions, no straightforward relationship between southwesterly wind strength, ocean temperatures, and sea ice is seen at centennial time scales. This conclusion is based on rather few sites and a limited number of proxies, and future multiproxy studies of more high-resolution and better-dated sites aimed at detecting these different steps of the feedback loop are needed to constrain BS air-ice-ocean relations at centennial time scales. Despite the lack of consistence at centennial times between the reconstructed wind forcing and ocean-ice response, there is an overall dominance of responses that can be related to weaker wind forcing from ~500 B.C. to ~700 A.D. and stronger wind from ~700 until 2000 A.D.

[128] The variability of the reconstructions has been compared with the relevant time series from the BCM 600 years control run, keeping in mind that the resolution and the length of the reconstructed time series are not directly

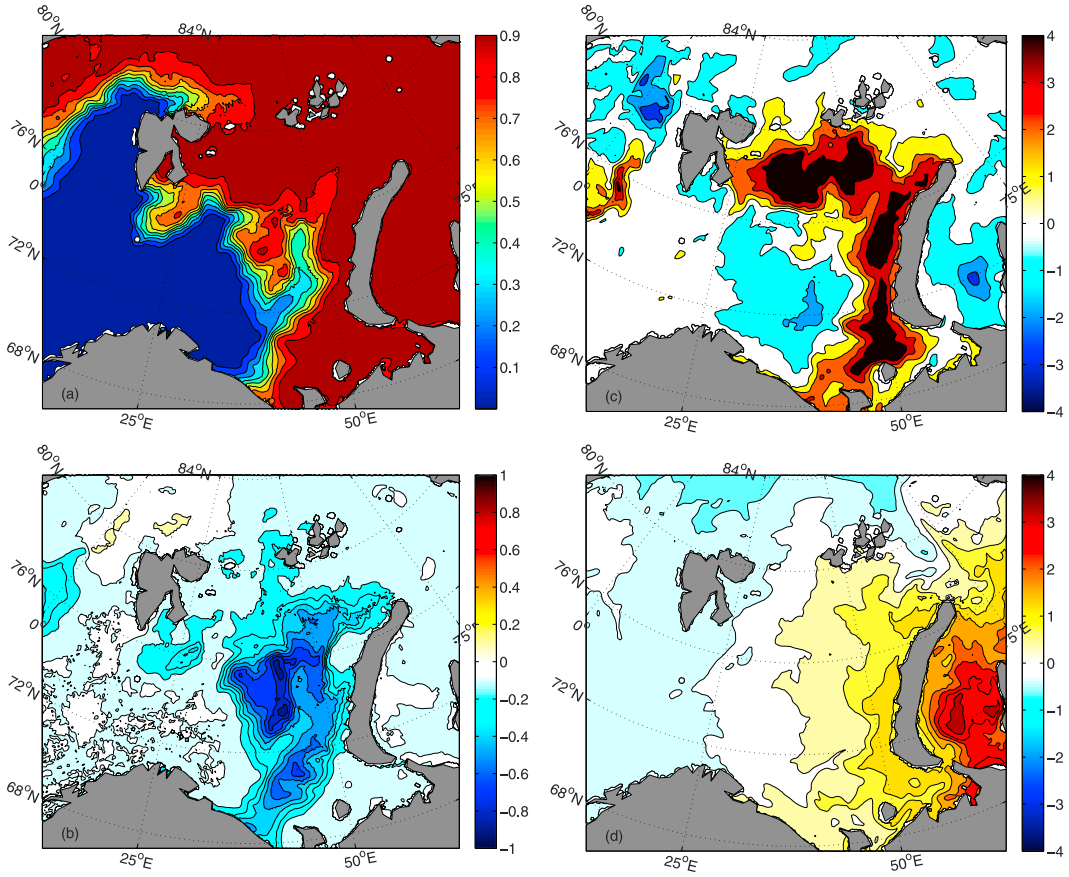


**Figure 20.** Selected fields describing the Barents Sea now and in 2050. (a) Ice concentration in March for the ROMS control run using GISS forcing representative of today. The other three subfigures show changes onward to 2050 using the A1B scenario. (b) Changes in sea ice concentration for March. (c) Changes in surface ocean temperature for July. (d) Changes in surface salinity for September.

comparable with the model simulations. Temperatures of AW, given by the mean of two benthic $\delta^{18}O$ records (422 m), suggest a range of ±2–3°C relative to 4.1°C recorded at the time of coring (August 2004). Events of predominant warmer or colder conditions last from 100 to 500 years [*Risebrobakken et al.*, 2010]. The simulated AW temperatures from a similar location (71°N, 23°E, 150 m depth) generally have a smaller range, and the mean is 5.5°C. For 25 to 50 year running means that would qualitatively be comparable with the benthic records, the variability is ±1°C. The maximum monthly simulated mean value is, however, 7°C and the minimum is 3°C, so variability through the seasons is larger. Periods of predominant cold and warm events lasts about 100 years (not shown).

[129] The range in annual mean wind speed, as simulated by the BCM, is 1.7 m/s around Sørøya (70°N, 22°E); however, the day-to-day or hour-to-hour variations would be much larger. For the 600 year period, there is clear wind-strength variability on a 10 to 50 year time scale, and up to 100 years long periods with predominantly stronger annual mean winds do exist (not shown). The difference in mean wind is on the order of 0.5 m/s for the 100 year periods. Absolute wind strength is not reconstructed by the aeolien sediment from Sørøya [*Sjögren*, 2009b]; however, 100 to 1000 year anomalies of relatively strong or weak wind forcing are indicated. Hence, the differences in resolution, length of records, and what is recorded hamper the comparison between the reconstructed and modeled wind conditions.

[130] Simulated sea ice concentration for the two positions southeast in the BS (Figure 1) also vary on decadal and centennial time scales in the 600 year BCM control run. There are clear similarities between the variability at the two positions, and the variability is close to that of the mean sea ice concentration (Figure 11b). The northern location has an annual mean sea ice cover about 40%, while it is around 25% in the more southern location. The amplitude of the variations on decadal scales is typically ±10%, again comparable to the mean sea ice concentration (Figure 11b). Both positions have minimum annual values close to zero and annual maximum values of up to 60% ice cover. The longest anomalies last 100–200 years, equal to the resolution of the dynocyst-based length of sea ice season reconstructions [*Voronina et al.*, 2001]. Thus, comparing the range of variability of the modeled and reconstructed sea ice is also prevented by the resolution of the reconstructions.

### 3.9. The Barents Sea in 2050

[131] To frame our understanding of the ongoing changes in the BS, we also include high-resolution downscaled scenarios for 2050 and compare with today. We apply a regional ice-

ocean model forced with global model simulations at the surface and boundaries and use a horizontal grid size of 10 km and 40 vertical levels. This generally reproduces most of the important processes discussed in section 2, such as a fractured sea ice cover, eddies, and vertical ocean stratification, and the bottom topography is realistic [*Melsom et al.*, 2009]. The model applied is the Regional Ocean Model System with a setup based on *Budgell* [2005]. Model performance was reviewed in section 2.8 and is generally good, and special emphasis was kept on the AW heat transport and the sea ice cover (A. B. Sandø et al., Downscaling IPCC control run and future scenario with focus on the Barents Sea, submitted to *Ocean Dynamics*, 2013, hereinafter referred to as Sandø et al., submitted manuscript, 2013).

[132] We compare two downscalings, each forced by one global model; none of them is the BCM. The two simulations are named after the global model, so ROMSG is the downscaling forced by the Goddard Institute for Space Studies (GISS) Global Atmosphere Ocean Model, and ROMSN is the downscaling using the National Center for Atmospheric Research Community Climate System Model. The two global models reproduced sea ice well in the Arctic Ocean [*Overland and Wang*, 2007]. We judge it as good to study the effects of using different global models and also note that an early version of the BCM did not pass the screening in these areas. The two downscalings (ROMSG and ROMSN) produce realistic hydrography and variability, despite a bias in the BS ice in the global forcing of ROMSG. Because the regional model is identical in the two, differences must be due to the different boundary conditions or the atmospheric forcing from the two global models. Differences were larger for 2050 than for today and thereby give interesting glimpses into the future (Sandø et al., submitted manuscript, 2013). Despite a better representation of sea ice in the ROMSN forcing, evaluation of the two models against observations showed that the ROMSG downscaling was most realistic (Sandø et al., submitted manuscript, 2013). In the following, the ROMSG simulations are shown as a possible realization of the BS future climate.

[133] In agreement with present observations, the present-day ROMSG ice extent and concentration are largest in March and April (Figure 20a) and smallest in September. The future scenario also shows most ice in March and April, but the sea ice minimum is delayed to October, with essentially no ice in the BS. A large loss of sea ice is predicted to occur in the northern and easternmost parts (Figure 20b), where the largest temperature increases are also found (shown for July) (Figure 20c). The largest change in salinity is fundamentally different to those of temperature and sea ice (Figure 20d). The maximum salinity increase occurs in September, a month with very low sea ice cover. The maximum salinity increase occurs in the Kara Sea, but the eastern and southern parts of the BS also get saltier, suggesting an increase of the AW-influenced areas.

[134] The seasonal volume and heat transports through the BSO for today and future runs are similar. Maximum departures of ±0.2 Sv for volume transport occur in February through April and for heat transport of ±5 TW for September through November. The BS response time for heat content from changes in heat transport is only 1 month [*Sandø et al.*, 2010]. The relatively large increase in temperature during summer (Figure 20c) is therefore likely caused by changes in heat flux as a function of ice cover and not increased transport of heat through the BSO. The annual mean volume transport decreases from 2.2 Sv today to 2.1 Sv in 2050, while the heat transport increases from 64 to 66 TW. The increase of 2 TW through the BSO is far below the observed interannual variability. The large summer temperature increase in the northern and eastern parts of the BS (Figure 20c) is therefore not caused by increased heat transport through the BSO but more likely by changes in solar heat flux as a function of ice cover [*Sandø et al.*, 2010].

## 4. SUMMARY

[135] The Barents Sea is a region where the air-ice-ocean coupling is especially strong. Decadal variability of all three elements in observations and in a long control simulation of the Bergen Climate Model has been documented here. During the recent decade, the Barents Sea ice has covered a smaller area than indicated by observations for the second half of the twentieth century and as simulated for the "preindustrial" climate. The Barents Sea ice anomalies dominate the recent ice loss in Northern Hemisphere winter. In contrast to the summer sea ice loss, which is concentrated in the Siberian sector of the Arctic Ocean and characterized by general thinning of the ice cover, the Barents ice loss is driven by an increased transport of heat into the region by the inflowing Atlantic Water. This increased Atlantic inflow leading to less sea ice and stronger heat loss to the atmosphere forms the main axis of two feedback loops that have been reviewed and evaluated in long-term simulations and data sets based on satellite observations. In the Barents Sea, the recent sea ice loss appears to be largely caused by more inflowing Atlantic Water, with the increased volume transport driven by atmospheric forcing. To what extent the changes in atmosphere and ocean circulation are related to global warming requires further investigation, a point we hope we have demonstrated and provided background for through the analyses presented here.

[136] The Northern Hemisphere surface air temperature north of 60°N relates strongly to variations in Arctic sea ice, and there are strong correlations between the surface air temperature, the Barents Sea ice cover, and the inflow of Atlantic Water to the Barents Sea. The correlations between the Barents Sea ice and the North Atlantic oscillation, or the Northern Annular Mode, are highly variable and low for extended periods of time in the simulated climate. Thus, these large-scale atmospheric patterns capture the dominating variability of the North Atlantic region but not the Barents Sea variability.

[137] The Barents Sea is an area of intense heat exchange. The added heat is dominated by the ocean heat transport, and without the 60–80 TW carried by the ocean currents, the Barents Sea would be substantially colder and have a larger winter sea ice cover. The heat loss is, on the other hand, almost

entirely governed by the surface heat fluxes as very little ocean heat is advected out of the sea. Without the surface heat loss, the Barents Sea outflow would have much higher temperatures, and the Barents Sea would be largely ice free during winter. The regional sea ice variability thus cannot be viewed as either driven by the ocean or the atmosphere. However, although large differences exist in the different data sets evaluated here, the heat loss generally increases when sea ice decreases, confirming the existence of the main axis of the feedback loops (Figure 3). Moreover, our conceptual analysis indicates that the sea ice cover is a component of the air-ice-ocean system that actively regulates the surface heat flux and the sensitivity to the ocean-air variability. With high ice cover, our results indicate that the ocean forcing dominates sea ice variability, but the importance of variations in heat flux driven by the atmosphere increases with decreasing sea ice concentrations.

[138] The inflowing ~2 Sv of Atlantic Water is effectively cooled to around 0°C, and at least 60% is transformed to dense water descending into the Arctic Ocean. This cooling and effective vertical mixing in the Barents Sea take up and transport $CO_2$ from the air and ocean surface layer down to great depths of the Arctic Ocean. About ~20 Mt of anthropogenic carbon is removed each year with this dense water formation in the Barents Sea. This removal, or sequestration, of anthropogenic carbon compares to previous estimates for the entire Arctic Ocean, but recent Arctic estimates are lacking to put our results properly into context.

[139] Associated with the cooling and the transformation to dense water is a possible positive feedback loop, supported by new results. Warm and cold periods with high and low Atlantic inflow will tend to be self-maintaining in the Barents Sea climate system. The limiting factor of the ocean feedback loop is likely external forcing from the large-scale atmospheric circulation. This also seems to be the main driver of sea level pressure variability in the simulated climate using the Bergen Climate Model. We could not find direct support for a wind feedback being steadily present. Instead, we found that many correlations vary extensively through the 600 year simulation. For example, does the North Atlantic oscillation correlate well with AW inflow for some periods. For others, it does not.

[140] Some recent studies have suggested teleconnections between the Barents Sea and continental Europe. For certain reductions in Barents Sea ice cover, cold winters become more prominent. The mechanism is an alteration of the frequent southwesterly winds toward a more north-south flow, leading warm southern air toward the Arctic, and more Arctic air southward. This pattern of large-scale flow is present in the Bergen Climate Model.

[141] We have examined the existing paleorecords for the Barents Sea and have found air-ice-ocean variability comparable to that of the simulated climate, although on somewhat longer than decadal time scales. For the future, the existing downscaling suggests a further loss of ice cover in the Barents Sea and continued warming amounting to ~4°C during summer.

[142] Based on the lessons learned here, we can state that the Early Warming of the 1930s was very likely connected to increased Atlantic Water heat transport into the Barents Sea. Consistent with the ocean feedback loop in Figure 3, the Early Warming probably had relatively limited Barents ice, large ocean heat loss, and efficient formation of dense water. Similarly, the Cool 1970s probably had less ocean heat transport than we have seen in the recent decade. The sea ice cover in the Barents Sea was large in the late 1970s and has decreased since then. The recent warming of the Barents Sea is found to be driven by increased ocean heat transport in combination with possible large-scale changes in the atmospheric circulation. The Barents Sea marine climate is set by the ocean and the presence of warm Atlantic Water, but the atmosphere governs variability on time scales shorter than a year. If the sea ice disappears, the atmosphere may be more dominant in the future.

## TERMS AND ABBREVIATIONS USED

Early Warming—The Warm period in the 1930s
Cool 1970s—The cold period around 1970
Transport—horizontal flow of mass, heat salt, and carbon
Flux—vertical fluxes of heat and carbon at the surface
Total heat flux =Sensible+Latent+Longwave+Shortwave
Most annually averaged heat transports and fluxes are winter centered averages, i.e., means from 1 July to 30 June, plotted on 1 January.
AW—Atlantic Water
BS—Barents Sea
BSO—Barents Sea Opening
BSX—Barents Sea Exit
BCM—Bergen Climate Model
CDW—Cold Deep Water
EOF—Empirical Orthogonal Function
DIC—Dissolved Inorganic Carbon
NAO—North Atlantic Oscillation
NAM—Northern Annular Mode
SAT—Surface Air Temperature
SLP—Sea Level Pressure
Names of reanalysis data in Table 1: NCEP, ERAI, ISCCP, HOAPS3, NOAA20C, OAFlux

[143] **ACKNOWLEDGMENTS.** The Kola section data were provided by the Polar Research Institute of Marine Fisheries and Oceanography (PINRO, http://www.pinro.ru). Time series of AW temperatures in the Faroe-Shetland Channel from *Yndestad et al.* [2008] were kindly provided by Bill Turrell, Marine Laboratory, Scotland, while air temperatures at Mayle Karmakuly, Novaya Zemlya, were taken from the National Climatic Data Center (http://www.ncdc.noaa.gov). NAO Index Data were provided by the Climate Analysis Section, NCAR, Boulder, USA. Reanalysis and heat flux data were taken from the different servers in Table 1. Thanks to Iselin Medhaug for the help in preparing the BCM data. This is publication no. A 421 from the Bjerknes Centre for Climate Research. CL, AO, and TE acknowledge the support from the Centre for Climate Dynamics (SKD) at the Bjerknes Centre.

[144] We would also like to thank the editor Eelco Rohling and two anonymous reviewers for their time, interest, and helpful suggestions.

## REFERENCES


Aagaard, K., and R. A. Woodgate (2001), Some thoughts on the freezing and melting of sea ice and their effects on the ocean, *Ocean Model*, *3*, 127–135.

Aagaard-Sørensen, S., K. Husum, M. Hald, and J. Knies (2010), Paleoceanographic development in the SW Barents Sea during the late Weichselian-Early Holocene transition, *Quat. Sci. Rev.*, *29*, 3442–3456, doi:10.1016/j.quascirev.2010.08.014.

Ådlandsvik, B., and H. Loeng (1991), A study of the climatic system in the Barents Sea, *Polar Res.*, *10*, 45–49.

Aksenov, Y., S. Bacon, A. Coward, and A. Nurser (2010), The North Atlantic inflow to the Arctic Ocean: High-resolution model study, *J. Mar. Syst.*, *79*(1–2), 1–22, doi:10.1016/j.jmarsys.2009.05.003.

Alexander, M. A., U. S. Bhatt, J. E. Walsh, M. S. Timlin, J. S. Miller, and J. D. Scott (2004), The atmospheric response to realistic Arctic sea ice anomalies in an AGCM during winter, *J. Clim.*, *17*(5), 890–905.

Alexeev, V. A., I. Esau, I. V. Polyakov, S. J. Byam, and S. Sorokina (2012), Vertical structure of recent Arctic warming from observed data and reanalysis products, *Clim. Change*, *111*(2), 215–239, doi:10.1007/s10584-011-0192-8.

Allan, R., and T. Ansell (2006), A new globally complete monthly historical gridded mean sea level pressure dataset (HadSLP2): 1850–2004, *J. Clim.*, *19*(22), 5816–5842.

Anderson, L. G., K. Olsson, and M. Chierici (1998a), A carbon budget for the Arctic Ocean, *Global Biogeochem. Cycles*, *12*, 455–465.

Anderson, L. G., K. Olsson, E. P. Jones, M. Chierici, and A. Fransson (1998b), Anthropogenic carbon dioxide in the Arctic Ocean: Inventory and sinks, *J. Geophys. Res.*, *103*(C12), 27,707–27,716.

Andersson, A., K. Fennig, C. Klepp, S. Bakan, H. Graßl, and J. Schulz (2010), The Hamburg Ocean Atmosphere Parameters and Fluxes from Satellite Data—HOAPS-3, *Earth Syst. Sci. Data*, *2*, 215–234, doi:10.5194/essd-2-215-2010.

Årthun, M., and C. Schrum (2010), Ocean surface heat flux variability in the Barents Sea, *J. Mar. Syst.*, *83*, 88–98, doi:10.1016/j.jmarsys.2010.07.003.

Årthun, M., R. B. Ingvaldsen, L. H. Smedsrud, and C. Schrum (2011), Dense water formation and circulation in the Barents Sea, *Deep Sea Res., Part I*, *58*, 801–817, doi:10.1016/j.dsr.2011.06.001.

Årthun, M., R. G. J. Bellerby, A. M. Omar, and C. Schrum (2012a), Spatiotemporal variability of air-sea $CO_2$ fluxes in the Barents Sea, as determined from empirical relationships and modeled hydrography, *J. Mar. Syst.*, *98–99*, 40–50.

Årthun, M., T. Eldevik, L. H. Smedsrud, Ø. Skagseth, and R. Ingvaldsen (2012b), Quantifying the influence of Atlantic heat on Barents Sea ice variability and retreat, *J. Clim.*, *25*, 4736–4743, doi:10.1175/JCLI-D-11-00466.1.

Arzel, O., T. Fichefet, and H. Goosse (2006), Sea ice evolution over the 20th and 21st centuries as simulated by current AOGCMs, *Ocean Model.*, *12*, 401–415.

Arzel, O., T. Fichefet, H. Goosse, and J. L. Dufresne (2008), Causes and impacts of changes in the Arctic freshwater budget during the twentieth and twenty-first centuries in an AOGCM, *Clim. Dyn.*, *30*(1), 37–58, doi:10.1007/s00382-007-0258-5.

Bengtsson, L., V. A. Semenov, and O. M. Johannessen (2004), The early twentieth-century warming in the Arctic—A possible mechanism, *J. Clim.*, *17*(20), 4045–4057.

Bjerknes, J. (1964), *Atlantic Air-Sea Interaction*, in Adv. in Geophys., edited by H. E. Landsberg, and J. van Mieghem, *10*, pp. 1–81, Academic Press Inc., New York.

Blindheim, J., V. Borovkov, B. Hansen, S. A. Malmberg, W. R. Turrell, and S. Østerhus (2000), Upper layer cooling and freshening in the Norwegian Sea in relation to atmospheric forcing, *Deep Sea Res., Part I*, *47*(4), 655–680.

Boitsov, V. D. (2006), *Variability of Temperature in the Barents Sea and its Forecasting*, PINRO Press, Murmansk, 292 pp.

Boitsov, V. D., A. L. Karsakov, and A. G. Trofimov (2012), Atlantic water temperature and climate in the Barents Sea, 2000–2009, *ICES J. Mar. Sci.*, *69*(5), 833–840, doi:10.1093/icesjms/fss075.

Bourassa, M. A., et al. (2013), High-Latitude ocean and sea ice surface fluxes: Requirements and challenges for climate research, *Bull. Am. Meteorol. Soc.*, *94*(3), 403–423, doi:10.1175/BAMS-D-11-00244.1.

Bracegirdle, T. J., and S. L. Gray (2008), An objective climatology of the dynamical forcing of polar lows in the Nordic seas, *Int. J. Climatol.*, *28*, 1903–1919.

Broecker, W. S., and T.-H. Peng (1974), Gas exchange rates between air and sea, *Tellus*, *26*, 21–35.

Brohan, P., J. J. Kennedy, I. Harris, S. F. B. Tett, and P. D. Jones (2006), Uncertainty estimates in regional and global observed temperature changes: A new dataset from 1850, *J. Geophys. Res.*, *111*, D12106, doi:10.1029/2005JD006548.

Brümmer, B. (1999), Roll and cell convection in wintertime arctic cold-air outbreaks, *J. Atmos. Sci.*, *56*, 2613–2636, doi:10.1175/1520-0469.

Brümmer, B., and S. Pohlmann (2000), Wintertime roll and cell convection over Greenland and Barents Sea regions: A climatology, *J. Geophys. Res.*, *105*(D12), *15*, 559–566, doi:10.1029/1999JD900841.

Budgell, P. (2005), Numerical simulation of ice-ocean variability in the Barents Sea region towards dynamical downscaling, *Ocean Dyn.*, *55*(3–4), 370–387, doi:10.1007/s10236-005-0008-3.

Cassou, C., L. Terray, J. W. Hurrell, and C. Deser (2004), North Atlantic winter climate regimes: Spatial asymmetry, stationarity with time and oceanic forcing, *J. Clim.*, *17*, 1055–1068.

Cavalieri, D. J., C. L. Parkinson, P. Gloersen, and H. J. Zwally *(*1996), Sea Ice Concentrations From Nimbus-7 SMMR and DMSP SSM/I-SSMI Passive Microwave Data, January 1979 to August 2011, Natl. Snow and Ice Data Cent., Boulder, Colo., [Updated daily].

Chapman, W. L., and J. E. Walsh (2007), Simulations of arctic temperature and pressure by global coupled models, *J. Clim.*, *20*, 609–632.

Chernokulsky, A., and I. I. Mokhov (2012), Climatology of total cloudiness in the Arctic: An intercomparison of observations and reanalyses, *Adv. Meteorol.*, *2012*, p. 15, doi:10.1155/2012/542093.

Chistyakova, N. O., E. V. Ivanova, B. Risebrobakken, E. A. Ovsepyan, and Y. S. Ovsepyan (2010), Reconstruction of postglacial environments in the south-western Barents Sea based on foraminiferal assemblages, *Oceanology*, *50*(4), 573–581, doi:10.1134/S0001437010040132.

Comiso, J. C. (2012), Large decadal decline of the Arctic multiyear ice cover, *J. Clim.*, *25*, 1176–1193, doi:10.1175/JCLI-D-11-00113.1.

Compo, G. P., J. S. Whitaker, and P. D. Sardeshmukh (2006), Feasibility of a 100 year reanalysis using only surface pressure data, *Bull. Am. Meteorol. Soc.*, *87*, 175–190.

Dee, D. P., with 35 co-authors (2011), The ERA-Interim reanalysis: Configuration and performance of the data assimilation system, *Q. J. R. Meteorol. Soc.*, *137*, 553–597.

Deser, C., and H. Teng (2008), Evolution of Arctic Sea ice concentration trends and the role of atmospheric circulation forcing, 1979–2007, *Geophys. Res. Lett.*, *35*, L02504, doi:10.1029/2007GL032023.

Deser, C., G. Magnusdottir, R. Saravanan, and A. Phillips (2004), The effects of North Atlantic SST and sea ice anomalies on the winter circulation in CCM3. Part II: Direct and indirect components of the response, *J. Clim.*, *17*, 877–889.

Dethloff, K., C. Abegg, A. Rinke, I. Hebestadt, and V. F. Romanov (2001), Sensitivity of Arctic climate simulations to different boundary-layer parameterizations in a regional climate model, *Tellus*, *53A*, 1–26.

Dickson, R. R., T. J. Osborn, J. W. Hurrell, J. Meincke, J. Blindheim, B. Adlandsvik, T. Vinje, G. Alekseev, and W. Maslowski (2000), The Arctic Ocean response to the North Atlantic oscillation, *J. Clim.*, *13*, 2671–2696.

Duplessy, J. C., E. Cortijo, E. Ivanova, T. Khusid, L. Labeyrie, M. Levitan, I. Murdmaa, and M. Paterne (2005), Paleoceanography of the Barents Sea during the Holocene, *Paleoceanography*, *20*, PA4004, doi:10.1029/2004PA001116.

Ellingsen, I., D. Slagstad, and A. Sundfjord (2009), Modification of water masses in the Barents Sea and its coupling to ice dynamics:

A model study, *Ocean Dyn*, *59*, 1095–1108, doi:10.1007/s10236-009-0230-5.

Fairall, C. W., E. F. Bradley, J. E. Hare, A. A. Grachev, and J. B. Edson (2003), Bulk parameterization of air-sea fluxes: Updates and verification for the COARE algorithm, *J. Clim.*, *16*, 571–591, doi:10.1175/1520-0442.

Fang, Z., and M. Wallace (1994), Arctic sea ice variability on timescale of weeks and its relation to atmospheric forcing, *J. Clim.*, *7*, 1897–1913.

Francis, J. A., and E. Hunter (2007), Drivers of declining sea ice in the Arctic winter: A tale of two seas, *Geophys. Res. Lett.*, *34*, doi:10.1029/2007GL030995.

Francis, J. A., and S. J. Vavrus (2012), Evidence linking Arctic amplification to extreme weather in mid-latitudes, *Geophys. Res. Lett.*, *39*, L06801, doi:10.1029/2012GL051000.

Fransson, A., M. Chierici, L. G. Anderson, I. Bussmann, G. Kattner, E. P. Jones, and J. H. Swift (2001), The importance of shelf processes for the modification of chemical constituents in the waters of the Eurasian Arctic Ocean: Implications for carbon fluxes, *Cont. Shelf Res.*, *21*, 225–242.

Gammelsrød, T., Ø. Leikvin, V. Lien, W. Budgell, H. Loeng, and W. Maslowski (2009), Mass and heat transports in the NE Barents Sea: Observations and models, *J. Mar. Syst.*, *75*, 56–69, doi:10.1016/j.marsys.2008.07.010.

Gerdes, R., and U. Schauer (1997), Large-scale circulation and water mass distribution in the Arctic Ocean from model results and observations, *J. Geophys. Res.*, *102*(C4), 8467–8483.

Gerland, S., A. H. H. Renner, F. Godtliebsen, D. Divine, and T. B. Løyning (2008), Decrease of sea ice thickness at Hopen, Barents Sea, during 1966–2007, *Geophys. Res. Lett.*, *35*, L06501, doi:10.1029/2007GL032716.

Gloor, M., N. Gruber, J. Sarmiento, C. L. Sabine, R. A. Feely, and C. Rödenbeck (2003), A first estimate of present and preindustrial air-sea $CO_2$ patterns based on ocean interior carbon measurements and models, *J. Geophys. Res.*, *30*, 1010, doi:10.1029/2002GL015594.

Goosse, H., and M. M. Holland (2005), Mechanisms of decadal arctic climate variability in the community climate system model, version 2 (CCSM2), *J. Clim.*, *18*(17), 3552–3570.

Goosse, H., F. M. Selten, R. J. Haarsma, and J. D. Opsteegh (2003), Large sea-ice volume anomalies simulated in a coupled climate model, *Clim. Dyn.*, *20*(5), 523–536, doi:10.1007/s00382-002-0290-4.

Grønås, S., and N. G. Kvamstø (1995), Numerical simulations of the synoptic conditions and development of Arctic outbreack polar lows, *Tellus*, *47A*, 797–814.

Gruber, N., J. L. Sarmiento, and T. F. Stocker (1996), An improved method for detecting anthropogenic $CO_2$ in the oceans, *Global Biogeochem. Cycles*, *10*, 809–837.

Gruber, N., et al. (2009), Ocean sources, sinks and transport of atmospheric $CO_2$, *Global Biogeochem. Cycles 23*, GB1005, doi:10.1029/2008GB003349.

Häkkinen, S., and D. J. Cavalieri (1989), A study of oceanic surface heat fluxes in the Greenland, Norwegian, and Barents Sea, *J. Geophys. Res.*, *94*, 6145–6157.

Hanzlick, D., and K. Aagard (1980), Freshwater and Atlantic water in the Kara Sea, *J. Geophys. Res.*, *85*, 4937–4942.

Harms, I. H. (1992), A numerical study of the barotropic circulation in the Barents and Kara Seas, *Cont. Shelf Res.*, *12*, 1043–1058.

Harms, I., C. Schrum, and K. Hatten (2005), Numerical sensitivity studies on the variability of climate-relevant processes in the Barents Sea, *J. Geophys. Res.*, *110*, C06002, doi:10.1029/2004JC002559.

Helland-Hansen, B., and F. Nansen (1909), The Norwegian Sea - Its physical oceanography based upon the Norwegian researches 1900-1904, *Rep. on Norw. Fish. and Marin. Invest.*, *11*(2), 360 pp.

Hibler, W., and K. Bryan (1987), A diagnostic ice-ocean model, *J. Phys. Oceanogr.*, *17*, 987–1015.

Honda, M., J. Inoue, and S. Yamane (2009), Influence of low Arctic sea-ice minima on anomalously cold Eurasian winters, *Geophys. Res. Lett.*, *36*, L08707, doi:10.1029/2008gl037079.

Hopsch, S., J. Cohen, and K. Dethloff (2012), Analysis of a link between fall Arctic sea ice concentration and atmospheric patterns in the following winter, *Tellus*, *64A*, 18624, doi:10.3402/tellusa.v64i0.18624.

Hurrell, J. W. (1995), Decadal trends in the North Atlantic oscillation regional temperatures and precipitation, *Science*, *269*, 676–679.

Ikeda, M. (1990), Decadal oscillations of the air-ice-ocean system in the Northern Hemisphere, *Atmos. Ocean*, *28*(1), 106–139, doi:10.1080/07055900.1990.9649369.

Ikeda, M., J. Wang, and J.-P. Zhao (2001), Hypersensitive decadal oscillation in the Arctic/subarctic climate, *Geophys. Res. Lett.*, *28*, 1275–1278.

Ingvaldsen, R. B. (2005), Width of the North Cape Current and location of the Polar Front in the western Barents Sea, *Geophys. Res. Lett.*, *32*, L16603, doi:10.1029/2005GL023440.

Ingvaldsen, R., H. Loeng, G. Ottersen, and B. Ådlandsvik (2003), Climate variability in the Barents Sea during the 20th century with focus on the 1990s, *ICES Mar. Sci. Symp.*, *219*, 160–168.

Ingvaldsen, R., L. Asplin, and H. Loeng (2004), The seasonal cycle in the Atlantic transport to the Barents Sea during the years 1997–2001, *Cont. Shelf Res.*, *24*, 1015–1032.

Inoue, J., M. E. Hori, and K. Takaya (2012), The role of Barents Sea ice in the wintertime cyclone track and emergence of a warm-Arctic cold-Siberian anomaly, *J. Clim.*, *25*, 2561–2568.

Ivanov, B. V., S. Gerland, J.-G. Winther, and H. Goodwin (2003), Energy exchange processes in the marginal ice zone of the Barents Sea, Arctic Ocean, during spring 1999, *J. Glaciol.*, *49*(166), 415–419.

Ivanov, V. V., V. A. Alexeev, I. Repina, N. V. Koldunov, and A. Smirnov (2012), Tracing Atlantic water signature in the Arctic Sea ice cover east of Svalbard, *Adv. Meteorol.*, *2012*, 11 pp., doi:10.1155/2012/201818.

Ivanova, D. P., J. L. McClean, and E. C. Hunke (2012), Interaction of ocean temperature advection, surface heat fluxes and sea ice in the marginal ice zone during the North Atlantic oscillation in the 1990s: A modeling study, *J. Geophys. Res.*, *117*, C02031, doi:10.1029/2011JC007532.

Jakobsson, M. (2002), Hypsometry and volume of the Arctic Ocean and its constituent seas, *Geochem. Geophys. Geosyst.*, *3*(5), 1028, doi:10.1029/2001GC000302.

Jeansson, E., A. Olsen, T. Eldevik, I. Skjelvan, A. M. Omar, S. K. Lauvset, J. E. Nilsen, R. G. J. Bellerby, and T. Johannessen (2011), The Nordic Seas carbon budget: Sources, sinks and uncertainties, *Global Biogeochem. Cycles*, *25*, GB4010, doi:10.1029/2010GB003961.

Johannesen, E., R. B. Ingvaldsen, P. Dalpadado, M. Skern-Mauritzen, J. E. Stiansen, E. Eriksen, H. Gjøsæter, B. Bogstad, and T. Knutsen (2012), The Barents Sea ecosystem state 1970-2009: climate fluctuations, human impact and trophic interactions, *ICES J. Mar. Sci.*, *69*(5), 880–889, doi:10.1093/icesjms/fss046.

Jones, E., B. Rudels, and L. Anderson (1995), Deep waters of the Arctic Ocean: Origins and circulation, *Deep Sea Res., Part I*, *42*(5), 737–760.

Jungclaus, J. H., and T. U. Koenigk (2010), Low-frequency variability of the arctic climate: The role of oceanic and atmospheric heat transport variations, *Clim. Dyn.*, *34*, 265–279, doi:10.1007/s00382-009-0569-9.

Junttila, J., S. Aagaard-Sørensen, K. Husum, and M. Hald (2010), Late Glacial-Holocene clay minerals elucidating glacial history in the SW Barents Sea, *Mar. Geol.*, *276*, 71–85.

Kalnay, E., 21 co-authors (1996), The NCEP/NCAR 40-year reanalysis project, *Bull. Am. Meteorol. Soc.*, *77*, 437–471.

Kaltin, S., L. G. Anderson, K. Olsson, A. Fransson, and M. Chierici (2002), Uptake of atmospheric carbon dioxide in the Barents Sea, *J. Mar. Syst.*, *38*, 31–45.

Keup-Thiel, E., H. Goettel, and D. Jacob (2006), Regional climate simulations for the Barents Sea region, *Boreal Environ. Res.*, *11*, 329–339.

Khatiwala, S., F. Primeau, and T. Hall (2009), Reconstruction of anthropogenic $CO_2$ concentrations in the ocean, *Nature*, *462*, 346–349, doi:10.1038/nature08526.

Kivimäe, C., R. G. J. Bellerby, A. Fransson, M. Reigstad, and T. Johannessen (2010), A carbon budget for the Barents Sea, *Deep Sea Res., Part I*, *57*, 1532–1542, doi:10.1016/j.dsr.2010.05.006.

Klimenko, V. V. (2008), Reconstruction of climate in the Russian Arctic over the last 600 years based on documentary evidence, *Dokl. Earth Sci.*, *418*(1), 95–98.

Koenigk, T., U. Mikolajewicz, J. H. Jungclaus, and A. Kroll (2009), Sea ice in the Barents Sea: Seasonal to interannual variability and climate feedbacks in a global coupled model, *Clim. Dyn.*, *32*(7), 1119–1138.

Koenigk, T., R. Doesher, and G. Nikulin (2011), Arctic future scenario experiments with a coupled regional climate model, *Tellus*, *63A*, 69–86.

Kolstad, E. W., and T. J. Bracegirdle (2008), Marine cold-air outbreaks in the future: An assessment of IPCC AR4 model results for the Northern Hemisphere, *Clim. Dyn*, *30*, 871–885, doi:10.1007/s00382-007-0331-0.

Kwok, R. (2009), Outflow of Arctic Ocean sea ice into the Greenland and Barents Seas: 1979–2007, *J. Clim.*, *22*(9), 2438–2457.

Kwok, R., and C. F. Cunningham (2010), Contribution of melt in the Beaufort Sea to the decline in Arctic multiyear sea ice coverage: 1993–2009, *Geophys. Res. Lett.*, *37*, L20501, doi:10.1029/2010gl044678.

Kwok, R., W. Maslowski, and S. W. Laxon (2005), On large outflows of Arctic sea ice into the Barents Sea, *Geophys. Res. Lett.*, *32*, L22503, doi:10.1029/2005GL024485.

Langehaug, H., I. Medhaug, T. Eldevik, and O. H. Otterå (2012), Arctic/Atlantic exchanges via the subpolar gyre, *J. Clim.*, *25*, 2421–2439.

Levitus, S., G. Matishov, D. Seidov, and I. Smolyar (2009), Barents Sea multidecadal variability, *Geophys. Res. Lett.*, *36*, L19604, doi:10.1029/2009GL039847.

Lind, S., and R. Ingvaldsen (2012), Variability and impacts of Atlantic Water entering the Barents Sea from the north, *Deep Sea Res., Part I*, *62*, 70–88.

van Linschoten, J. H. (1601), Map of Barentsz Voyages, Journal of Jan Huyghens van Linschoten.

Liu, J., J. A. Curry, H. Wang, M. Song, and R. M. Horton (2012), Impact of declining Arctic sea ice on winter snowfall, *Proc. Natl. Acad. Sci. U. S. A.*, doi:10.1073/pnas.1114910109.

Loeng, H. (1991), Features of the physical oceanographic conditions of the Barents Sea, *Polar Res.*, *10*(1), 5–18.

Loeng, H., V. Ozhigin, and B. Adlandsvik (1997), Water fluxes through the Barents Sea, *ICES J. Mar. Sci.*, *54*(3), 310–317, doi:10.1006/jmsc.1996.0165.

van Loon, H., and J. Rogers (1978), The seesaw in winter temperature between Greenland and northern Europe. Part I: General description, *Mon. Weather Rev.*, *106*, 296–310.

Lubinski, D. J., L. Polyak, and S. L. Forman (2001), Freshwater and Atlantic water inflow to the deep northern Barents and Kara seas since ca 13 $^{14}$C ka: Foraminifera and stable isotopes, *Quat. Sci. Rev.*, *20*, 1851–1879.

Lundberg, L., and P. M. Haugan (1996), A Nordic Seas-Arctic Ocean carbon budget from volume flows and inorganic carbon data, *Global Biogeochem. Cycles*, *10*(3), 493–510, doi:10.1029/96GB00359.

Macias Fauria, M., A. Grinsted, S. Helama, J. Moore, M. Timonen, T. Martma, E. Isaksson, and M. Eronen (2010), Unprecedented low 20th century winter sea ice extent in the western Nordic Seas since A.D. 1200, *Clim. Dyn.*, *34*(6), 781–795, doi:10.1007/s00382-009-0610-z.

Magnusdottir, G., C. Deser, and R. Saravanan (2004), The effects of North Atlantic SST and sea ice anomalies on the winter circulation in CCM3. Part I: Main features and storm track characteristics of the response, *J. Clim.*, *17*, 857–876, doi:10.1175/1520-0442.

Maslowski, W., D. Marble, W. Walczowski, U. Schauer, Clement J. L., and A. J. Semtner (2004), On climatological mass, heat, and salt transports through the Barents Sea and Fram Strait from a pan-Arctic ice-ocean model simulation, *J. Geophys. Res.*, *109*, C03032, doi:10.1029/2001JC001039.

Mauritzen, C. (1996), Production of dense overflow waters feeding the North Atlantic across the Greenland-Scotland Ridge. Part 1: Evidence for a revised circulation scheme, *Deep Sea Res., Part I*, *43*(6), 769–806.

Medhaug, I., H. Langehaug, T. Eldevik, T. Furevik, and M. Bentsen (2011), Mechanisms for decadal scale variability in a simulated Atlantic meridional overturning circulation, *Clim. Dyn.*, doi:10.1007/s00382-011-1124-z.

Meier, W. N., J. C. Stroeve, and F. Fetterer (2006), Whither Arctic sea ice? A clear signal of decline regionally, seasonally and extending beyond the satellite record, *Ann. Glaciol.*, *46*, 428–434.

Melsom, A., V. S. Lien, and W. P. Budgell (2009), Using the Regional Ocean Modeling System (ROMS) to improve the ocean circulation from a GCM 20th century simulation, *Ocean Dyn.*, *59*, 969–981.

Midttun, L. (1985), Formation of dense bottom water in the Barents Sea, *Deep Sea Res., Part A*, *32*(10), 1233–1241.

Moritz, R. E., C. M. Bitz, and E. J. Steig (2002), Dynamics of recent climate change in the Arctic, *Science*, *297*, 1497–1502.

Mosby, H. (1938), Svalbard waters, *Geofys. Publ.*, *12*(4), 1–86.

Mosby, H. (1962), Water, salt and heat balance of the North Polar Sea and of the Norwegian Sea, *Geofys. Publ.(Geophys. Norv.)*, *24*, 289–313.

Mysak, L. A., and S. A. Venegas (1998), Decadal climate oscillations in the Arctic: A new feedback loop for atmosphere-ice-ocean interactions, *Geophys. Res. Lett.*, *25*(19), 3607–3610.

Nakaoka, S., S. Aiki, T. Nakazawa, G. Hashida, S. Morimoto, T. Yamanouchi, and H. Yoshikawa-Inoue (2006), Temporal and spatial variations of oceanic $pCO_2$ and air-sea $CO_2$ flux in the Greenland Sea and the Barents Sea, *Tellus, Ser. B*, *58*, 148–161, doi:10.1111/j.1600-0889.2006.00178.x.

Noer, G., Ø. Saetra, T. Lien, and Y. Gusdal (2011), A climatological study of polar lows in the Nordic Seas, *Q. J. R. Meteorol. Soc.*, doi:10.1002/qj.846.

Olsen, A., A. M. Omar, E. Jeansson, L. G. Anderson, and R. G. J. Bellerby (2010), Nordic Seas transit time distributions and anthropogenic CO2, *J. Geophys. Res.*, *115*, C05005, doi:10.1029/2009JC005488.

Omar, A., T. Johannessen, S. Kaltin, and A. Olsen (2003), The anthropogenic increase of oceanic $pCO_2$ in Barents Sea surface waters since 1967, *J. Geophys. Res.*, *108*(C12), 3388, doi:10.1029/2002JC001628.

Omar, A., T. Johannessen, R. Bellerby, A. Olsen, L. Anderson, and C. Kivimàe (2005), Sea ice and brine formation in Storfjorden: Implications for the Arctic winter time air-sea CO2 flux, in *The Nordic Seas: An Integrated Perspective Oceanography, Climatology, and Modelling*, edited by H. Drange, et al., pp. 177–187, AGU, Washington, D. C.

Omar, A. M., T. Johannessen, A. Olsen, S. Kaltin, and F. Rey (2007), Seasonal and interannual variability of the air-sea CO2 flux in the Atlantic sector of the Barenst Sea, *Mar. Chem.*, *104*, 203–213.

Otterå, O. H., M. Bentsen, I. Bethke, and N. G. Kvamstø (2009), Simulated pre-industrial climate in Bergen Climate Model (version 2): Model description and large-scale circulation features, *Geosci. Model Dev.*, *2*, 197–212.

Otterå, O. H., M. Bentsen, H. Drange, and L. Suo (2010), External forcing as a metronome for Atlantic multidecadal variability, *Nat. Geosci.*, *3*, 688–694, doi:10.1038/NGEO0955.

Overland, J. E., and M. Wang (2005a), The Arctic climate paradox: The recent decrease of the Arctic Oscillation, *Geophys. Res. Lett.*, *32*, L06701, doi:10.1029/2004gl021752.

Overland, J. E., and M. Wang (2005b), The third Arctic climate pattern: 1930s and early 2000s, *Geophys. Res. Lett.*, *32*, L23808, doi:10.1029/2005gl024254.

Overland, J. E., and M. Wang (2007), Future climate of the North Pacific Ocean, *Eos Trans. AGU*, *88*(16), 178, doi:10.1029/2007EO160003.

Overland, J. E., and M. Wang (2010), Large-scale atmospheric circulation changes are associated with the recent loss of Arctic sea ice, *Tellus, Ser. A*, *62*(1), 1–9.

Overland, J. E., M. Wang, and S. Salo (2008), The recent Arctic warm period, *Tellus, Ser. A*, *60*(4), 589–597.

Ozhigin, V. K., S. S. Drobysheva, N. G. Ushakov, N. A. Yaragina, O. V. Titov, and A. L. Karsakov (2003), Interannual variability in the physical environment: Zooplankton, capelin (*Mallotus villosus*), and Northeast Arctic cod (*Gadus morhua*) in the Barents Sea, *ICES Mar. Sci. Symp.*, *219*, 283–293.

Ozhigin, V., R. B. Ingvaldsen, H. Loeng, V. Boitsov, and A. Karsakov (2011), Introduction to the Barents Sea, in *The Barents Sea Ecosystem, Resources, Management. Half a Century of Russian-Norwegian Cooperation*, edited by T. Jakobsen, and V. Ozhigin, pp. 39–76, Tapir Acad. Press, Trondheim, Norway.

Palm, S. P., S. T. Strey, J. Spinhirne, and T. Markus (2010), Influence of Arctic sea ice extent on polar cloud fraction and vertical structure and implications for regional climate, *J. Geophys. Res.*, *115*, D21209, doi:10.1029/2010JD013900.

Peters, G. P., G. Marland, C. Le Quéré, T. Boden, J. G. Canadell, and M. R. Raupach (2012), Rapid growth in CO2 emissions after the 2008–2009 global financial crisis, *Nat. Clim. Change*, *2*, 2–4, doi:10.1038/nclimate1332.

Petoukhov, V., and V. A. Semenov (2010), A link between reduced Barents-Kara sea ice and cold winter extremes over northern continents, *J. Geophys. Res.*, *115*, D21111, doi:10.1029/2009jd013568.

Pfirman, S. L., D. Bauch, and T. Gammelsrød (1994), The Northern Barents Sea: Water mass distribution and modification, in *The Polar Oceans and Their Role in Shaping the Global Environment: The Nansen Centennial Volume*, Geophys. Monogr. Ser., vol. 85, edited by O. Johannessen, R. Muench, and J. Overland, pp. 77–94, AGU, Washington, D. C.

Polyak, L., and A. Solheim (1994), Late- and postglacial environments in the northern Barents Sea west of Franz Josef Land, *Polar Res.*, *13*(2), 1997–1207.

Polyakov, I. V., and M. A. Johnson (2000), Arctic decadal and interdecadal variability, *Geophys. Res. Lett.*, *27*, 4097–4100, doi:10.1029/2000GL011909.

Polyakov, I. V., R. V. Bekryaev, G. V. Alekseev, U. S. Bhatt, R. L. Colony, M. A. Johnson, A. P. Maskshtas, and D. Walsh (2003), Variability and trends of air temperature and pressure in the maritime Arctic, 1875–2000, *J. Clim.*, *16*, 2067–2077, doi:10.1175/1520-0442.

Rinke, A., et al. (2006), Evaluation of an ensemble of Arctic regional climate models: Spatiotemporal fields during the SHEBA year, *Clim. Dyn.*, *26*(5), 459–472.

Risebrobakken, B., M. Moros, E. V. Ivanova, N. Chistyakova, and R. Rosenberg (2010), Climate and oceanographic variability in the SW Barents Sea during the Holocene, *Holocene*, *20*(4), 609–621.

Risebrobakken, B., T. Dokken, L. H. Smedsrud, C. Andersson, E. Jansen, M. Moros, and E. V. Ivanova (2011), Early Holocene temperature variability in the Nordic Seas: The role of oceanic heat advection versus changes in orbital forcing, *Paleoceanography*, *26*, PA4206, doi:10.1029/2011PA002117.

Rogers, J. C. (1997), North Atlantic storm track variability and its association to the north Atlantic oscillation and climate variability of Northern Europe, *J. Clim.*, *10*, 1635–1647, doi:10.1175/1520-0442.

Rogers, J. C., and E. Mosley-Thompson (1995), Atlantic Arctic cyclones and the mild Siberian winters of the 1980s, *Geophys. Res. Lett.*, *22*(7), 799–802.

Rossow, W. B., and E. N. Dueñas (2004), The International Satellite Cloud Climatology Project (ISCCP) Web site: An online resource for research, *Bull. Am. Meteorol. Soc.*, *85*, 167–172.

Rudels, B., B. Jones, L. Anderson, and G. Kattner (1994), On the intermediate depth waters of the Arctic Ocean, in *The Polar Oceans and Their Role in Shaping the Global Environment: The Nansen Centennial Volume*, Geophys. Monogr. Ser., vol. 85, edited by O. Johannessen, R. Muench, and J. Overland, pp. 33–46, AGU, Washington, D. C.

Rudels, B., L. G. Anderson, and E. P. Jones (1996), Formation and evolution of the surface mixed layer and halocline of the Arctic Ocean, *J. Geophys. Res.*, *101*, 8807–8821.

Sandø, A. B., J. E. Ø. Nilsen, Y. Gao, and K. Lohmann (2010), Importance of heat transport and local air-sea heat fluxes for Barents Sea climate variability, *J. Geophys. Res.*, *115*, C07013, doi:10.1029/2009JC005884.

Sandvik, A. D., and B. R. Furevik (2002), Case study of a coastal jet at Spitsbergen—Comparison of SAR- and model-estimated wind, *Mon. Weather Rev.*, *130*, 1040–1051.

Schauer, U., R. Muench, B. Rudels, and L. Timokov (1997), Impact of eastern Arctic shelf waters on the Nansen Basin intermediate layers, *J. Geophys. Res.*, *102*, 3371–3382.

Schauer, U., H. Loeng, B. Rudels, V. K. Ozhigin, and W. Dieck (2002), Atlantic Water flow through the Barents and Kara Seas, *Deep Sea Res., Part I*, *49*, 2281–2298.

Schlichtholz, P. (2011), Influence of oceanic heat variability on sea ice anomalies in the Nordic Seas, *Geophys. Res. Lett.*, *38*, L05705, doi:10.1029/2010GL045894.

Screen, J. A., and I. Simmonds (2010), Increasing fall-winter energy loss from the Arctic Ocean and its role in Arctic temperature amplification, *Geophys. Res. Lett.*, *37*, L16707, doi:10.1029/2010GL044136.

Segtnan, O. H., T. Furevik, and A. D. Jenkins (2011), Heat and freshwater budgets of the Nordic seas computed, *J. Geophys. Res.*, *116*, C11003, doi:10.1029/2011JC006939.

Seierstad, I. A., and J. Bader (2009), Impact of a projected future Arctic sea ice reduction on extratropical storminess and the NAO, *Clim. Dyn.*, *33*(7–8), 937–943.

Semenov, V. A. (2008), Influence of oceanic inflow to the Barents Sea on climate variability in the Arctic region, *Dokl. Earth Sci.*, *418*(1), 91–94, doi:10.1134/S1028334X08010200.

Semenov, V. A., and L. Bengtsson (2003), Modes of the wintertime Arctic temperature variability, *Geophys. Res. Lett.*, *30*(15), L1781, doi:10.1029/2003GL017112.

Semenov, V. A., and M. Latif (2012), The early twentieth century warming and winter Arctic sea ice, *Cryosphere*, *6*, 1231–1237.

Semenov, V. A., W. Park, and M. Latif (2009), Barents Sea inflow shutdown: A new mechanism for rapid climate changes, *Geophys. Res. Lett.*, *36*, L14709, doi:10.1029/2009gl038911.

Semenov, V. A., M. Latif, D. Dommenget, N. S. Keenlyside, A. Strehz, T. Martin, and W. Park (2010), The impact of North Atlantic-Arctic multidecadal variability on Northern Hemisphere surface air temperature, *J. Clim.*, *23*, 5668–5677.

Serreze, M., and R. G. Barry (2011), Processes and impacts of Arctic amplification: A research synthesis, *Global Planet. Change*, *77*(1–2), 85–96, doi:10.1016/j.gloplacha.2011.03.004.

Serreze, M., A. Barrett, A. Slater, M. Steele, J. Zhang, and K. Trenberth (2007), The large-scale energy budget of the Arctic, *J. Geophys. Res.*, *112*, D11122, doi:10.1029/2006JD008230.

Shapiro, I., R. Colony, and T. Vinje (2003a), April sea ice extent in the Barents Sea, 1850–2001, *Polar Res.*, *22*(1), 5–10.

Shapiro, G. I., J. M. Hutnance, and V. V. Ivanov (2003b), Dense water cascading off the continental shelf, *J. Geophys. Res.*, *108*, 3390, doi:10.1029/2002JC001610.

Simonsen, K., and P. M. Haugan (1996), Heat budgets for the Arctic Mediterranean and sea surface heat flux parameterizations for the Nordic Seas, *J. Geophys. Res.*, *101*, 6553–6576.

Sjögren, P. (2009a), Sand mass accumulation rate as a proxy for wind regimes in the SW Barents Sea during the past 3 ka, *Holocene*, *19*(4), 591–598.

Sjögren, P. (2009b), Climate, cod, and corps: Coastal land use in the SW Barents Sea region during the past 2.5 ka, *Holocene*, *19*(5), 703–716.

Skagseth, Ø., T. Furevik, R. Ingvaldsen, H. Loeng, K. A. Mork, K. A. Orvik, and V. Ozhigin (2008), Volume and heat transports to the Arctic Ocean via the Norwegian and Barents Seas, in *Arctic*

*Subarctic Ocean Fluxes: Defining the Role of the Northern Seas in Climate*, edited by R. Dickson, J. Meincke, and P. Rhines, pp. 45–64, Springer, New York.

Skagseth, Ø., K. F. Drinkwater, and E. Terrile (2011), Wind- and buoyancy-induced transport of the Norwegian Coastal Current in the Barents Sea, *J. Geophys. Res.*, *116*, C08007, doi:10.1029/2011JC006996.

Skeie, P. (2000), Meridional flow variability over Nordic seas in the Arctic Oscillation framework, *Geophys. Res. Lett.*, *27*, 2569–2572.

Skeie, P., and S. Grønås (2000), Strongly stratified easterly flows across Spitsbergen, *Tellus*, *52A*, 473–486.

Smedsrud, L. H., R. Ingvaldsen, J. E. Ø. Nilsen, and Ø. Skagseth (2010), Heat in the Barents Sea: Transport, storage and surface fluxes, *Ocean Sci.*, *6*(1), 219–234.

Smedsrud, L. H., A. Sirevaag, K. Kloster, A. Sorteberg, and S. Sandven (2011), Recent wind driven high sea ice area export in the Fram Strait contributes to Arctic sea ice decline, *Cryosphere*, *5*, 821–829, doi:10.5194/tc-5-821-2011.

Sorokina, S. A., and I. N. Esau (2011), Meridional energy flux in the Arctic from data of the IGRA radio sounding archive, *Izv. Atmos. Oceanic Phys.*, *47*(5), 572–583, doi:10.1134/S0001433811050112.

Sorteberg, A., and B. Kvingedal (2006), Atmospheric forcing on the Barents Sea winter ice extent, *J. Clim.*, *19*, 4772–4784.

Sorteberg, A., V. Kattsov, J. E. Walsh, and T. Pavlova (2007), The Arctic surface energy budget as simulated with the IPCC AR4 AOGCMs, *Clim. Dyn.*, *29*, 131–156, doi:10.1007/s00382-006-0222-9.

Takahashi, T., et al. (2009), Climatological mean and decadal change in surface ocean $pCO_2$ and net sea-air $CO_2$ flux over the global oceans, *Deep Sea Res., Part II*, *56*, 554–577.

Tanhua, T., E. P. Jones, E. Jeansson, S. Jutterström, W. M. Smethie Jr, D. W. R. Wallace, and L. G. Anderson (2009), Ventilation of the Arctic Ocean: Mean ages and inventories of anthropogenic CO2 and CFC-11, *J. Geophys. Res. 114*, C01002, doi:10.1029/2008JC004868.

Tjernström, M., M. Žagar, G. Svensson, J. Cassano, S. Pfeifer, A. Rinke, K. Wyser, K. Dethloff, C. Jones, and T. Semmler (2005), Modeling the Arctic Boundary Layer: An evaluation of six ARCMIP regional-scale models with data from the SHEBA project, *Boundary Layer Meteorol.*, *117*, 337–381.

Tjiputra, J., K. A. Assmann, and C. Heinze (2010), Anthropogenic carbon dynamics in the changing ocean, *Ocean Sci.*, *6*, 605–614.

Tremblay, L.-B. (2001), Can we consider Arctic Oscillation independently from the Barents Oscillation?, *Geophys. Res. Lett.*, *28*, 4227–4230.

Trenberth, K. E., and D. P. Stepaniak (2004), The flow of energy through the Earth's climate system, *Q. J. R. Meteorol. Soc.*, *130*, 2677–2701, doi:10.1256/qj.04.83.

Tsubouchi, T., S. Bacon, A. C. Naveira Garabato, Y. Aksenov, S. W. Laxon, E. Fahrbach, A. Beszczynska-Möller, E. Hansen, C. M. Lee, and R. B. Ingvaldsen (2012), The Arctic Ocean in summer: A quasi-synoptic inverse estimate of boundary fluxes and water mass transformation, *J. Geophys. Res.*, *117*, C01024, doi:10.1029/2011JC007174.

Van der Swaluw, E., S. Drijfhout, and W. Hazeleger (2007), Bjerknes compensation at high northern latitudes: The ocean forcing the atmosphere, *J. Clim.*, *20*, 6023–6032.

Vare, L. L., G. Massé, and S. T. Belt (2010), A biomarker-based reconstruction of sea ice conditions for the Barents Sea in recent centuries, *Holocene*, *20*(4), 637–643.

Vihma, T., J. Hartmann, and C. Lüpkes (2003), A case study of an on-ice air flow over the Arctic marginal sea ice zone, *Boundary Layer Meteorol.*, *107*, 189–217.

Vinje, T. (2001), Anomalies and trends of sea-ice extent and atmospheric circulation in the Nordic Seas during the period 1864-1998, *J. Clim.*, *14*(3), 255–267.

Voronina, E., L. Popyak, A. de Vernal, and O. Peyron (2001), Holocene variations of sea-surface conditions in the southeastern Barents Sea, reconstructed from dinoflagellate cyst assemblages, *J. Quat. Sci.*, *16*(7), 717–726.

Vorren, T. O., J. Landvik, K. Andreassen, and J. S. Laberg (2011), Glacial history of the Barents Sea region, in *Quaternary Glaciations—Extent and Chronology—A Closer Look*, *Dev. in Quat. Sci*., edited by J. Ehlers, P. L. Gibbard, and P. D. Hughes, pp. 361–372, Elsevier, Netherlands, Amsterdam.

Walker, G. T. (1925), Correlation in seasonal variations of weather —A further study of world weather, *Mon. Weather Rev.*, *53*, 252–254, doi:10.1175/1520-0493.

Wilson, L. J., M. Hald, and F. Godtliebsen (2011), Foraminiferal faunal evidence of twentieth-century Barents Sea warming, *Holocene*, *21*(4), 527–537.

Winton, M. (2006), Amplified Arctic climate change: What does surface albedo feedback have to do with it?, *Geophys. Res. Lett.*, *33*, L03701, doi:10.1029/2005GL025244.

Yang, S., and J. H. Christensen (2012), Arctic sea ice reduction and European cold winters in CMIP5 climate change experiments, *Geophys. Res. Lett.*, *39*, L20707, doi:10.1029/2012GL053338.

Yndestad, H., W. R. Turrell, and V. Ozhigin (2008), Lunar nodal tide effects on variability of sea level, temperature, and salinity in the Faroe-Shetland Channel and the Barents Sea, *Deep Sea Res., Part I*, *55*(10), 1201–1217, doi:10.1016/j.bbr.2011.03.031.

Yu, L., and R. A. Weller (2007), Objectively analyzed air-sea heat fluxes for the global ice-free oceans (1981–2005), *Bull. Am. Meteorol. Soc.*, *88*, 527–539.

Zahn, M., and H. von Storch (2008), A long-term climatology of North Atlantic polar lows, *Geophys. Res. Lett.*, *35*, L22702, doi:10.1029/2008GL035769.

Zhang, X., and J. Zhang (2001), Heat and freshwater budgets and pathways in the Arctic Mediterranean in a coupled ocean/sea-ice model, *J. Oceanogr.*, *57*, 207–234.

Zhang, X., A. Sorteberg, J. Zhang, R. Gerdes, and J. C. Comiso (2008), Recent radical shifts of atmospheric circulations and rapid changes in Arctic climate system, *Geophys. Res. Lett.*, *35*, L22701, doi:10.1029/2008GL035607.